

**SURFACE ELECTRON DONATING PROPERTIES
AND CATALYTIC ACTIVITY OF FERROSPINELS
CONTAINING Co, Zn AND Ni**

THESIS SUBMITTED TO THE
COCHIN UNIVERSITY OF SCIENCE AND TECHNOLOGY
IN PARTIAL FULFILMENT OF THE
REQUIREMENTS FOR THE DEGREE OF

DOCTOR OF PHILOSOPHY

IN

CHEMISTRY

IN THE FACULTY OF SCIENCE

BY

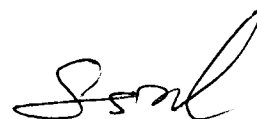
SREEKUMAR KURUNGOT

DEPARTMENT OF APPLIED CHEMISTRY
COCHIN UNIVERSITY OF SCIENCE AND TECHNOLOGY
KOCHI - 682 022

FEBRUARY 1999

CERTIFICATE

This is to certify that the thesis herewith is an authentic record of research work carried out by the author under my supervision, in partial fulfilment of the requirements for the degree of Doctor of Philosophy of Cochin University of Science and Technology, and further that no part thereof has been presented before for any other degree.



Dr. S. Sugunan
(Supervising Teacher)
Professor in Physical Chemistry
Department of Applied Chemistry
Cochin University of Science and Technology
Kochi-22

Kochi -22.
19th February '99.

CONTENTS

CHAPTER I	INTRODUCTION & LITERATURE SURVEY	
1.0	INTRODUCTION	1
1.1	HETEROGENEOUS CATALYSIS	1
1.1.1	Solid acid-base concept in heterogeneous catalysis	3
1.1.2	Methods of preparation	6
1.1.3	Transition metal oxides as catalysts	8
1.2	DISCUSSION OF THE SPINEL STRUCTURE	10
1.2.1	Normal and inverse spinels	13
1.2.2	The individual site preference of some cations	14
1.2.3	Ferrospinel	16
1.2.4	Magnetic and electric properties of ferrites	17
1.2.5	Spinel as catalysts	17
1.3	SURFACE ELECTRON DONATING PROPERTIES	21
1.4.	ALCOHOL DECOMPOSITION REACTION- a probe reaction for surface acidity/basicity determination	24
1.5	DEHYDROGENATION OF ETHYL BENZENE	27
1.6	ALKYLATION OF ANILINE AND PHENOL	28
1.7	OBJECTIVES OF THE PRESENT WORK	28
	REFERENCES	31
CHAPTER II	EXPERIMENTAL	
2.1	CATALYST PREPARATION	36
2.2	CATALYST CHARACTERIZATION	37
2.2.1	X-ray diffraction analysis	38
2.2.2	Diffuse reflectance infrared spectroscopy	38
2.2.3	Surface area determination by BET method	39
2.2.4	Pore volume determination using mercury porosimetry	40
2.2.5	Scanning electron microscope (SEM) and energy disperse X- ray analysis (EDX)	41
2.2.6	Mössbauer spectroscopy	42

2.2.7	Thermal analysis	43
2.2.8	Determination of surface electron donor properties	43
2.3	VAPOUR PHASE REACTIONS	44
	REFERENCES	47
CHAPTER III	CHARACTERIZATION AND SURFACE PROPERTIES OF FERRITES	
3.1	PHYSICAL CHARACTERIZATION	48
3.1.1	X-ray diffraction analysis	48
3.1.2	Scanning electron micrograms and energy dispersive X-ray analysis	50
3.1.3	Diffuse reflectance infrared spectra	52
3.1.4	Thermal analysis	54
3.1.5	Surface area and pore volume distribution	56
3.2	SURFACE PROPERTIES - ACIDITY/BASICITY	58
3.2.1	Surface electron donating properties	58
3.3	Alcohol decomposition reactions	67
3.3.1	Isopropyl alcohol decomposition	67
3.3.2	Cyclohexanol conversion	74
3.4	OXIDATIVE DEHYDROGENATION OF ETHYLBENZENE	77
	REFERENCES	87
CHAPTER IV	ALKYLATION OF ANILINE	
4.1	INTRODUCTION	89
4.2	Zn _{1-x} Co _x Fe ₂ O ₄ -TYPE SYSTEMS	91
4.2.1	Effect of methanol to aniline molar ratio	91
4.2.2	Effect of time-on-stream	93
4.2.3	Effect of catalyst composition	94
4.2.4	Effect of reaction temperature and feed flow rate	94
4.3	Zn _{1-x} Ni _x Fe ₂ O ₄ -TYPE SYSTEMS	97
4.3.1	Effect of methanol to aniline molar ratio	97
4.3.2	Effect of contact time	98

4.3.3	Effect of reaction temperature	99
4.3.4	Effect of time-on stream	100
4.3.5	Effect of catalyst composition	101
4.4	$\text{Co}_{1-x}\text{Ni}_x\text{Fe}_2\text{O}_4$ -TYPE SYSTEMS	103
4.4.1	Effect of catalyst composition	103
4.4.2	Effect of reaction temperature	103
4.4.3	Effect of feed flow rate and time-on-stream	104
4.5	GENERAL CATALYTIC PATHWAY	105
4.6	ACTIVITY AND SURFACE PROPERTIES OF THE PRESENT SYSTEMS	106
4.6.1	$\text{Zn}_{1-x}\text{Co}_x\text{Fe}_2\text{O}_4$ -type systems	108
4.6.2	$\text{Zn}_{1-x}\text{Ni}_x\text{Fe}_2\text{O}_4$ -type systems	113
4.6.3	$\text{Co}_{1-x}\text{Ni}_x\text{Fe}_2\text{O}_4$ -type systems	114
4.7	DIMETHYL CARBONATE FOR ENVIRONMENTALLY BENIGN REACTIONS	116
4.7.1	Effect of reaction temperature	117
4.7.2	Effect of feed molar ratio	118
4.7.3	Effect of contact time	118
4.8	KINETICS OF ANILINE ALKYLATION	119
4.9	COMPARISON OF ACTIVITY WITH γ -ALUMINA AND ZEOLITES	122
	REFERENCES	125
CHAPTER V	ALKYLATION OF PHENOL	
5.1	INTRODUCTION	127
5.2	$\text{Co}_{1-x}\text{Ni}_x\text{Fe}_2\text{O}_4$ -TYPE SYSTEMS	131
5.2.1	Effect of reaction temperature	131
5.2.2	Selection of phenol to methanol molar ratio	132
5.2.3	Effect of contact time	133
5.2.4	Composition effect of catalysts	134
5.2.5	Effect of time-on-stream	135
5.2.6	Effect of water in the feed	136

5.3	Zn _{1-x} Co _x Fe ₂ O ₄ -TYPE SYSTEMS	137
5.3.1	Effect of catalyst composition	137
5.3.2	Effect of reaction temperature	138
5.3.3	Effect of feed flow rate	139
5.3.4	Selection of feed molar ratio	139
5.4	Zn _{1-x} Ni _x Fe ₂ O ₄ -TYPE SYSTEMS	140
5.4.1	Influence of catalyst composition	140
5.4.2	Effect of reaction temperature and contact time	141
5.5	GENERAL CATALYTIC PATHWAY	142
5.6	ACTIVITY AND SURFACE PROPERTIES OF THE PRESENT SYSTEMS	144
5.7	ALKYLATION OF PHENOL USING DIMETHYL CARBONATE	149
	REFERENCES	151
CHAPTER VI	SUMMARY AND CONCLUSIONS	
6.1	SUMMARY OF THE WORK	153
6.2	CONCLUSIONS	154

PREFACE

Binary and ternary oxides possessing spinel structure have attracted much attention due to their remarkable transport, magnetic and catalytic properties. Spinel oxides containing iron are called ferrospinels. Simple ferrospinels, $A^{II}B_2O_4$, as well as mixed ferrospinels of the general formula $A^{II}B^{III}Fe_2O_4$ are known. The catalytic effectiveness of ferrites for many reactions arises because of the ease with which iron can change oxidation state between 2 and 3. However, the most important property of these materials is their stability to withstand under extremely reducing conditions. Thus the reduction of Fe^{3+} to Fe^{2+} takes place without altering the lattice configurations so that upon reoxidation the original state can be regained.

Ferrites are generally produced by the conventional ceramic processes involving high temperature (≥ 1200 °C) solid state reaction between the constituent oxides or carbonates. This method provides non-homogeneous, coarser ferrite particles with very low surface areas; thus the material does not match with the properties essentially required for a good catalyst. Recently reported, low temperature controlled co-precipitation methods have overcome these drawbacks and produced homogeneous, fine and reproducible ferrite powders with significantly high surface areas.

This work is oriented to evaluate the catalytic activities of ferrospinels containing Zn, Co and Ni prepared via low temperature route. The major reactions carried out were methylation of aniline and phenol, oxidative dehydrogenation of ethyl benzene to styrene and alcohol decomposition. Various physico-chemical methods have been adopted for the characterization of the systems.

The last chapter of the thesis summarises the general conclusions drawn by us from the results presented in the earlier chapters. These materials offer interesting opportunities as potential catalysts in alkylating both aniline and phenol. There is plenty of scope for further research in this field for alkylating various substituted phenols and anilines, and also various heterocyclic compounds.

CHAPTER I

INTRODUCTION & LITERATURE SURVEY

1.0 INTRODUCTION

Catalyst development and synthesis have become a wide spread research field because of the increasing global demand for better systems in chemical industry. Today, the chemical industry has been blamed for producing environmentally hazardous substances, which cause acid rain, a reduction of stratospheric ozone levels and so on. Many industrial processes have become a burden on the environment, and, therefore, must be essentially replaced by more eco-friendly or compatible processes. In addition to this, disposing of by-products or converting them into environmentally nonhazardous substances consume much energy. The successful exploitation of a material as a catalyst will give value-added products with improved yields and also eliminate or minimize environmental pollutants.

The two catalyst systems, homogeneous and heterogeneous, have been implemented widely in chemical industries. Although, well known homogeneous catalytic systems such as ‘Wacker’ and ‘oxo’ processes have been successfully used on an industrial scale, there are ever increasing problems associated with these catalytic reactions. Homogeneous systems often perform better selectivity, activity and reproducibility, however, they are more vulnerable to extraneous materials. Low thermal stability and shorter catalyst life-time amplify the cost of production. Synthesis of new heterogeneous systems to replace the existing homogeneous systems has become a challenging task in the catalytic field.

1.1 HETEROGENEOUS CATALYSIS

The field of heterogeneous catalysis is one of the most rapidly expanding fields of chemistry. The world market for heterogeneous catalysts is expected to reach highest peak in the coming years. Here reactants and catalysts are present in different phases. Commonly, the catalyst is a solid, and the reactants are either gases or liquids. Chemisorption of the substrates on the surface of the catalyst is the first step in heterogeneous catalysis, which is followed by the reaction of the chemisorbed molecules and the diffusion of the products away from the active sites of the catalyst. The main advantage of the heterogeneous catalytic process is that it can be operated

continuously in a reactor without interruption. Since the catalyst is present in a phase different from the reactants and the products, the separation of the catalyst from the final reaction mass is also quite easy.

A commercial catalyst should be stable, active and selective. Sufficiently high surface area, good porosity and stable mechanical strength are essential for an effective heterogeneous catalyst. The properties of a heterogeneous catalyst for industrial use can be classified broadly into two [1]:

1. Properties which determine directly catalytic activity and selectivity: Here factors such as bulk and surface chemical composition, local microstructure and phase composition are important.
2. Properties which ensure their successful implementation in the catalytic process: Here thermal, mechanical and chemical stability, porosity, shape and dimension of catalyst particle enter.

Experiments show that in the majority of cases the chemical composition of the principal component of a catalyst exerts considerably greater influence on its catalytic activity than the method of preparation.

Heterogeneous catalysts are classified into several ways. Based on their physico-chemical nature they can be classified as follows:

1. Metal oxides: Simple metal oxides, mixed metal oxides, supported metal oxides, modified metal oxides.
2. Supported metals / bimetallic catalysts.
3. Zeolites / molecular sieves.
4. Clays and hydrotalcites.
5. Solid supported heteropoly acids.

A wide range of reactions can be catalysed by heterogeneous systems. However, heterogeneous based reactions can be separated mainly into two types[2].

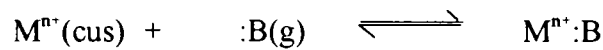
1. Oxidation-reduction (electronic): Reactions pertaining to this type are those of oxidation, reduction, hydrogenation, dehydrogenation, decomposition of unstable oxygen containing compounds and others. The reactions are catalyzed by solids possessing free or easily excited electrons *i.e.* metals and semiconductors. The mechanism of these reactions is a characteristic transfer of electron in an elementary act of catalysis from the catalyst to the reacting substance or vice versa.

2. Acid-base (ionic): Catalytic cracking, hydration, dehydration, hydrolysis, many reactions of isomerization, and a series of other reactions pertaining to this type. Such reactions are accelerated under the influence of acid or base. For this type of reactions the elementary act is the characteristic transfer of proton or the production of heteropolar donor-acceptor pair. Acid-base property of a heterogeneous surface is the important factor in determining the catalytic efficiencies for these type of reactions. Many chemical reactions are initiated by acid-base interactions followed by catalytic cycles. In acid catalyzed reactions, reactants act as bases toward catalysts which act as acids. On the other hand in a base catalyzed reaction reactants act as acids toward catalysts which act as bases.

1.1.1 Solid acid-base concept in heterogeneous catalysis:

A large number of solids have surface acidic and /or basic properties. Many materials possess inherent acid-base centers. Activity and selectivity of these systems for particular reactions depend predominantly on the strength and distributions of the acid-base centers. The inherent acid-base properties can be further improved by adopting some surface modification techniques and also by adopting proper synthesis/post-synthesis treatments. These solid acids and bases have usually been employed as catalysts on various acid-base catalyzed reactions. Surface hydroxyl groups and coordinatively unsaturated metal cations and oxygen anions are responsible for the surface acidity and basicity on a partially hydroxylated oxide surface. Exposed

coordinatively unsaturated (cus) cations may act as acceptors for free electron pairs of adsorbed molecules.

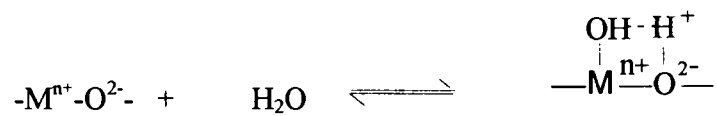


Such cations are Lewis acid sites. The strength of these acid sites depends on the charge and size of the cations. According to the concept of hard and soft acids, cations of a higher oxidation states are harder.

Surface hydroxyl groups may act as Brønsted acid sites. They may dissociate to protonate adsorbed bases:



The resulting conjugate acids and bases are stabilized on the surface by electrostatic interaction with the oxide. Brønsted acid sites are present only when hydroxyl groups are present. Therefore, the number of such sites depends on the extent of hydroxylation of the surface. Hydroxylation and dehydroxylation involve the interaction between a water molecule and surface coordinately unsaturated cations and oxygen anions:



This means that both dehydroxylation and disappearance of Brønsted acidity are responsible for the formation of Lewis acid sites, and vice versa. However in some cases this interconversion may not be demonstrated so readily due to the fact that the surface oxygen anion is very strongly basic such that its protonated form is only a very weak Brønsted acid and it protonates only strongly basic molecules.

An exposed coordinatively unsaturated oxygen ion participates in an acid base reaction acting as a base.

Heterogeneous acid catalysis attracted much attention primarily because in petroleum industry, heterogeneous acid catalysts are used as the main catalyst in the cracking process which is the largest process among the industrial chemical processes. Extensive studies of heterogeneous cracking catalysts undertaken during 1950s revealed that the essential feature of cracking catalysts is acidity, and, therefore, generation of acidic sites on the solids was extensively studied. As a result, amorphous silica-alumina was utilized as a cracking catalyst, and crystalline aluminosilicate (zeolite) was used afterwards.

In many cases good correlation has been found between the total amount of acid (Brønsted + Lewis) and catalytic activities of solid acids. For example the rates of both catalytic decomposition of cumene [3] and polymerization of propylene [4] over $\text{SiO}_2\text{-Al}_2\text{O}_3$ catalysts were found to increase with increasing acid amounts. Uchida and Imami have found that both the ethylene polymerization activity of $\text{SiO}_2\text{-Al}_2\text{O}_3$ and its acid amounts are increased by the addition of nickel oxide [5]. Alumina's catalytic activity in a range of reactions such as isomerization of hydrocarbons, the polymerization of olefins, etc have been attributed to the acidic properties of the surface [6,7]. Another important observation was the higher activity of $\text{Al}_2\text{O}_3\cdot\text{B}_2\text{O}_3$ compared to $\text{SiO}_2\cdot\text{Al}_2\text{O}_3$ in the trans alkylation of aromatic compounds and in the Beckmann rearrangement of cyclohexanone oxime. This higher activity seems to be due to the higher concentrations of acid sites on $\text{Al}_2\text{O}_3\cdot\text{B}_2\text{O}_3$ [8].

In contrast to these extensive studies of heterogeneous acidic catalysts, fewer efforts have been given to the study of heterogeneous basic catalysts. The first study of heterogeneous basic catalysts, that sodium metal dispersed on alumina acted as an effective catalyst for double bond migration of alkenes, was reported by Pines *et al.* [9].

The various types of heterogeneous basic catalysts are [10]:

1. Single component metal oxides, alkaline earth oxides, alkali metal oxides and rare earth oxides.

2. Zeolites and alkali ion-exchanged zeolites.
3. Supported alkali metal ions, alkali metal ions on alumina and silica and alkaline earth oxides
4. Clay minerals, hydrotalcite and Sepiolite
5. Non-oxide and KF supported on alumina

Following the report by Pines *et al.*, the 1-butene isomerization over calcium and magnesium oxide was recognized as a base catalyzed reaction in which the reaction was initiated by the abstraction of a proton from 1-butene by the basic site on the catalyst surfaces [11]. The catalytic activities of basic zeolites were also reported during this period. The first reported base catalyzed reaction by alkali-cation exchanged zeolite was the side chain alkylation of toluene as reported by Yashima *et al.* [12].

In addition to the above mentioned catalysts, a number of materials have been reported to act as heterogeneous base catalysts. Except for non-oxide catalysts, the basic sites are believed to be surface O atoms. Oxygen atoms existing on any materials may act as basic sites because any O atoms would be able to interact attractively with a proton.

1.1.2 Methods of preparation:

For the exact reproducibility of the heterogeneous catalysts, utmost care must be taken during the preparation stages. In metal oxide catalysts, both composition and preparation methods are equally crucial in determining their properties. Even minor variation in the preparation method can drastically alter their catalytic properties irrespective of their composition. Therefore, designing metal oxide catalyst involves a judicious selection of metal components and the preparation method. The most common preparation methods are precipitation, co-precipitation, sol-gel method, complexation method, and ceramic method

The formation of a precipitate from the homogeneous liquid phase may occur as a result of the addition of bases, acids or by the use of complex forming agents. In

almost all cases, the formation of a new solid phase in a liquid medium results from two elementary processes; nucleation (*i.e.*, the formation of the smallest elementary particles of the new phase) and growth or agglomeration of the particles. Supersaturation, pH, temperature, nature of the reagents, presence of impurities and the method of preparation are the critical factors in determining the morphology, the texture and the structure of the particles [13].

In the co-precipitation method, hydroxides or carbonates of metal ions are precipitated out of a solution containing the precursor compounds [14,15]. This is followed by filtration, washing and calcination of the product to form the oxide. In a system with two or more metallic compounds, the composition of the precipitate depends on the difference in solubility between the components. When there is a large difference in the solubility products of the compounds involved, the sequential precipitation route can be adopted [16].

Sol-gel method involves the continuous transformation of a solution into a hydrated solid precursor [17]. This method allows control of texture, composition, homogeneity and structural properties of the finished solids. This method generally involves controlled hydrolysis and polymerization of ionic species in aqueous media. The preliminary stage involves the formation of hydrosols, and this is followed by aggregation of primary particles. The discovery of new and faster methods to produce aerogels substantially enhanced the popularity of this method, as an efficient way to control the texture, composition, homogeneity and structural properties of the catalyst materials.

The complexation method involves chemical reactions which transform slowly and without physical discontinuity the homogeneous solution of catalyst precursor into a homogeneous or amorphous phase [18]. The resulting precursor is then dried and decomposed to yield better intermixed and more highly dispersed oxides than those prepared by usual precipitation routes [19]. The multifunctional organic chelating agents will perform smooth gelation of the homogeneous solution of catalyst precursors.

Ceramic method involves the direct calcination of appropriately mixed metal salts at high temperatures. Metal salts (usually oxalates or carbonates) are ground well in wet or dry condition [20]. Solid solutions of the spinel and perovskite type oxides are generally prepared by ceramic route.

In addition to the above discussed common methods, some other methods like combustion synthesis, freeze drying technique, spray drying technique and hydrothermal method are also applied in catalyst synthesis.

1.1.3 Transition metal oxides as catalysts:

The high catalytic activity of transition metals appears to be one of the most significant facts of heterogeneous catalysis. Not only do the transition metals themselves possess high catalytic activity, but also do their alloys and compounds with nonmetals, sulfides and oxides etc. Transition metal oxides are the functional components in catalysts used in a large number of reactions such as oxidation, oxidative and non-oxidative dehydrogenation, reduction, ammoxidation, metathesis (production of long chain alkenes) and water gas shift reaction (production of hydrogen). Of these, selective oxidation, ammoxidation and selective dehydrogenation constitute the most important catalytic uses of transition metal oxides [21]. Another important application of transition metal oxides is that these can be used as precursors for other important catalysts. Cobalt-molybdenum sulfide catalyst for hydro desulphurization of petroleum crude and chromium based catalysts are examples. The important properties of transition metal oxides, that make these systems catalytically important material, are summarized below.

1. Presence of cations and anions in stoichiometric ratios and in well-defined spatial (structural) relationships
2. Possibility of covalent and ionic bonding between cations and anions
3. Presence of strong electric field normal to the surface due to the coulombic nature of the ionic lattice
4. Presence of charged adsorbed species
5. Presence of surface acidity and basicity

6. Presence of cationic and anionic vacancies
7. Ability of cations to undergo oxidation and reduction
8. High mobility of lattice oxygen and the possibility that the lattice oxygen are reactants in a reaction

Generally transition metal oxides in the series Ti → Cu, Zr → Ag, and Ta → Au, are especially active in reactions of the oxidation-reduction class. Many workers have explained the high catalytic activity on the basis of the fact that the cations exert an abnormally strong deforming action and that there is a gradual decrease in the potential of the chemical forces in bonds that are formed by d-electrons, in comparison with bonds formed by s- and p-electrons.

The developments in surface science techniques have provided very detailed idea about the surface structures, chemical composition and electronic properties of the surfaces. In particular, the advances in instrumentation and experimental techniques have made it possible to study the chemistry of the interface between the transition metal oxide and the fluid phase in greater detail than ever before.

Corundum, rocksalt, wurtzite, spinel, perovskite, rutile and layer structure are the important structural classes of transition metal oxides. In addition to these structures, there exist many other structures such as schelite, pyrochlore and wolframite. The difference in these structures is mainly due to difference in the close packing of oxygen anions. Ionic radius of transition metals are smaller than O^{2-} . Thus the oxygen ions are usually close packed with smaller metal ions situated in the octahedral and tetrahedral holes among the oxygen ions.

In the present investigation, iron based spinel oxides of Co, Ni and Zn are chosen. Materials are prepared by soft-chemical route, and their surface properties and catalytic applications are discussed in the present study. A detailed account of the catalyst systems and literature overview are given below.

1.2 DISCUSSION OF THE SPINEL STRUCTURE

Spinel is the structure type of a wide variety of compounds with the general formula AB_2O_4 . The spinel structure can be approximated by a cubic close packing of O^{2-} ions in which A and B ions occupy certain interstices. The unit cell of a spinel contains 8 formula units and, hence, can be represented as $8[AB_2O_4]$. The 32 oxygen anions per unit cell form a face centered cubic cage, while the metallic cations occupy interstitial sites. In an ideal spinel the metallic cations represented as A occupy tetrahedral (Tet.) sites and comprises the tetrahedral sublattice, while those metallic cations represented as B occupy octahedral (Oct.) sites, and comprise the octahedral sublattice. Close packing of 32 O^{2-} ions form 64 tetrahedral interstices and 32 octahedral interstices. Of these, 8 Tet. holes and 16 Oct holes are occupied by cations. In other words, 1/8 of the Tet. interstices and 1/2 of the Oct. interstices are occupied by cations. The unit cell of an ideal spinel structure is shown in Fig.1.2.1. The non-ideal structure is derived from the ideal one by moving the anion from the ideal position in a (111) plane away from the nearest T- ion. The deviation of the ideal pattern is given by the oxygen parameter 'u' (*the difference in the expansion of octahedral and tetrahedral sites, in order to accommodate larger cations (such as Co, Cu, Mg, Mn, Ni and Zn) is characterized by a parameter, and it is generally represented as oxygen parameter 'u'. The tetrahedral interstices in an ideal close packed structure can accommodate only those metal ions with a radius $r_{tet} \leq 0.30 \text{ \AA}$ and in the octahedral sites only ions with a radius $r_{oct} \leq 0.55 \text{ \AA}$. Hence the lattice has to be expanded to accommodate larger cations*). In all ideal spinels the parameter 'u' has a value in the neighbourhood of 0.375. But in actual spinel lattices this ideal pattern is slightly deformed, usually corresponds to $u > 0.375$ [23-25].

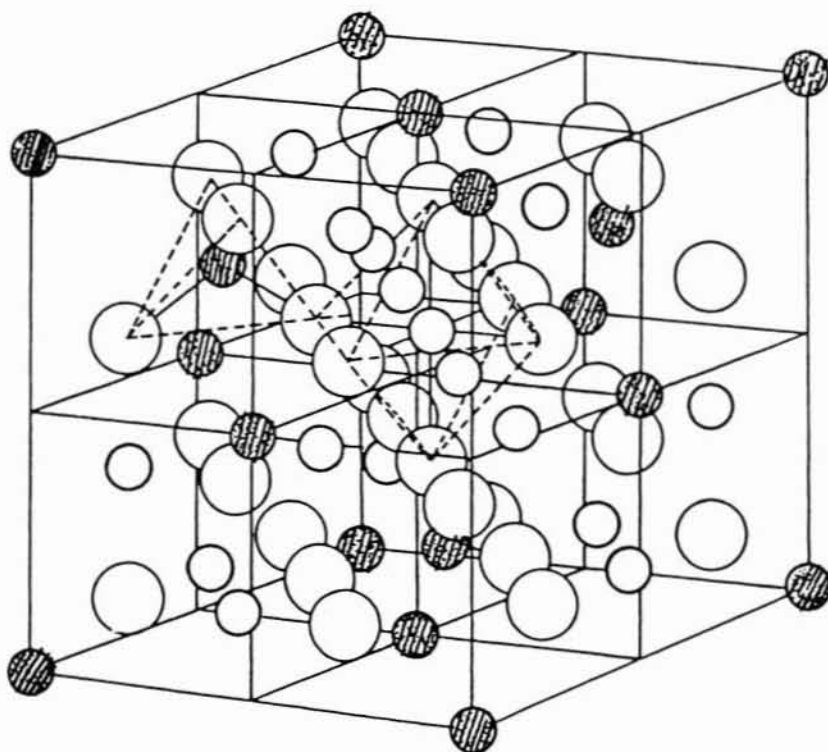


Fig. 1.2.1. The unit cell of an ideal spinel structure. Hatched circles indicate A cations, small unhatched circles indicate B cations and large unhatched circles indicate oxygen anions.

Fig. 1.2.2 represents the immediate neighbours of an anion in the spinel structure. One A and three B cations are around each anion as represented in the figure. If 'a' denotes the cell edge of the spinel unit cell, the AX distance is $a(u-1/4)$ and BX distance is $a(5/8-u)$ for small deviations from the ideal lattice. The angle AXB is about 125° and the angle BXB about 90° .

$$AX = a(u-1/4),$$

$$BX = a(5/8-u).$$

But for an ideal spinel 'u' = 0.375. Hence,

$$AX = a(0.375-1/4)$$

$$= 0.125 a,$$

$$BX = a(5/8-0.375)$$

$$= 0.25 a.$$

This difference in the bond length of two types of cations with the anions is an important factor in determining their electrical and catalytic properties [25].

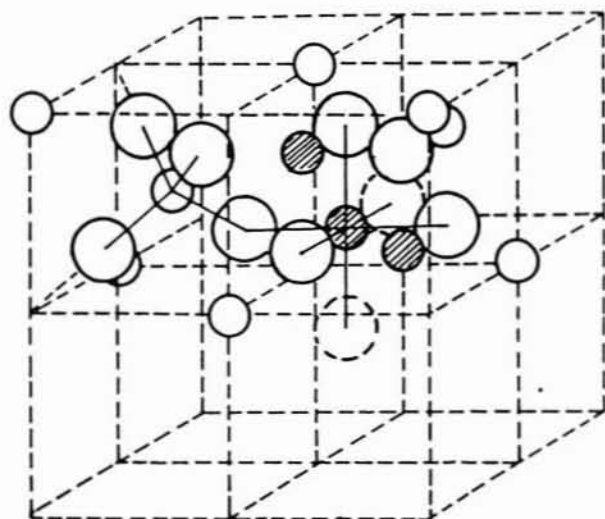


FIG. 1.22. UNIT CELL OF THE IDEAL SPINEL STRUCTURE. THE POSITION OF THE IONS IN ONLY TWO OCTANTS SHOWN. THE DASHED CIRCLES BELONG TO OTHER OCTANTS. LARGE CIRCLES : ANIONS ; SMALL HATCHED CIRCLES B - SITE CATIONS ; SMALL UNHATCHED CIRCLES : A - SITE CATIONS.

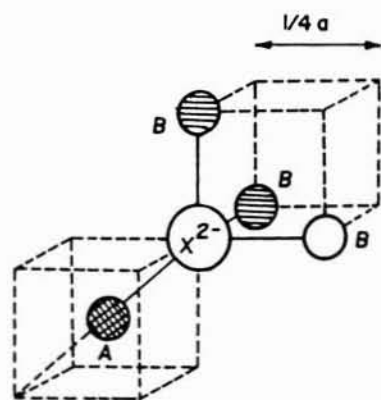


FIG. 1.23. THE NEAREST NEIGHBOURS OF ANION IN THE SPINEL STRUCTURE : X : ANION, A : A - SITE CATION, B : B - SITE CATION, a : CELL EDGE.

1.2.1 Normal and inverse spinels:

As mentioned above the general formula of a spinel can be represented as AB_2O_4 . Mainly three different valency distribution for the cations are possible.

1. $A = +2$ $B = +3$
2. $A = +4$ $B = +2$
3. $A = +6$ $B = +1$

However, the third possibility represented as $A = +6$ and $B = +1$ is very rare.

A spinel is called “normal” if the Tet. sites are occupied only by A-type ions and the Oct. sites by B-ions. The A ions of a normal spinel occupy the 8 Tet. sites of the O_h^7 space group and have a point symmetry T_d . The B ions of a normal spinel occupy the 16 Oct. sites of O_h^7 and have a point symmetry D_{3d} . But Barth and Posenjak [26] pointed out a second possibility, in which half of the B cations occupy the Tet. sites and all A cations together with the other half of the B cations in the Oct. sites. This type of spinel configuration is called “inverse” spinels. Recent work such as that of Datta and Roy [27] and Hafner and Laves [28] have shown that there are many “intermediate” or “random” spinels which are in between the pure normal and pure inverse arrangements. This intermediate spinel structure is due to the averaged distribution of all ions about all spinel cation positions (Table 1.2.1).

Type	Structure	Examples
Normal	$(A^{+2})[B_2^{+3}]O_4$	$ZnFe_2O_4$, $ZnCrFeO_4$, $ZnCr_2O_4$, $MgCr_2O_4$
Inverse	$(B^{+3})[A^{+2}B^{+3}]O_4$	$MgFe_2O_4$, $NiFe_2O_4$, $CoFe_2O_4$
Random	$(A_x^{+2}B_y^{+3})[A^{+2}_{1-x}B^{+3}_{2-y}]O_4$	$MgCrFeO_4$

Table 1.2.1. Examples of some normal and inverse spinels.

1.2.2 The individual site preference of some cations:

It is well known that cations sometimes have a pronounced preference for certain coordination numbers. This phenomenon influences the cation distribution in spinel structure. The following three factors are the major influencing factors in the cation distribution in the spinel lattice [29-31].

1. **Cation size:** Large divalent ions tend to occupy Tet. sites as this is favoured by polarization effects. If the A site ions have lower valency and the B site ions have higher valency, the intermediate O^{2-} ions will become polarized towards B sites. Thus polarization favours normal spinel configuration [31]. Also, as the $+3$ cation in 2:3 spinel is usually smaller than the $+2$ ion, it would be expected to confer greater stability on the lattice by occupying the smaller Tet. sites. This is realized when $rB^{3+} \ll rA^{2+}$, the tendency being towards the inverse form.

2. **Madelung constant:** Verweg, de Boer and Van Sonten [32,33] calculated the Madelung constant for normal and inverse spinels with divalent, trivalent and tetravalent ions as a function of the oxygen parameter 'u'. Their result is shown in Fig. 1.2.3. Some important points can be generalised from this figure. For a fixed value of the lattice constant a normal structure is stable for $u > 0.379$ in the case of 2-3 spinels, and for $u < 0.385$ for 2-4 spinels. Otherwise inverse spinels are stable. The most favourable situation is a small 'u' (0.375) for normal 2-4 spinels and a large 'u' (0.385) for normal 2-3 spinels. The Madelung constant of inverse 2-3 spinel is hardly dependent upon 'u'. This result was reproduced later by Gorter [34] by plotting Madelung constant M as a function of the anion parameter q_A for different values of 'u'. They pointed out that for electrostatic reasons it is favourable to have either large ions with low charge or small ions with high charge on A sites. The Madelung constant and therefore the lattice energy for the structure is greatest when the cations of greater charge has highest coordination number. This factor favours the occupancy of octahedral sites by $+3$ ions (*i.e* the normal spinel lattice) in a 2-3 spinel lattice.

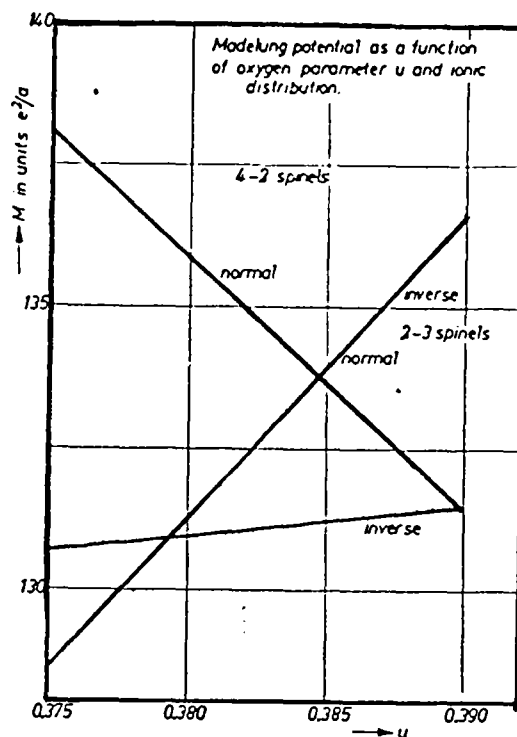


Fig. 1.2.3. Electrostatic contribution to the lattice energy of spinels (in units of e^2/a , where electronic charge, a = lattice constant)

3. Ligand field stabilization energy: Certain ions tend to occupy octahedral holes because the arrangement confers the maximum ligand field stabilization energy. For example Ni^{2+} ions (d^8 configuration) always displaces other ions from octahedral sites and the spinels containing it are always inverse. The Mn^{3+} ions (d^3) displaces all other ions except Ni^{2+} from octahedral holes, consequently all its spinels except $\text{Mn}[\text{NiMn}]\text{O}_4$ are normal. This tendency of d^3 and d^8 ions to occupy oct. holes can be explained in terms of the ligand field theory. According to this theory, the cations will occupy those sites where it will gain maximum ligand field stabilization energy. Thus d^3 and d^8 ions will prefer oct. sites due to the high value of stabilization energy in the

octahedral environment. The ligand field stabilization energy calculated for different 'd' systems is summarized in the following table (Table 1.2.2).

Configuration	Ligand field energy Stabilization	
	Octahedral field	Tetrahedral field
d ¹ and d ⁶	0.4Δ _o	0.6Δ _t
d ² and d ⁷	0.8Δ _o	1.2Δ _t
d ³ and d ⁸	1.2Δ _o	0.8Δ _t
d ⁴ and d ⁹	0.6Δ _o	0.4Δ _t
d ⁵ and d ¹⁰	0	0

Table. 1.2.2. Ligand field stabilization energies calculated for different 'd' systems.

From the table it is seen that ions with d⁵ and d¹⁰ configurations have no site preference at all. d⁴ and d⁹ ions can be further stabilized by Jahn-Teller distortion. If the regular octahedron of surrounding anions is elongated or compressed, the doublet and triplet levels of d orbitals further split [35]. The splitting of the doublet is larger. In the case of elongation the dz² orbital is stabilized compared to the dx²-y² orbital. Fe[CuFe]O₄ and Zn[Mn³⁺]O₄ are examples of tetragonally distorted spinels.

When the various factors as mentioned above are counter balancing one another there can be a completely random arrangement of metal ions among the eight Tet. and sixteen Oct. Sites.

1.2.3 Ferros spinels:

Spinel oxides containing iron are called ferros spinels. The interesting electrical, magnetic and catalytic properties of these compounds are governed critically by their chemical composition. Hence preparation of ferros spinel composites with specific properties has gained much importance. Simple ferros spinels (A^{II}Fe₂O₄), as well as mixed ferrite spinels of the general formula A^{II}_{1-x}B^{III}_xFe₂O₄ are known.

1.2.4 Magnetic and electric properties of ferrites:

Historically ferrites attracted the attention of physicists and technologists since they are magnetic semiconductors. Due to the occupancy of cations in two crystallographically different sites (*i.e.* octahedral B and tetrahedral A sites) three kinds of magnetic interactions are possible between the metallic ions, through the intermediate O^{2-} ions, namely A-A interactions, B-B interactions and A-B interactions. Generally for inverse ferrites, the resultant moment is that of the divalent ions in B sites. This can be explained by taking magnetite (Fe_3O_4) as a specific example. Here, half of the Fe^{3+} ions are in A sites and the rest of the ions (*i.e.* Fe^{3+} and Fe^{2+}) in B sites. The spins of A site and B site Fe^{3+} ions will cancel mutually due to the negative A-B interaction, and the resultant moment is only due to the Fe^{2+} ions in the B sites. But in $ZnFe_2O_4$, a normal spinel, there can be neither A-B interaction nor A-A interaction since Zn^{2+} is a nonmagnetic ion. Therefore, the only prevalent magnetic interaction is B-B interaction between Fe^{3+} ions, which is antiferromagnetic [36].

Electrical conductivity of spinel ferrites is low when compared to those of the magnetic materials. This factor is responsible for a wide use of ferrites at microwave frequencies. Generally they are semiconductors with their conductivity values varying between 10^2 and 10^{-11} $ohm^{-1} cm^{-1}$.

Nickel-zinc ferrites have been found to be one of the most versatile ferrites for general use. They present a wide range of choice in permeability, coercive force and magnetic and electric losses [37]. In a similar way, cobalt-zinc ferrites [38], lithium ferrites [39] and copper-zinc ferrites [40] also were extensively studied and were used in technological fields.

1.2.5 Spinel as catalysts:

Spinel shows interesting catalytic properties. In these compounds the properties are controlled by the nature of ions, their charge and site distribution among Tet. and Oct. sites. Bautiles and Barboax [41] investigated the surface composition of normal spinel oxides using Differential Neutron Diffraction (DND) techniques. This method suggested that the surface of normal spinel consists of a mixture of (110) and

(111) planes. But, in the case of a distorted spinel like γ -alumina, 80% of the exposed faces have the (110) direction. By comparing the experimental results of DND with some models involving argon-oxygen anions, these workers observed that such planes (*i.e.* both (111) and (110)) contain only octahedral cation and oxygen anion, respectively. Probing the surface layer of materials has become more accurate after introducing Low Energy Ion Scattering (LEIS) technique in catalytic field. The most characteristic feature of the LEIS is that the peaks in the spectra result from scattering by topmost atomic layer. Jacobs *et al.* [42], in a recent work, applied this technique to evaluate spinel surface composition. Their work clearly revealed that Oct. sites are exposed almost exclusively at the surface of the spinel oxide and the catalytic activity of many such systems is mainly due to Oct. cations. Several other workers also believed that Tet. ions are either inactive or contributing only a little to the catalytic properties [43]. Another possible reason for the lower activity of Tet. cations comes from the fact that, due to lower coordination number, the metal oxygen bonds will be stronger and, hence, such cations are not easily accessible to the reactants.

Catalytic activities of different spinel compounds have been well established for various reactions like oxidative dehydrogenation of hydrocarbons, hydrodesulphurization of petroleum crude, treatment of automobile exhaust gases, oxidation of carbon monoxide, hydrogen and methane etc. Among the spinel compounds, ferrites have been used as effective catalysts for a number of industrially important reactions as those mentioned above. The catalytic effectiveness of ferrites for many such reactions arises because of the ease with which iron can exchange its oxidation state between 2 and 3. Another important attribute of these materials, from the commercial stand point, is that spinel structure provides high stability so that these materials can withstand extremely reducing conditions. Even if reduction of Fe^{3+} to Fe^{2+} occurs, spinel structure remains unaltered and upon reoxidation the original state can be retained [44].

Perhaps the most widely studied reaction using spinel type catalyst is the catalytic selective oxidation of carbon monoxide. Selective removal of CO from CO/H₂ mixed gas is a key step for fuel cell or sensor technology [45,46]. Among the

metal oxides, spinel type cobalt oxide (Co_3O_4) is the most active catalyst for the oxidation of CO. For determining the active species of Co_3O_4 , Oh *et al.* [45] replaced $\text{Co}_{\text{Tet.}}^{2+}$ and $\text{Co}_{\text{Oct.}}^{3+}$ with Zn^{2+} and Al^{3+} , respectively, because ZnO and Al_2O_3 are inactive for CO oxidation. This substitution method has been employed to study the activity of different cobalt sites separately. Later Barbaoux *et al.* [47] studied the bulk cobalt species and activity and reported that the factor which determined the activity for complete oxidation was $\text{Co}_{\text{Oct.}}^{3+}$. Systems like ZnCo_2O_4 , CoAl_2O_4 and CoFe_2O_4 were also employed for selective CO oxidation by Takada *et al.* [48], and it was concluded that $\text{Co}_{\text{Oct.}}^{3+}$ is an active site for oxidation while $\text{Co}_{\text{Tet.}}^{2+}$ is inactive. One probable reason, why $\text{Co}_{\text{Oct.}}^{3+}$ is effective for oxidation is that the valence of cation in the Tet. sites is lower than that in the Oct. sites, and, therefore the stronger tetrahedral metal-oxygen bond retards the oxidation. Another reason is that the surface site is an Oct. site and the Tet. one is not accessible. In a recent work Omata *et al.* [49] synthesized some substituted spinel oxides such as $\text{Zn}_x\text{Co}_{3-x}\text{O}_4$ ($x = 0-1$), $\text{Al}_x\text{Co}_{3-x}\text{O}_4$ ($x = 0-2.5$) and $\text{Fe}_x\text{Co}_{3-x}\text{O}_4$ ($x = 0-2.5$) to clarify the relation between the surface cobalt species and the oxidation activity/selectivity. The substituted cobalt oxide showed high oxidation activity and CO oxidation selectivity only when $\text{Co}_{\text{Oct.}}^{3+}$ was available on the surface, while it showed quite low activity and selectivity when little $\text{Co}_{\text{Oct.}}^{3+}$ was available on the surface.

The oxidation of methanol has been studied over chromium-containing spinel, $\text{MgAl}_{2-x}\text{Cr}_x\text{O}_4$, by Awe *et al.* [50] and compared its activity with corundum ($\alpha\text{-Al}_2\text{O}_3$). The spinel catalyst was found to be more active, but less selective for HCHO, whereas the corundum system showed high selectivity and low activity to HCHO.

Another synthetically important reaction is the synthesis of methyl formate. Actually it was prepared via the process of dehydrocoupling of methanol catalyzed by copper-containing catalysts. Vapour phase dehydrocoupling of methanol to methyl formate over CuAl_2O_4 spinel has been reported recently. $\text{CuO-Al}_2\text{O}_3$ systems with different Cu/Al ratios were prepared by the amorphous citrate precursors and, their

catalytic activities for the reaction were examined. CuAl_2O_4 activated at $1100\text{ }^\circ\text{C}$ showed highest activity for the formation of methyl formate at a reaction temperature $310\text{ }^\circ\text{C}$. According to the authors, Cu^{II} ion in the CuAl_2O_4 is the effective site for the dehydrocoupling above $250\text{ }^\circ\text{C}$ [51].

Many single and mixed metal oxides have been mentioned as catalysts for the oxidative dehydrogenation of olefins. Ferrite spinels such as CoFe_2O_4 and CuFe_2O_4 are active catalysts for oxidative dehydrogenation of n-butene to butadiene [52]. In addition to these, various other ferrite spinel structures seemed well suited for this type of reactions; as the cation distributions in the spinels are well established and the ferric ions offer the availability of a reducible cation. Surface and lattice oxygen atoms participate in the reactions. Selectivity for the dehydrogenation reaction was strongly dependent on the presence of gaseous oxygen in the case of CoFe_2O_4 , although the selectivity over the Cu catalyst was not a strong function of gaseous oxygen. The copper catalyst was more active, but, selectivity of the oxidation reaction to butadiene was much poorer on the copper ferrite. A probable reason, as suggested by the authors, for the difference in activity of two catalysts is the greater reducibility of the copper ion relative to the cobalt.

Magnesium ferrite catalyst is effective for the oxidative dehydrogenation of hydrocarbons containing four to six carbon atoms. Its first use for this process was reported in a patent granted to Bajars, Croce and Gabliks [53]. After this a number of other studies have been reported over ferrites mainly aimed at improving the selectivity and extending the activity maintenance for desired reactions [54,55]. Zinc-chromium ferrites and magnesium-chromium ferrites also have been developed for the oxidative dehydrogenation of butene to butadiene [56,57]. Further, the substitution of chromium for iron in both zinc and magnesium-ferrites increases the efficiency of the catalyst for the oxidative dehydrogenation and stabilizes the catalyst against the bulk reduction in a hydrocarbon atmosphere. The formation of butadiene over these catalysts is postulated to proceed via a redox cycle involving Fe^{3+} and Fe^{2+} , with the active hydrocarbon intermediate being an allylic C_4 radical complexed with an Fe^{3+} ion [58].

During the past 10 years, there has been considerable interest in developing processes for the synthesis of higher alcohols (C₂ and higher) from syn gas for use as additives to gasoline to reduce air pollution and increase the octane number. Catalysts for higher alcohol synthesis have evolved primarily from modified methanol-synthesis catalysts. The original methanol synthesis catalysts were based on a Zn/Cr spinel. A commercially available Zn/Cr spinel methanol-synthesis catalyst is Engelhard Zn-0312. Epling *et al.* [59] promoted this catalyst with potassium to achieve a high isobutanol production rate and a low hydrocarbon production rate. Interestingly, they observed that the addition of 3 or 5 % K decreases the hydrocarbon by-product formation rate, consequently increasing the selectivity to total alcohols.

The heterogeneous decomposition of hydrogen peroxide is a more convenient alternative to the electrolysis of water for the production and storage of oxygen. Some ferrospinels seem to be a potential alternative to the noble metal catalysts such as silver oxide and platinum black [60,61]. Cobalt ferrite, CoFe₂O₄, catalyses the decomposition of hydrogen peroxide to the same extent as noble metal catalysts. Several workers reported the catalytic properties of CoFe_{3-x}O₄, NiFe_{3-x}O₄ and CuFe_{3-x}O₄ (0 ≤ x ≤ 3) for H₂O₂ decomposition[62-64]. According to them the catalytic activity follows the order Co > Cu > Ni and that Co_{1.5}Fe_{1.5}O₄ is the most active one.

In addition to the above mentioned reactions lots of other reactions are also catalyzed by spinel type oxides. Hydrodesulphurization of petroleum crude with CoFe₂O₄ and NiFe₂O₄ [65] and oxidation of carbon monoxide with various inverse spinels are some examples.

1.3 SURFACE ELECTRON DONATING PROPERTIES

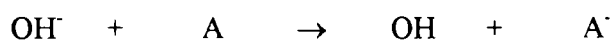
The utility of electron acceptor adsorption for the study of the electron donor properties of the surface has been well established. The electron donor strength of the metal oxide can be defined as the conversion power of an electron acceptor (EA) adsorbed on the surface into its anion radical. When an electron acceptor is adsorbed on a metal oxide, it has often been observed that electron transfer occurs from the metal oxide surface to the electron acceptor, resulting in the formation of the

corresponding anion radical on the metal oxide. Considerable attention has been paid to determine the strength and distribution of electron donor sites on the metal oxide surfaces using electron acceptors with different electron affinity values. Perhaps the first work of this type is the one reported by Folkhart *et al.* [67], who investigated the electron donor properties of an alumina surface by the adsorption of tetracyanoethylene (TCNE). Following this, similar studies on the metal oxides such as titania [68-70], magnesia [71,72], zinc oxide [73,74] and two component metal oxides [75-77] have also been reported by several other workers.

If a strong electron acceptor is adsorbed on the metal oxide, its anion radical is formed at strong as well as weak donor sites present on the surface. On the otherhand if a weak electron acceptor is adsorbed, the formation of anion radical is expected only at the strong donor sites. Finally, in the case of a very weak electron acceptor adsorption, its anion radical will not be formed even at the strongest donor sites. This means that, by comparing the limiting amount of EAs adsorbed on the catalyst surface and the electron affinity values of the respective EAs used, it is possible to assign valuable information regarding the strength and distribution of the donor sites on the surface.

7,7,8,8-tetracyanoquinodimethane (TCNQ), 2,5-dichloro-p-benzoquinone (DCQ), p-dinitrobenzene (PDNB) and m-dinitrobenzene (MDNB) with electron affinity values 2.84, 2.30, 1.77 and 1.26 eV respectively were widely employed as EAs to probe the donor sites on the surface [78]. The adsorption of EAs with electron affinity from 1.26 to 2.84 eV on the surface of alumina has been studied by measuring the adsorption isotherms, ESR and electronic spectra by Meguro *et al.* [79]. They observed that, the radical concentrations formed were directly related to the electron affinity values of the respective EAs used. In other words, radical concentrations decreased with decreasing electron affinity of EAs from 2.84 to 1.77 eV. Two possible electron sources existing on the alumina surface are electron trapped at intrinsic defects and the hydroxyl ions. Folkhart *et al.* [67] have suggested that the electron donor defect on the surface of alumina was created at activation temperatures of above 500 °C. On the otherhand, the hydroxyl groups present on the surface of

alumina have comparatively small ionization potential (≈ 2.6 eV in the gas phase) [80]. Therefore, the possibility of its participation in oxidation-reduction processes of the type:

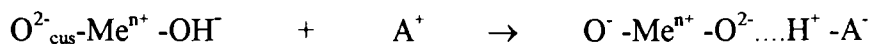


where A is an EA, can be included. It has been reported that the electron donor site on the alumina surface might be associated with the presence of unsolvated hydroxyl ions on the surface.

In a similar way, using TCNQ as the probe molecule, it was understood that the OH^- ions act as a plausible cause of the electron donor property of $\text{ZrO}_2\text{-TiO}_2$ system [81]. The electron donor sites of titania, one of the parent oxides in the zirconia-titania system, have been associated with the surface hydroxide ions and Ti^{3+} ions [82]. Infrared spectroscopy of zirconia has shown that the surface of zirconia contains hydroxide ions [83]. Therefore the electron transfer adsorption of TCNQ on the zirconia-titania surface may result from surface hydroxide ions and Ti^{3+} ions.

Adsorption of tetrachloro-p-benzoquinone (chloranil) from basic and acidic solvents on metal oxides such as alumina and titania was carried out [84]. The amount of chloranil adsorbed was successfully correlated with the acid base interaction at the interface.

The electron donor properties of several oxides like CaO, MgO, ZnO, Al_2O_3 , silica-alumina were investigated using ESR spectral studies of adsorbed nitrobenzene. A correlation between electron donor sites (EDS) and Lewis base strength was established. The active sites were described as an acid-base pair, and the interaction of EDS to an acceptor is as follows:



Me^{n+} is the surface cation and O^{2-} is a surface oxygen ion in a low coordinate state. The radical is bound to the surface by static interaction [85].

The adsorption of EA from its organic solvent changes the zeta potentials of the metal oxide. Esumi and co-workers [86] observed that the zeta potential of alumina was dependent on two factors, when TCNQ was used as the EA; (1) the concentration of TCNQ (2) acidity/basicity of the solvents. Zeta potential of alumina decreased with concentration of TCNQ, and the magnitude in the decrement of the zeta potential is of the order: acetonitrile > ethylacetate > 1-4 dioxane. The TCNQ anion radical is formed by the electron transfer from the alumina surface to the adsorbed TCNQ molecule. Furthermore, the adsorption of TCNQ depends on the interaction between the TCNQ and organic solvent. This interaction is best explained by applying the Drago equation [87]:

$$\Delta H^{AB} = E_A E_B + C_A C_B$$

where ΔH^{AB} is acid-base enthalpy, and the two constants (E,C) are given for the acid (A) and for the base (B). In the present case, it was observed that $-\Delta H^{AB}$ between TCNQ and the organic liquids increased in the order 1-4 dioxane ($-5.2 \text{ kcal mol}^{-1}$) > ethyl acetate ($-4.3 \text{ Kcal mol}^{-1}$) > acetonitrile ($-3.5 \text{ kcal mol}^{-1}$). This result indicates that the adsorption of TCNQ on alumina is depressed with increasing acid-base interaction between TCNQ and the organic liquid.

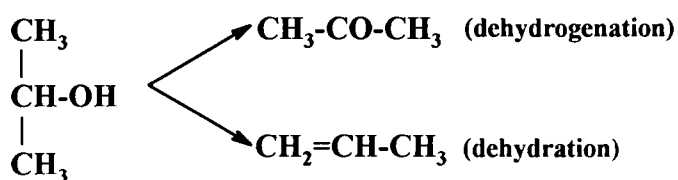
The electron donor properties of rare earth oxides such as Pr_6O_{11} [88], CeO_2 [89], Sm_2O_3 [90], La_2O_3 [91] and Nd_2O_3 [92,93] and their mixed oxides with alumina were investigated as a function of composition and activation temperature. The extent of electron transfer was characterised by magnetic measurement.

1.4 ALCOHOL DECOMPOSITION REACTION-A PROBE REACTION FOR SURFACE ACIDITY/BASICITY DETERMINATION:

The catalytic decomposition of alcohols on oxide has been extensively performed to study the catalytic properties of oxide surfaces. The two basic modes of

reactions are (a) dehydrogenation to form an aldehyde (in the case of primary alcohols) or a ketone and hydrogen (in the case of secondary alcohols), and (b) dehydration to form an olefin and water. At high temperatures decomposition of an alcohol may occur leading to the cleavage of carbon-carbon bonds and the resultant formation of parafins, CO, CO₂ etc. At near ambient temperature ether is the major reaction product. Dehydration and dehydrogenation of isopropyl alcohol has gained a prominent place as a model reaction for studying the principles of catalyst selection [94]. The selectivity effects on dehydration and dehydrogenation give deep insight into the nature of the catalyst and aid in catalyst selection. This type of multipathway (dehydration and dehydrogenation) conversion of alcohols has frequently been employed as a diagnostic or model reaction for studying the catalytic properties of metal oxides. Several authors have suggested correlations between the observed activity/selectivity behaviour of oxides and their chemical and physical properties [94,95].

The two main paths of decomposition of isopropanol are:



According to the generally accepted concept, dehydration is an acidic reaction and, therefore, should be catalysed by solid and liquid protic and aprotic acid; and dehydrogenation activity is due to the combined effect of both acidic and basic sites on the system. This means that the dehydration activity gives the direct measure of the acidity of the system, whereas the ratio of the dehydrogenation activity to the dehydration activity gives the basicity of the system [96,97]. However, another conclusion has been drawn by Krylov [94], based on the electronic theory of catalysis. According to this concept, the rate limiting step for dehydrogenation is the migration of vacancies while for dehydration it is the migration of free electrons in the catalyst. Consequently dehydrogenation is expected to be catalysed by p-type semiconductors and dehydration by n-type semiconductors.

It is possible to classify the dehydration mechanism in three routes as shown below [98] (Fig. 1.4.1):

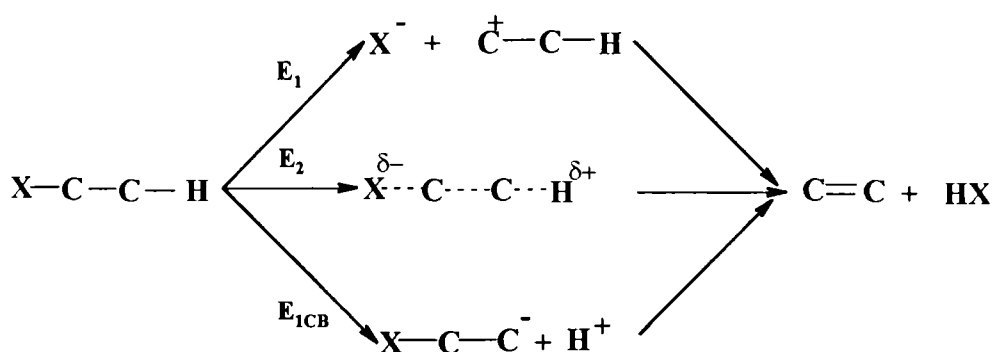


Fig. 1.4.1. Three routes of dehydration reaction.

In E1 mechanism rupture of C-OH bond occurs with carbonium ion formation, the latter being capable of positional and geometrical isomerization. Hence all possible alkenes are formed. E2 reaction is concerted, single step with no intermediate formation. Saytzeff alkene orientation occurs from 2-ols, i.e there are more alk-2-enes than alk-1-enes. In E1_{CB} route C-H bond rupture occurs via the most acidic proton. Hoffmann orientation of alkenes occurs, i.e alk-1-enes are formed preferentially from 2-ols and there is a tendency for dehydrogenation to occur.

The nature of alcohol is very important. The order of ease of dehydration is tertiary > secondary > primary and tertiary alcohols tend to react via an E1 mechanism because of the relative stability of tertiary carbonium ion.

Bakshi and Gavalas [99] investigated a number of aluminas, silica aluminas, and clays for ethanol dehydration. According to them, for ethylene formation, the best group associated is an acid and a weak base site and for ether formation two acid-base site pairs were required, allowing a dissociatively adsorbed alcohol and a surface alkoxide to interact. At temperatures below 300 °C most oxides favour ether production and only at higher temperatures does dehydration predominate.

Most research seeking to relate dehydration/dehydrogenation activity and surface acid base properties has involved mixed rather than single oxides as the former provide a means of varying acidity through composition changes. Iron oxide possesses inherent dehydrogenation properties but it was reported that in the presence of Al_2O_3 these properties are lost and it becomes a dehydrogenation catalyst [100]. Decomposition of isopropyl alcohol was carried out on the solid solution system $\text{MgAl}_{2-x}\text{Fe}_x\text{O}_4$ ($x = 0$ to 2) by Narasimhan *et al.* [96]. The system exhibited both dehydrogenation and dehydration activities. It was predicted that Fe^{3+} sites act as the active site for the adsorption of alcohol while Fe^{3+} site may be reduced to Fe^{2+} state during adsorption and subsequent reaction. However, it regains the Fe^{3+} state by diffusing the electron to an adjacent Fe^{3+} ion. In a similar way $\text{Ga}_{1-x}\text{Fe}_x\text{CuMnO}_4$ spinel system has been studied for the decomposition of 1-octanol by Dube *et al.* [101]. They observed that increase in the percentage of Fe^{3+} ions at the A site increased the octyl alcohol decomposition rate. According to them, when Fe^{3+} replaces Ga^{3+} ions the number of active centres for the adsorption of alcohol molecule increase due to the hopping of A site ion between $+2$ and $+3$ states. Decomposition of cyclohexanol has been carried out by Joshi *et al.* over $\text{Mg}_{1-x}\text{Zn}_x\text{Al}_2\text{O}_4$ and good correlation has been established between surface acidity and catalytic behaviour [102].

1.5 DEHYDROGENATION OF ETHYL BENZENE

Styrene is manufactured industrially by the dehydrogenation of ethyl benzene in the vapour phase at 850-950 K, just below the region where thermal cracking becomes insignificant. This is an endothermic reaction effected by an equilibrium which favours the products as the temperature is increased and the pressure reduced [103]. A typical catalyst for the production on a commercial basis is bismuth-molybdenum catalyst [104]. Mn, Co, Ni and Ni-W oxides supported on Al_2O_3 [105] and Mg-Mo and MgMo-Mo oxide catalysts [106,107] have also been examined, but only insufficient conversion and selectivity.

Iron based systems are widely employed as catalysts for this reaction. The K-promoted iron oxide catalyst exhibits higher activity compared to all other type of catalysts. Several studies have been carried out for the identification of the active sites

on the K-promoted iron oxide surface. Several models have been proposed, all pointing to the importance of Fe^{3+} ions in the dehydrogenation process. The catalyst activity and selectivity were found to be dependent on the surface concentration of Fe^{3+} ions and K^+ ions. Potassium suppresses the extent of carbonaceous deposits on the surface. Spinel oxides, having cation distribution at two crystallographic environments are reported to have more activity for the dehydrogenation of hydrocarbons and alcohols [108,109].

Studies on the dehydrogenation of ethyl benzene over simple spinel oxide has revealed that the activity of the spinels is significantly varied with respect to cations at octahedral sites. In the present work, the activity of ferrite systems such as $\text{Zn}_{1-x}\text{Co}_x\text{Fe}_2\text{O}_4$, $\text{Zn}_{1-x}\text{Ni}_x\text{Fe}_2\text{O}_4$ and $\text{Co}_{1-x}\text{Ni}_x\text{Fe}_2\text{O}_4$ were evaluated, and, hence, the influence of parameters such as metal concentration and their distributions among tetrahedral and octahedral sublattice have been discussed. The screening of the catalysts was carried out with a continuous flow vapor phase reactor.

1.6. Alkylation of Aniline and Phenol:

Alkylation of aniline and phenol are industrially important reactions owing to the numerous uses of the alkylated products. The most synthetically valuable alkyl anilines are N-methylaniline, N,N-dimethylaniline, toluidines and xylydines. Alkylation of phenol gives a wide variety of products; the most important among them are cresols and xylenols. Detailed discussions of each type of reactions are made in chapter IV and chapter V

1.7 Objectives of the present work:

Conventionally ferrites are prepared by solid solution high temperature methods. These methods are associated with some inherent drawbacks such as chemical inhomogeneity, low surface area and aggregate and large particles. Recently there have been reports dealing with the preparation of ferrites via co-precipitation route. The most attractive feature of these methods is the exclusive formation of spinel phase at low temperature leading to materials having sufficiently high surface area. Such materials are also seemed to be chemically homogeneous and very fine in

nature. So in this work we prepared some ferrospinels containing Zn, Co and Ni by adopting a soft chemical route. The three series of ferrites studied in the present case involve $Zn_xCo_{1-x}Fe_2O_4$, $Zn_{1-x}Ni_xFe_2O_4$ and $Co_{1-x}Ni_xFe_2O_4$; where 'x' varies as 0,0.2,0.5,0.8 and 1. In the first two series the spinel changes from inverse to normal as 'x' increases from 0 to 1; whereas in the last series of compounds the cation configuration remains unaltered in the Tet sites and only the Co-Ni ratio in the Oct. sites isomorphically varies. In both cases the acido-basic and redox properties of the systems vary with the 'x' value. The present work is carried out with an objective to evaluate the variation of surface electron properties and catalytic activities of the systems as a function of composition.

The main objectives of the present work can be summarised as follows:

⇒ To prepare ferrospinels containing Zn, Co and Ni by low temperature method and to characterize these materials by adopting various physico-chemical techniques.

⇒ To evaluate the nature of surface basicity, using electron acceptors having different electron affinity values. By comparing the limiting concentrations and electron affinity values of the respective electron acceptors adsorbed, valuable information can be obtained regarding the strength and distribution of electron donor sites.

⇒ Alcohol decomposition reaction can be used for predicting the nature of the surface active sites. Dehydration and dehydrogenation activities can be correlated with acidity and basicity. So another objective of the work was to perform such experiments and to correlate acid base properties with composition in different ferrite series.

⇒ To understand the redox property of the systems by carrying out dehydrogenation of ethyl benzene.

⇒ An important objective of the present work was to evaluate the catalytic activity of the systems for aniline alkylation using methanol as the alkylating agent and to

optimize the process parameters to get the synthetically valuable mono N-methyl aniline selectively and in better yield.

⇒ To understand the mechanism and kinetics of the above reaction and to compare the catalytic activity of the present systems with some of the earlier reported systems like alumina and γ -zeolite.

⇒ To evaluate the catalytic activity of the systems for phenol alkylation using methanol as the alkylating agent and to optimize the process parameters to achieve maximum selectivity and yield for the industrially valuable ortho derivatives viz. o-Cresol and 2,6 Xylenol.

⇒ To understand the plausible mechanism of the above reaction.

⇒ To try the choice of a less expensive alkylating agent dimethyl carbonate for the alkylation of both aniline and phenol and, hence, to highlight the merits and demerits over the alkylation experiments using methanol as the alkylating agent.

REFERENCES:

- [1] J.A. Schwarz; Chem. Rev., 95 (1995) 477.
- [2] O.Legv. Krylov; in Catalysis by Non-metals- Rules for Catalyst Selection, Academic Press, New York.
- [3] M.W. Tamele, Discussions Faraday Soc. 8 (1950) 270.
- [4] O. Johnson, J. Phy. Chem., 59 (1955) 827.
- [5] H. Uchida and H. Imami, Schokhai (Tokyo) 3, No.2 (1961) 202.
- [6] H. Pines and W.O. Haag, J. Am. Chem. Soc., 82 (1960) 2471.
- [7] S.E. Tung and E. Meininch, J. Catal., 3 (1964) 229.
- [8] Y. Izumi and T. Shiba, Bull. Chem. Soc. Jpn, 37 (1964) 1797.
- [9] H. Pines, J.A. Verseley, V.N. Ipatieff, J. Am. Chem. Soc. 77 (1961) 6314.
- [10] H. Hattori, Chem. Rev., 95 (1995) 538.
- [11] H. Hattori; N. Yoshii; K. Tanabe, Proceedings of the International Congress of Catalysis, Miami Beach, FI, 233 (1972).
- [12] T. Yashima, K. Sato, T. Hayasaka, N. Hara, J. Catal. 26 (1972) 303.
- [13] C. Marcilly; Rev. Inst. Fr. Pet., 39, (1984) 189.
- [14] P. Courty, C. Macilly; in Preparation of Catalysts.I, B. Delmon, P.A. Jacobs and G. Poncelet (Edn); Stud. Surf. Sci. Catal., 1 (1976) 119.
- [15] K.R. Barnard, K. Foger, T.W. Turney and R.D. Williams; J. Catal., 125 (1990) 265.
- [16]. J. A. Swwarz, C. Contescu and A. Contescu; Chem. Rev. 95 (1995) 484.
- [17] L. Hench and J.K. West; Chem. Rev., 90, 33 (1990).
- [18] J. A. Swwarz, C. Contescu and A. Contescu; Chem. Rev. 95 (1995) 484.
- [19] C. Marcilly, P. Chourty and B. Delmon; J. Amer. Cerm. Soc., 53 (1970) 56.
- [20] A.K. Cheetand and P. Day; Solid State Chemistry Techniques, Oxford University Press, 1987.
- [21] K. Tanabe, M. Misono, Y. Ono and H. Hattori; Stud. In Surf. Sci. And Catalysis, Vol. 51, New Solid Acids and Bases. Their Catalytic Properties, 1989.
- [22] Pratibha, L. Gai-boyes; Catal. Rev. Sci. And Eng., 34 (1992)1-54.

- [23] F.C. Romeijn; Philips Research Reports; 18 (1953) 304.
- [24] E.J.W. Verwey and E.L. Heilmann; J. Chem. Phys., 15 (1947) 174.
- [25] G. Blasse; Philips Research Rep. Supplement, 3 (1964) 40.
- [26] T.F.W. Barth and E. Posenjak; Zs. Kristallographie, 84 (1952) 325.
- [27] R.K. Datta and K. Roy, Nature 191 (1961) 169.
- [28] S. Hafner and F. Laves, Z. Krist. 115 (1961) 321.
- [29] E.W. Gorter; Philips Res. Rept., 9 (1954) 302.
- [30] J. Smith; Magnetic Properties of Materials, McGraw-Hill, New York, p.20 (1971).
- [31] Ferrite Materials Science and Technology; Edited by B. Viswanathan and V.R.K Murthy, Springer-Verlag and Narosha Publishing House, Page No. 5.
- [32] F. De Boer, J.H. van Santen and E.J.H Verwey, J. Chem. Phys. 16 (1948) 1091.
- [33] F. De Boer, J.H. van Santen and E.J.H Verwey, J. Chem. Phys. J. Chem. Phys. 18 (1950) 1932.
- [34] E.W. Gorter, Philips. Res. Repts. 9 (1954) 295-320.
- [35] G. Blasse; Philips Res. Rept. Supplement, 3 (1964) 40.
- [36] B. Viswanathan; in: Ferrite materials-Science and Technology, Edtrs. B. Viswanathan and V.R.K. Murthy, Narosha Publishing House, p.8 (1990).
- [37] J. Sobhanadri and R. Raman in 'Ferrite Materials Science and Technology'; Edited by B. Viswanathan and V.R.K Murthy, Springer-Verlag and Narosha Publishing House, Page No. 76.
- [38] O.S. Josyulu and J. Sobhanadri, Phys. Stat. Sol. (A), 59 (1980) 323.
- [39] R. Raman, Ph.D Thesis, Indian Institute of Technology, Madras, India (1989).
- [40] G. Srinivasan and C.M. Srivastava, Phy. Stat. Sol. (B), 103 (1981) 665.
- [41] J.P. Beaufils and Y. Barbaux, J. Appl. Cryst., 15 (1982) 301.
- [42] J.P. Jacobs, A. Maltha, J.G.H. Reintjes, J. Drimal, V. Ponec and H.H. Brongersma, J. Catal. 147 (1994).
- [43] J. Ziolkowski and Y. Barbaun, J. Mol. Catal., 67 (1991) 199.
- [44] C.S. Narasimhan and C.S. Swamy, Appl. Catal., 2 (1982) 315.
- [45] S.H. Oh and R.M. Sinkevitch. J. Catal. 142 (1993) 254.

- [46] T. Takada, S.Kasahara, K. Omata and M. Yamada, *Nippon Kagaku Kaishi* (1994) 793.
- [47] Y. Barbaux, L.S. Coustuner, J.P. Bonnelle, *J. Chem. Res.*, (1994) 218.
- [48] T. Takada, S.Kasahara, K. Omata and M. Yamada, *Nippon Kagaku Kaishi* (1994) 793
- [49] K. Omata, T. Takada, s. Kasahara, M. Yamada, *Appl. Catal. A. General* 146 (1996) 253.
- [50] A.A. Awe, G. Miliades and J.C. Vickerman; *J. Catal.* 62 (1980) 202-210.
- [51] S. Sato, M. Iijima, T. Nakayama, T. Sode Sewa and F. Nozaki; *J. Catal.* 169(1997)447.
- [52] W. Ronald Cares and J.W. High Tower; *J. Catal.* 23 (1971) 193.
- [53] I. Bajars, J.L Croce and M. Gabliks; U.S patent 3, 284, 536 issued to Petro-Tex Chemical Corporation, Nov. 8, 1966.
- [54] F.E. Massoth and D.A Scarpillo; *J. Catal.* 21 (1971) 294.
- [55] W.R. Cares and J.W. Hightower. *J. Catal.* 23 (1971) 193.
- [56] W.L Kehl and R.J. Rennard; U.S. Patent 3,450,788 June 17, 1969.
- [57]. W.L Kehl and R.J. Rennard; U.S. Patent 3,450,787 June 17, 1969.
- [58] R.J. Rennard and W.C. Kehl; *J. Catal.* 21 (1971) 282-293.
- [59] W.S. Epling, G.B Hoflund, W.M. Hartand D.M. Minahan; *J. Catal.*, 169 (1997) 438-446.
- [60] H.M Cota, J.Katan, M.Chin and F.J. Schoenweis; *Nature, London*, 203 (1964) 1281.
- [61] S.K. Senguptha and P.Lehiri; *Indian Journal of Technology*. 30, 1992
- [62] J.R. Goldstein and A.C.C. Tsemg; *J. Catal.* 32 (1974) 452.
- [63] A.I. Onuchukwa ; *J. Chem. Soc. Faraday. Trans.I*, 80 (1984) 1447.
- [64] A.I. Onuchukwa and A.B. Zuru; *Mat. Chem. Phys.* 15 (1986) 131
- [65] P.N. Rylader. Jr., and W.J. Zimmerschied., U.S. Pat. 2, 805 (1957) 187.
- [66] G.M. Schwab, E. Roth, C.H. Grinteoz and N. Mararokis, in R. Gomer and C.S. Smith (edn), *Structural and properties of solid surfaces*, University of Chickago press, Chickago, IL, 1953.
- [67] B.D. Folkhart, I.R. Leith and R.C. Pink; *Trans. Faraday Soc.* 65 (1969) 542.

- [68] K. Esumi and K. Meguro; *Shikizai Kyokaiishi*, 48 (1975) 544.
- [69] K. Esumi and K. Meguro; *Bull. Chem. Soc. Jpn.*, 55 (1982) 1647-1648.
- [70] R.S. Davidson and R.M. Slater; *J.C.S. Faraday I*, 72 (1976) 2416.
- [71] M. Che, C. Naccache and B. Imlik; *J. Catal.*, 24 (1972) 328.
- [72] A.J. Tech and R.L. Nelson; *Trans. Faraday Soc.*, 63 (1967) 2254.
- [73] H. Hosaka, T. Fujiwara and K. Meguro; *Bull. Chem. Soc. Japan*, 44 (1971) 2616.
- [75] K. Esumi, H. Shimada and K. Meguro; *Bull. Chem. Soc. Japan*, 50 (1977) 2795.
- [76] B.D. Folkhart, Kong Yong Liew and R.C. Pink; *J. Catal.*, 32 (1974) 20.
- [77] H. Hosaka, N. Kawashima and K. Meguro; *Bull. Chem. Soc. Japan*, 45 (1972) 3371.
- [78] K. Esumi and K. Meguro; *Journal of Colloid and Interface Science*, 66(1), (1978).
- [79] K. Meguro and K. Esumi; *Journal of Colloid and Interface Science*, 59(1) (1977) 93.
- [80] J.B. Perri; *J. Phy. Chem.*, 69 (1965).
- [81] K. Esumi, H. Shimada and K. Meguro; *Bull. Chem. Soc. Japan*, 50(10) (1977) 2795.
- [82] M. Che, C. Naccache and B. Imclik; *J. Catal.* 24 (1972) 328.
- [83] D.A. Agron, E.I. Fuller and H.F. Hobiari; *J. Colloid Interface Sci.*, 52 (1975) 533
- [84] K. Esumi, K. Miyata, F. Waki and K. Meguro; *Bull. Chem. Soc. Jpn.*, 59, (1986) 3363-3366.
- [85] D. Gordishi and V. Indovino; *Bull Chem. Soc. Jpn.*, 49 (1976) 2341.
- [86] K. Esumi, K. Magara and K. Meguro; *Journal of Colloid and Interface Science*, 141 (2) (1991) 578.
- [87] R.S. Drago, L.B. Parr and C.S. Chambelain; *J. Am. Chem. Soc.*, 99 (1977) 3203.
- [88] S. Sugunan, G.D. Devika Rani and P.A. Unnikrishnan; *J. Mater. Sci. Technol.*, 10 (1994) 425.

- [89] S. Sugunan and J.M. Jalaja; *Collect. Czech. Chem. Commun.*, 59 (1994) 2605
- [90] S. Sugunan and J.J. Malayan; *J. Adhesion Sci. Technol.*, 9(1) (1995) 73.
- [91] S. Sugunan and K.B. Sherly; *Indian Journal of Chemistry*, 32(A) (1993) 689.
- [92] S. Sugunan and G.D. Devika Rani; *Indian Journal of Chemistry*, 32(A) (1993) 993.
- [93] S. Sugunan and G.D. Devika Rani; *Journal of Material Science*, 29 (1993) 4811.
- [94] O.V. Krylov; "Catalysis by Nonmetals", Academic press, New York.
- [95] M.P. Rosynek, R.J. Koprowski and G.N. Dellisante; *J. Catal.*, 122 (1990) 80.
- [96] C.S. Narasimhan and C.S. Swamy; *Applied Catal.*, 2 (1982) 315-328.
- [97] M.P. Rosynek, R.J. Koprowski and G.N. Dellisante; *J. Catal.*, 122 (1990) 80-94.
- [98] H. Vinek, H. Noller, N. Ebel and K. Schwarz; *J. Chem. Soc., Faraday Trans.*, 73 (1977) 734.
- [99] K.R. Bakshi and G.R. Gavalas; *J. Catal.*, 38 (1975) 312.
- [100] R. Venkatachalam and J.C. Kuriacose; *proc. Natl. Acad. Sci., India, Sect. A1* (1977) 245.
- [101] G.R. Dube and V.S. Darshane; *J. Mol. Catal.*, 79 (1993) 285-296 .
- [102] M. V. Joshi, S.G. Oak and V.S. Darshane; *Catalysis: Modern Trends*, Edited by H.M. Gupta and D.K. Chakrabarty, Narosha Publishing House, 1995.
- [103] W.W. Kaeding; *Catal. Rev.*, 8 (1974) 307.
- [104] Y. Murakami, K. Iwayama, H. Uchida, T. Hattori and T. Tagawa; *Appl. Catal.*, 2 (1992) 67.
- [105] J.C. Conesa, A. Cortes, J. Marti, J.C. Seoane and J. Soria., *J. Catal.*, 58 (1979) 34.
- [106] J. Houza, B. Jezowska-Trzebatowska and W. Ognowski; *J. Mol. Catal.*, 4 (1978) 271.
- [107] W. Oganowski, J. Hanuza, B. Jezowska-Trzebatowska and J. Wrzyszc; *J. Catal.*, 39 (1975) 161.
- [108] H.H. Kung and M.C. Kung, *J. Phys. Chem*; 84 (1980) 383.
- [109] K. Balasubramanian and V. Krishnasamy; *Indian J. Chem.*, 21 A (1982) 813.

CHAPTER II
EXPERIMENTAL

2.1 CATALYST PREPARATION

Three series of substituted ferrites of the general formula $A^{II}_{1-x}B^{III}_xFe_2O_4$ (A and B are metal cations like Zn, Co or Ni, and $x = 0, 0.2, 0.5, 0.8$ and 1.0) were prepared for the present work. Their compositions and cation distributions are summarized in the following table:

x	Composition	Cation at	
		Tetrahedral site	Octahedral site
	<u>$Zn_{1-x}Co_xFe_2O_4$</u>		
0	$ZnFe_2O_4$	Zn^{2+}	Fe_2^{3+}
0.2	$Zn_{0.8}Co_{0.2}Fe_2O_4$	$Zn_{0.8}^{2+}Fe_{0.2}^{3+}$	$Fe_{1.8}^{3+}Co_{0.2}^{2+}$
0.5	$Zn_{0.5}Co_{0.5}Fe_2O_4$	$Zn_{0.5}^{2+}Fe_{0.5}^{3+}$	$Fe_{1.5}^{3+}Co_{0.5}^{2+}$
0.8	$Zn_{0.2}Co_{0.8}Fe_2O_4$	$Zn_{0.2}^{2+}Fe_{0.8}^{3+}$	$Fe_{1.2}^{3+}Co_{0.8}^{2+}$
1.0	$CoFe_2O_4$	Fe^{3+}	$Fe^{3+}Co^{2+}$
	<u>$Zn_{1-x}Ni_xFe_2O_4$</u>		
0	$ZnFe_2O_4$	Zn^{2+}	Fe_2^{3+}
0.2	$Zn_{0.8}Ni_{0.2}Fe_2O_4$	$Zn_{0.8}^{2+}Fe_{0.2}^{3+}$	$Fe_{1.8}^{3+}Ni_{0.2}^{2+}$
0.5	$Zn_{0.5}Ni_{0.5}Fe_2O_4$	$Zn_{0.5}^{2+}Fe_{0.5}^{3+}$	$Fe_{1.5}^{3+}Ni_{0.5}^{2+}$
0.8	$Zn_{0.2}Ni_{0.8}Fe_2O_4$	$Zn_{0.2}^{2+}Fe_{0.8}^{3+}$	$Fe_{1.2}^{3+}Ni_{0.8}^{2+}$
1.0	$NiFe_2O_4$	Fe^{3+}	$Fe^{3+}Ni^{2+}$
	<u>$Co_{1-x}Ni_xFe_2O_4$</u>		
0	$CoFe_2O_4$	Fe^{3+}	$Fe^{3+}Co^{2+}$
0.2	$Co_{0.8}Ni_{0.2}Fe_2O_4$	Fe^{3+}	$Fe^{3+}Ni_{0.2}^{2+}Co_{0.8}^{2+}$
0.5	$Co_{0.5}Ni_{0.5}Fe_2O_4$	Fe^{3+}	$Fe^{3+}Ni_{0.5}^{2+}Co_{0.5}^{2+}$
0.8	$Co_{0.2}Ni_{0.8}Fe_2O_4$	Fe^{3+}	$Fe^{3+}Ni_{0.8}^{2+}Co_{0.2}^{2+}$
1.0	$NiFe_2O_4$	Fe^{3+}	$Fe^{3+}Ni^{2+}$

Table 2.1. Catalyst compositions and cation distributions of ferrosinels containing Zn, Co and Ni.

For the synthesis of all compositions of ferrosinels the soft chemical method reported by Datte *et al.* [1] was adopted. AR grade chemicals supplied by Qualigens Chemicals were used as such, without any further purification. Metals were precipitated as their hydroxides from their nitrate solutions using sodium hydroxide as

the precipitating alkali. Solutions of metal nitrates and sodium hydroxide of the following concentrations (molar, M) were prepared in distilled water.

1. Ferric nitrate	2.6 M
2. Cobalt nitrate	3.4 M
3. Nickel nitrate	3.4 M
4. Zinc nitrate	3.4 M
5. Sodium hydroxide	5.3 M

Solutions of the metal nitrates in the required stoichiometric ratios were mixed, and was rapidly added to sodium hydroxide solution with intermittent stirring. Temperature of the slurry was reached upto 50 °C due to the exothermic nature of the precipitation reaction. pH of the final slurry was carefully adjusted between 10 and 11, except for all zinc containing systems, where the pH was not exceeded 9. This was to prevent the dissolution of zinc as sodium zincate complex, which would alter the spinel composition. Aging of the precipitates was done for overnight, and were washed several times with distilled water to make the final precipitates free from both sodium hydroxide and nitrate ions. The precipitates were filtered and dried in an air oven at 80 °C for about 64 hours and were calcined at 300 °C for 12 hours to achieve complete spinel phase transformation. The dried materials were powdered and sieved to get the mesh size below 100 μ .

Unlike the spinels prepared by the conventional high temperature solid solution methods which provide non-homogeneous, aggregate, large particles with very low surface area, the spinels prepared by low temperature co-precipitation route provides chemically homogeneous, fine particles with high surface areas.

2.2. CATALYST CHARACTERIZATION

The prepared samples were characterized by adopting various physico-chemical methods such as X-ray diffraction analysis, infrared spectroscopy, surface area determination, pore volume measurements, surface electron micrograms, Mössbauer

spectroscopy, electron acceptor adsorption studies and alcohol decomposition reactions. A brief discussion of the various methods adopted is presented below.

2.2.1 X-Ray Diffraction Analysis:

X-Ray Diffraction (XRD) is a powerful tool for the qualitative and quantitative analysis of solid phases and can provide valuable information about the heterogeneous catalyst phase. The XRD method involves the interaction between the incident X-rays monochromatized (like CuK α or MoK α source) with the periodic structures of polycrystalline material. A fixed wave length is chosen for the incident radiation and Bragg peaks are measured by observing the intensity of the scattered radiation as a function of scattering angle 2θ . The interplanar distances or d-spacing are calculated from the values of the peaks observed from the Bragg equation,

$$n\lambda = 2d \sin \theta,$$

where, 'n' is order of reflection and the values are 1,2,3 etc. [2].

XRD allows a tridimensional characterization of a complete surface. It allows to characterize different phases and eventually their modification during catalytic reaction. Such studies are particularly important for mixed oxides used in mild oxidation reactions since lattice oxygen atoms are often involved in the reaction. XRD can clearly trace the changes in crystallographic arrangements occurring, particularly at the surface of the system.

2.2.2 Diffuse Reflectance Infrared Spectroscopy:

Infrared spectroscopy is an extremely versatile tool which may be used to study the characteristics of the surface of a catalyst. Various types of information, on the nature of the active sites of catalyst, the structural transformations in catalysts, the identification of surface groups, the surface acidic properties of catalysts and the identification of intermediates in surface transformations, can be obtained by the application of IR spectroscopy.

Better results can be achieved by using a Fourier Transform Infrared (FTIR) spectrophotometer. Here detector is used to simultaneously record the entire frequency range of electromagnetic waves transmitted through the sample. The output of a detector is fed a computer which reconstructs the spectrum using Fourier Transformation. Latest advance in this series is the Diffuse Reflectance Infrared Fourier Transform (DRIFT) instruments. Diffuse reflectance was originally developed for the UV-Visible range for analysis of highly scattering samples. The enormously increased throughput provided by FTIR instruments has led to its routine use in the infrared also. The theory of diffuse reflectance was developed by Kubelka and Munk [3] and extended by Kortun *et al.* [4] According to this theory,

$$f(R_{\infty}) = (1-R_{\infty})^2/2R_{\infty} = K/S$$

where R_{∞} is the diffuse reflectance from an 'infinitely' thick sample, K is the extinction coefficient and S is a scattering coefficient. A diffuse reflectance spectrum of a dilute sample in a nonabsorbing matrix will resemble its absorption spectrum. It is obvious that in the case of highly scattering samples employed in heterogeneous catalysis, the technique of diffuse reflectance will be very useful. It is known that structure plays an important role in the catalytic activity of many heterogeneous systems. In many cases, the positions of the infrared bands are sensitive to the changes in the ratio of metal cations in the catalyst composition. Since, in spinels metal ions are distributed in two different environments, the spinel phase formation can be very well assigned by the appearance of two broad IR bands. The infrared spectra were recorded through a DR-IR (Shimadzu) in the range 400 cm^{-1} to 1000 cm^{-1} .

2.2.3 Surface area determination by BET method:

Brunauer, Emmett and Teller, in 1938, extended Langmuir's kinetic theory to multilayer adsorption. The effectiveness of the BET theory is that it enables an experimental determination of the number of molecules required to form a monolayer despite the fact that exactly one monolayer is never formed. The basic equation to find

out surface area is as follows:

$$\frac{P}{V_{ads}(P_o - P)} = \frac{1}{V_m C} + \frac{C - 1}{V_m C} \frac{P}{P_o}$$

where P = adsorption equilibrium pressure, P_o = saturated vapour pressure of the adsorbent, V_{ads} = volume at STP occupied by molecules adsorbed at pressure P , V_m = volume of adsorbate required for a monolayer coverage, C = constant related to heat of adsorption.

A plot of $\frac{P}{V_{ads}(P_o - P)}$ Vs $\frac{P}{P_o}$ will yield a straight line usually in the range $0.05 \leq P/P_o \leq 0.35$. The slope (s) and intercept (i) of the BET plot are $s = \frac{C - 1}{V_m C}$ and $i = \frac{1}{V_m C}$. Solving these equations permits the calculation of V_m . Then the specific surface area of the catalyst can be calculated as,

$$\text{Specific surface area, m}^2\text{g}^{-1}\text{ cat.} = \frac{V_m N_a}{22414 \times W_t} \times A_m$$

A_m = mean cross sectional area occupied by adsorbate molecule (16.2 \AA^2 for N_2), W_t = weight of the catalyst sample, N_a = Avagadro number, V_m = monolayer volume in ml at STP.

For surface area determinations the ideal adsorbent should exhibit BET C values sufficiently low to preclude localized adsorption. A very high or very low C value will create considerable error in calculating the effective adsorbate cross-sectional area. Nitrogen as an adsorbate exhibits the unusual property that on almost all surfaces its C value is sufficiently small to prevent localized adsorption and yet adequately large to prevent the adsorption layer from behaving as a two-dimensional gas [5].

2.2.4 Pore volume determination using mercury porosimetry:

Dubinin [6] has classified the pores on the catalyst surface according to their diameter as micropores ($<20 \text{ \AA}$), macropores ($>200 \text{ \AA}$) and intermediate pores (between 20 and 200 \AA). The pore size can be determined either from an adsorption

isotherm or by using a mercury porosimeter. The underlying principle of mercury porosimeter is to relate the force necessary to intrude a non wetting liquid, such as mercury, to the average radius of the pores which are filled. The number of these pores is related to the volume of mercury to fill pores of a certain average diameter. The relationship between the pressure, surface tension, contact angle and radius of curvature is given by,

$$\Delta P = -\frac{2\sigma\cos\theta}{r},$$

where, ΔP = pressure, σ = surface tension, r = radius of the pore, θ = contact angle.

Usually the working fluid is mercury, for which $\sigma = 480$ dynes / cm and $\theta = 140^\circ$. So the above equation becomes,

$$\Delta P = \frac{72,500}{r}$$

This equation allows to calculate the pressure that will be needed to force mercury into pores of radius 'r'. The apparatus consist of a calibrated piston pump, connected to a thermostated high pressure cell and a pressure gauge. The zero penetration volume is noted when the pressure just begins to rise. Usually these instruments are automated such that the volume and pressure signals drive an X-Y recorder or the data are collected on computer for post-run processing and manipulation.

2.2.5 Scanning electron microscope (SEM) and energy dispersive X-ray (EDX) analysis:

Electrons interact much more strongly with matter than do X-rays or neutrons and can thus be scattered appreciably by quite small atomic clusters. They can also be conveniently deflected and focused by electronic or magnetic fields so that magnified real space images can be formed. This property of electron beams is used in the Scanning Electron Microscope (SEM) to obtain an image of the region under analysis. In the SEM the electron optics act before the specimen is reached to convert the beam into a fine probe which can be as small as 100 Å in diameter at the specimen surface. This makes the technique suitable for producing very impressive, in-focus images to be

obtained from a highly irregular structures typical of catalyst specimens [7]. The technique is of great interest in catalysis particularly because of its high spacial resolution. However, a serious drawback is that, the result need not be really representative of the whole sample. This can be overcome by making any analysis at different location of the sample particles and for many catalyst particles. Metal ion compositions were determined using EDX analysis. Using this technique the bulk composition can be determined in the accuracy level of 95-98 %.

SEM analysis of the samples were done using Stereoscan 440: Cambridge, U.K scanning electron microscope. The sample was dusted on alumina and coated with a thin film of gold to prevent surface charging and to protect the material from thermal damage by electron beam. A uniform film thickness of about 0.1 mm was maintained for all the samples.

2.2.6. Mössbauer spectroscopy:

Mössbauer spectroscopy is a versatile technique to investigate the bulk and surface characteristics of catalyst systems. The phenomenon of recoil free emission or absorption of gamma rays from nuclei bound in a solid is called Mössbauer effect. The effect has been observed for a number of nuclei emitting low energy γ -rays and finds wide applications in solid state studies because of the fact that the line width of these transitions is comparable to the energy of hyperfine interactions. Due to the presence of surrounding electronic charges, the nuclear energy levels are perturbed and the scanning of these levels gives valuable information about the nature of bonding in solids. The main advantage of Mössbauer technique over the other commonly used techniques for probing the structural properties of catalysts is that Mössbauer spectroscopy is well suited for “in situ” study of crystalline and non-crystalline materials. Mössbauer isomer shift (IS) is a parameter by which the nature of different cationic oxidation states and the character of chemical binding in a catalyst may be monitored. Similarly quadrupole splitting data may be used to access the structural properties of catalysts and the distribution of electronic charge around the probe atoms.

The room-temperature Mössbauer spectra were obtained using a constant acceleration Mössbauer spectrometer with the ferrite powders pressed firmly between the two mylar foils of an adsorber holder.

2.2.7 Thermal analysis:

The term thermal analysis incorporates those techniques in which some physical parameters of the system are determined or recorded as a function of temperature. It is an important tool for determining the properties of many solid acid catalyst. Properties such as phase composition, hydration, purity, melting, decomposition etc. can be determined using thermogravimetry (TG) and differential thermal analysis (DTA).

Thermogravimetry is a technique whereby the weight of a sample can be followed over a period of time while its temperature being raised linearly. Recording analytical balances with provision for controlled heating of a sample are called thermobalances. In a thermogravimetric curve the horizontal portions point out the regions where there is no weight change, whereas the weight loss is indicated by the curved portions.

Differential thermal analysis is a technique by which phase transition or chemical reaction can be followed through observation of heat adsorbed or liberated. It is especially suited to studies of structural changes within a solid at elevated temperatures, where few other methods are available. Here, the temperature difference between a sample and an inert reference material is monitored while both are subjected to a linearly increasing environmental temperature. With a constant heating rate, any transition or thermally induced reaction in the sample will be recorded as a peak or dip in an otherwise straight line graph [8].

Thermal analysis of the dried samples were carried out using simultaneous TG & DTA instrument (SETARAM-TG-DTA-92) using finely powdered α -alumina as a reference material.

2.2.8 Determination of Surface Electron donor properties:

(a) Reagents used and purification methods:

The electron acceptors used in the study are:

7,7,8,8-tetracyanoquinodimethane (TCNQ)

2,3,5,6-tetrachloro-p-benzoquinone (chloranil) and

p-dinitrobenzene

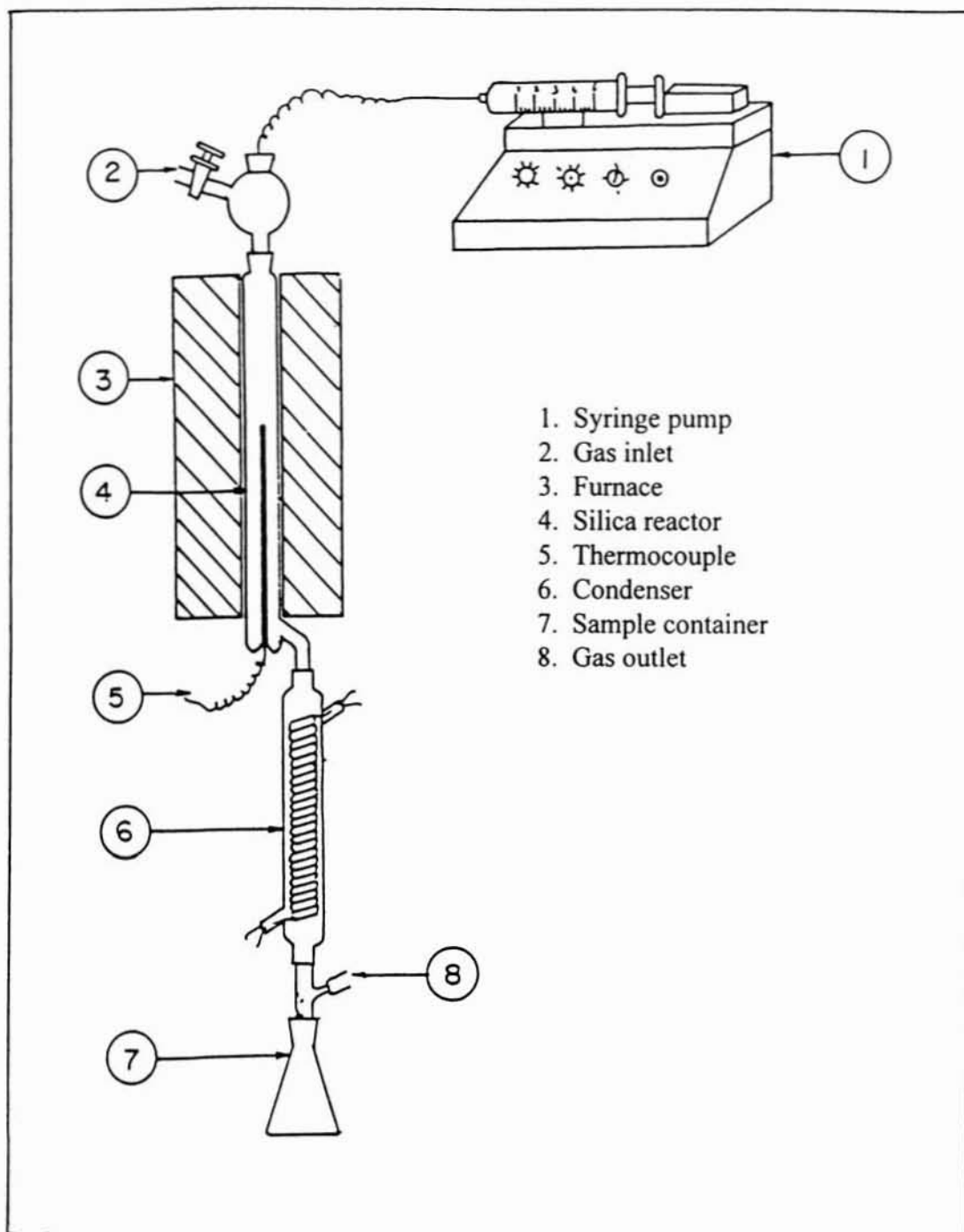
TCNQ was obtained from Merk-Schuchardt and was purified by repeated recrystallization from acetonitrile [9]. Chloranil was obtained from Sisco research laboratories Pvt. Ltd. was purified by recrystallization from benzene [10], and p-dinitrobenzene was purified by crystallization from chloroform [11]. Acetonitrile was used as the solvent. SQ grade acetonitrile obtained from Qualigens Fine chemicals was first dried by passing through a column filled with silica gel 60-120 mesh size activated at 110⁰C for 2 hours. It was then distilled with anhydrous phosphorous pentoxide and the fraction between 79-82⁰C was collected [12].

(b) Method adopted for adsorption studies:

The catalysts were activated at the particular temperatures for two hours prior to each experiment. Adsorption study was carried out over 0.5 gram catalyst placed in a cylindrical glass vessel fitted with a mercury sealed stirrer. Before sealing, the sample was outgassed at 10 torr for one hour. 10 ml of a solution of an electron acceptor in acetonitrile was then admitted to the catalyst. Stirring was continued for 4 hours in a mechanically driven stirrer at 28 ⁰C in a thermostated bath, and the oxide was collected by centrifuging the solution. The amount of electron acceptor adsorbed was determined from the difference in the concentration of electron acceptor in solution before and after adsorption, which was measured by means of a Shimadzu UV-VIS spectrophotometer (λ_{\max} of electron acceptors in solvent: 393.5 nm for TCNQ, 288 nm for chloranil and 262 nm for PDNB). The amount adsorbed was calculated from the difference in the absorbance before and after adsorption.

2.3. VAPOUR-PHASE REACTIONS

Vapour-phase experiments were performed at atmospheric pressure in a fixed-bed, vertical, down-flow, integral silica reactor placed inside a double-zone furnace (gèomècanique, France). Schematic diagram of a reactor setup is shown in Fig. 2.3.1. The catalysts were pressed, pelleted and sieved to obtain catalyst particles of size 10-20 mesh. About 3 g catalyst was charged each time in the centre of the reactor in such a way that the catalyst was sandwiched between the layers of inert porcelain beads. The upper portion of the reactor served as a vaporizer cum pre-heater. All heating and temperature measurements were carried out using 'Aplab' temperature controller and indicator instruments. A thermocouple was positioned at the centre of the catalyst bed to monitor the exact temperature of the catalyst bed. Activation of the catalyst consist of heating in a sufficient flow of dry air at 773 K for at least 6 hours before each run. The catalyst bed was cooled to the desired reaction temperature in presence of nitrogen. The liquid reactant mixture was fed by a syringe pump (SAGE Instruments, Model 352, USA). The products of the reaction were collected downstream from the reactor in a receiver connected through a cold water circulating condenser. Products were collected at various time intervals and analyzed by gas chromatography (Shimadzu, Model 15 A connected with FID and TCD). Identification of the products were done by using GC-MS and GC-FTIR.



1. Syringe pump
2. Gas inlet
3. Furnace
4. Silica reactor
5. Thermocouple
6. Condenser
7. Sample container
8. Gas outlet

Fig. 2.3.1. Reactor set-up for reactions carried out in vapour-phase.

REFERENCES

- [1] P.S. Anil Kumar, J.J. Shrotri, S.D. Kulkarni, C.E. Deshpande and S.K. Date; *Materials Letters*, 27 (1996) 293.
- [2] J.C. Vedrine in "Surface Properties and Catalysis by Non-metals", edited by J.P. Bonnelle, B. Delmon and E. Derouane, NATO ASI series, page 139 (1983).
- [3] P. Kubelka and F. Munk; *Z. Tech. Phys.*, 12 (1931) 593.
- [4] P. Kortum, W. Braun and C. Harzog; *Angew. Chem. Int. Ed. Engl.*, 2 (1963) 333.
- [5] S. Lowell and J.E. Shields "Powder Surface Area and Porosity", third edition, Chapman and Hall, page 38 (1991).
- [6] M.M. Dubinin; *Chem. Rev.*, 60 (1960) 235.
- [7] A. Howie; in: *Characterization of Catalysts*, Edited by J.M. Thomas and R.M. Lambert, John-Wiley & Sons, p. 89 (1980).
- [8] D.A. Skoog, D.M. West and F.J. Holler; "Analytical Chemistry-An Introduction" Sanders College Publishing, p. 108.
- [9] D.S. Acker and W.R. Hertler; *J. Am. Chem. Soc.*, 84 (1962) 3370.
- [10] L.F. Fieser and M. Fieser; "Reagents for Organic Synthesis", John Wiley, New York, p. 125 (1967).
- [11] B.S. Furness, A.J. Hannaford, V. Rogers, P.W.G. Smith and A.R. Tatchel; "Vogel's Text Book of Practical Organic Chemistry", 4th edn., ELBS, London (1978) p. 708.
- [12] A.I. Vogel; "A Text Book of Practical Organic Chemistry", 3rd edn., ELBS, London, p. 407 (1973).

CHAPTER III

**CHARACTERIZATION AND SURFACE
PROPERTIES**

3.1. PHYSICAL CHARACTERIZATION

The prepared samples were characterized by adopting various physical methods, such as X-ray diffraction analysis, scanning electron micrograph, diffuse reflectance infrared studies, surface area measurements, pore volume determination and thermal analysis. The results obtained in each case are discussed below.

3.1.1 X-ray diffraction analysis:

The X-ray diffractograms of the powdered samples were recorded using Rigaku (model D/MAX-VC) instrument with Cu K α radiation. X-ray diffractograms of some samples are presented in Figs: 3.1.1, 3.1.2 and 3.1.3. All peaks in the pattern matched well with the characteristic reflections of Zn-Ni, Zn-Co and Co-Ni ferrites reported in ASTM card. Close resemblance of the 'd' values (calculated using Bragg's equation) with the standard values clearly indicates the formation of single spinel phase. An important observation from the XRD pattern is the slightly broad peaks, indicating fine particle nature of the ferrite formed at 80 °C, as reported by Date *et al.* [1]. However, it was observed that the intensity of the XRD pattern progressively becomes sharper with the temperature of calcination. This implies growth of particle size and better crystallinity at higher calcination temperatures.

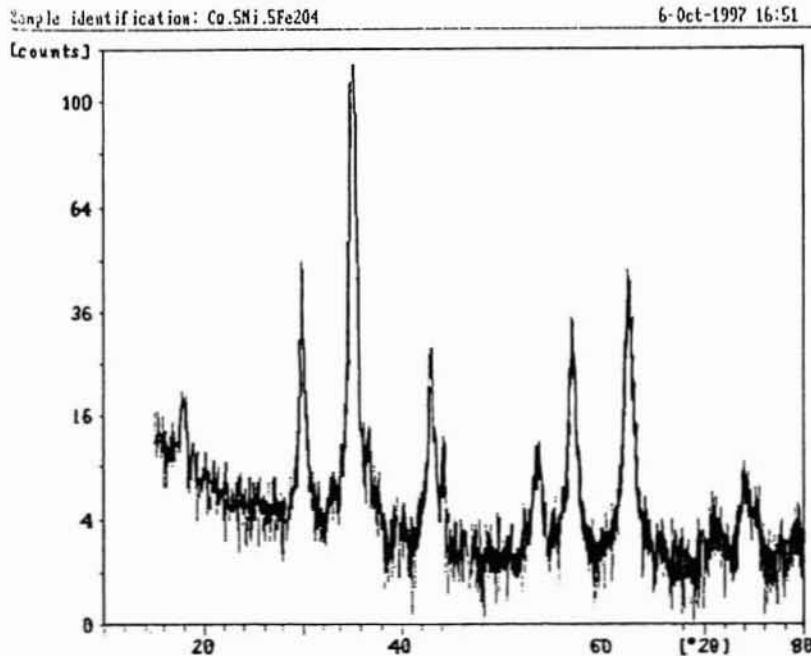


Fig. 3.1.1. Powder X-ray diffraction pattern of $\text{Co}_{0.5}\text{Ni}_{0.5}\text{Fe}_2\text{O}_4$.

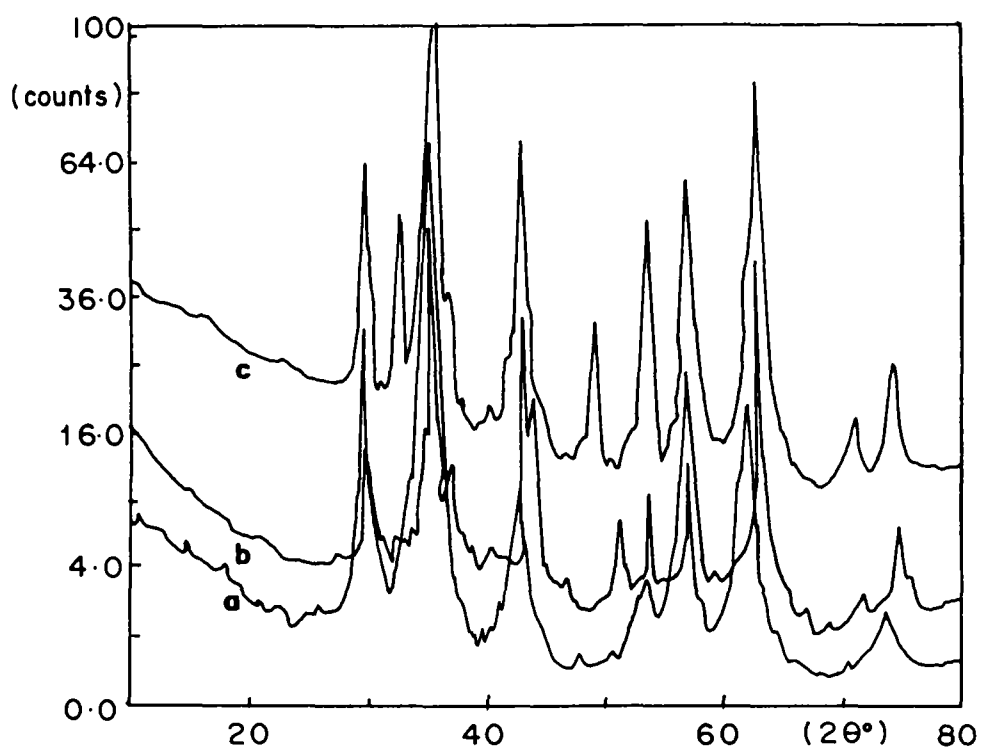


Fig. 3.1.2. Powder X-ray diffraction patterns of (a) CoFe_2O_4 (b) $\text{Zn}_{0.2}\text{Co}_{0.8}\text{Fe}_2\text{O}_4$ (c) $\text{Zn}_{0.8}\text{Co}_{0.2}\text{Fe}_2\text{O}_4$.

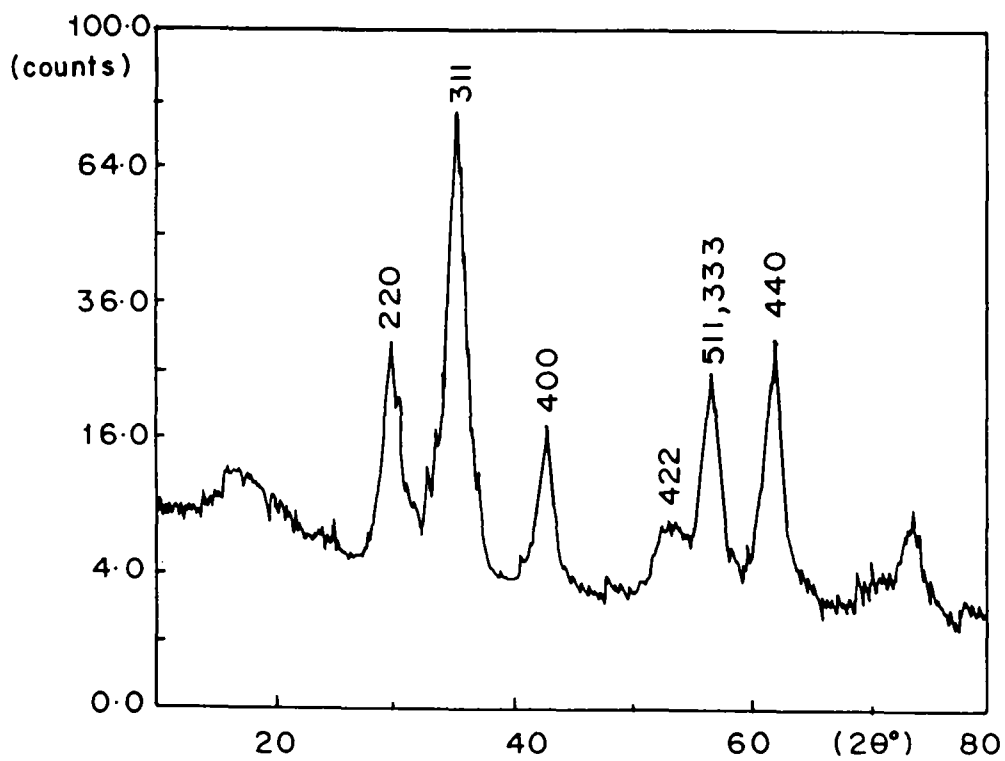


Fig. 3.1.3. Powder X-ray diffraction pattern of ZnFe_2O_4 .

3.1.2. Scanning Electron Micrograms Energy Dispersive X-ray analysis:

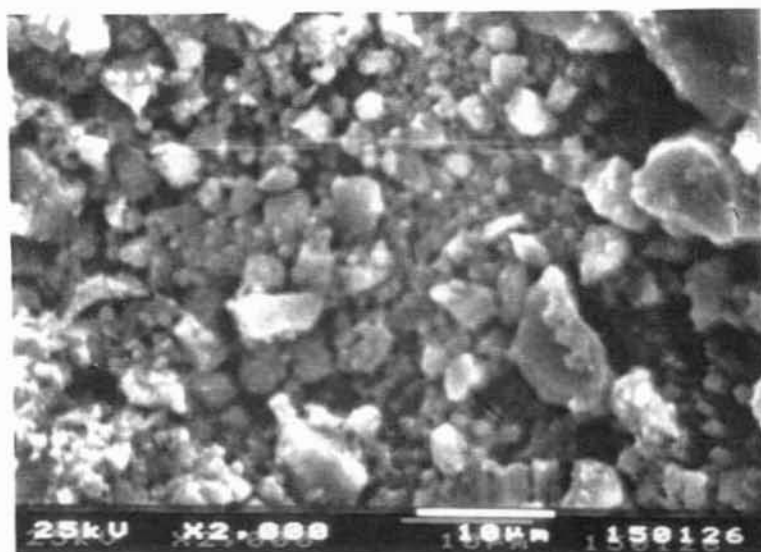
Scanning electron micrograms of the samples as dried at 80 °C showed fine particles of uniform size \approx 50 nm; as against larger, aggregate, non-uniform particles appeared for the samples prepared by adopting conventional ceramic method (Fig: 3.1.4). Thus, the growth of particles at higher calcination temperatures, as revealed from the XRD data, is supported by SEM images.

Metal ion concentrations in each series of the systems were estimated by EDX analysis. Results are summarized in the following table (Table 3.1.1):

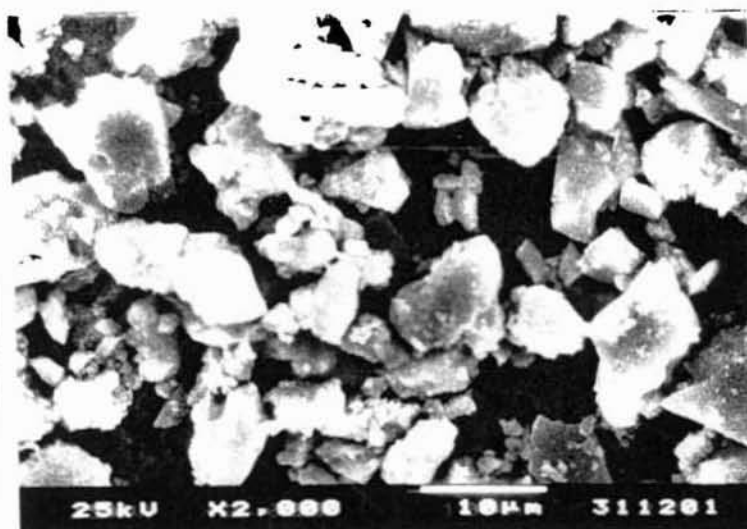
x	Catalyst composition	Metal ion concentration, Wt %	
		Zn ²⁺	Ni ²⁺
	Zn _{1-x} Ni _x Fe ₂ O ₄ --series	Zn ²⁺	Ni ²⁺
0	ZnFe ₂ O ₄	27.0 (27.1)	-----
0.2	Zn _{0.8} Ni _{0.2} Fe ₂ O ₄	21.6 (21.8)	4.9 (4.9)
0.5	Zn _{0.5} Ni _{0.5} Fe ₂ O ₄	13.7 (13.8)	12.4 (12.3)
0.8	Zn _{0.2} Ni _{0.8} Fe ₂ O ₄	5.4 (5.6)	19.8 (20.0)
1.0	NiFe ₂ O ₄	-----	25.2 (25.1)
	Zn _{1-x} Co _x Fe ₂ O ₄ ---series	Zn ²⁺	Co ²⁺
0	ZnFe ₂ O ₄	27.0 (27.1)	-----
0.2	Zn _{0.8} Co _{0.2} Fe ₂ O ₄	21.7 (21.8)	4.6 (4.8)
0.5	Zn _{0.5} Co _{0.5} Fe ₂ O ₄	13.7 (13.7)	12.3 (12.4)
0.8	Zn _{0.2} Co _{0.8} Fe ₂ O ₄	5.7 (5.5)	20.0 (20.0)
1.0	CoFe ₂ O ₄	-----	24.7 (24.8)
	Co _{1-x} Ni _x Fe ₂ O ₄ --series	Co ²⁺	Ni ²⁺
0	CoFe ₂ O ₄	24.7 (24.8)	-----
0.2	Co _{0.8} Ni _{0.2} Fe ₂ O ₄	19.9 (20.2)	5.1 (5.0)
0.5	Co _{0.5} Ni _{0.5} Fe ₂ O ₄	12.5 (12.6)	12.5 (12.5)
0.8	Co _{0.2} Ni _{0.8} Fe ₂ O ₄	4.9 (5.0)	19.9 (20.0)
1.0	NiFe ₂ O ₄	-----	25.1 (25.1)

* Quantities in the parentheses indicate theoretical values.

Table 3.1.1. EDX analysis data of ferrospinels containing Zn, Co and Ni.



(b)



(c)

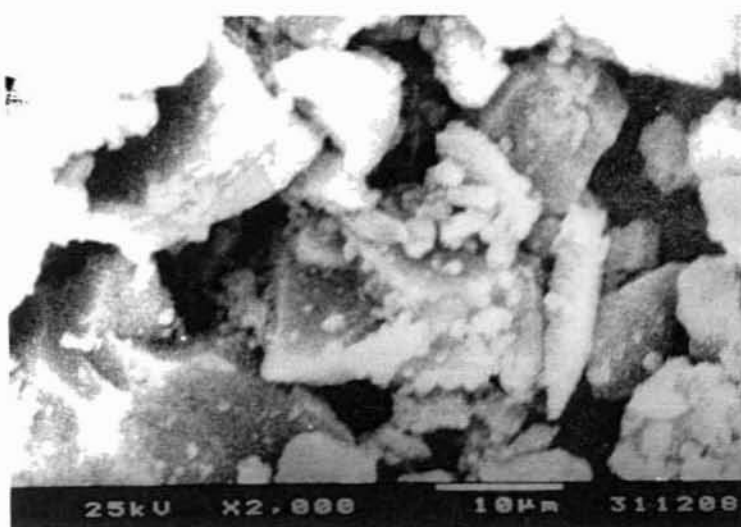


Fig 3.14: Scanning electron micrographs (SEM) of (a) CoFe₂O₄ (b) ZnFe₂O₄, as dried at 300^oC and (c) calcined ZnFe₂O₄ at 1400^oC

3.1.3. Diffuse reflectance infrared spectra:

All compositions of the samples showed two strong IR bands, ν_1 and ν_2 around 700 and 500 cm^{-1} (Fig. 3.1.6 and 3.1.7). It was systematically assigned by Waldren *et al.* [2] and White *et al.*[3] that the high frequency band at 700 cm^{-1} due to the stretching vibration of the tetrahedral M-O group and the lower frequency band at 500 cm^{-1} due to the vibration of the octahedral M-O group. The conclusion made by Waldren is as follows:

In a spinel lattice every oxygen anion is bonded to 3 octahedral and 1 tetrahedral cation as shown below [Fig. 3.1.5].

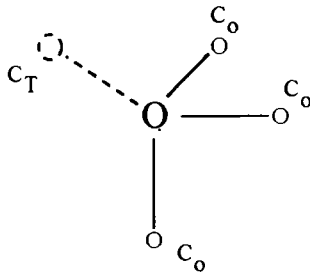


Fig. 3.1.5. The nearest cationic neighbours of the oxygen anion in the spinel lattice. C_o: octahedral cation, C_T: tetrahedral cation.

The three octahedral bonds are perpendicular to each other and thus provide an isotropic force field in the three directions if the tetrahedral bond was absent. The tetrahedral cation C_T introduces a supplementary restoring force in a preferential direction along the C_{T-O} bond. This is responsible for the ν_1 mode in which the oxygen is forced to oscillate along the C_{T-O} bond, and thus appears as a stretching vibration of the tetrahedral group. Vibration of this group corresponds to the highest restoring force and thus assigned to the highest frequency band. If we now consider an oxygen vibration at right angles with the preceding one, the restoring force due to the tetrahedral cation C_T will be negligible. This leads to ν_2 mode, which may be considered as a stretching vibration of the octahedral group.

Waldren's assignment is fairly acceptable for all inverse spinels, where cations with $+2$ and $+3$ oxidation states are distributed both in tetrahedral and octahedral sites. But an opposite conclusion was made for normal 2-3 spinels by J. Preudhomme and P. Tarte [4]; according to which, in the case of normal spinels the high frequency band should be assigned to the stretching vibration of the octahedral groups, since the tetrahedral sites are solely occupied by $+2$ cations and, hence, the bonding force of C_{T-O} will be lesser than the bonding force of C_{O-O} .

Thus, the two bands in the two distinct frequency regions clearly indicated the distribution of metal cations in the two coordinated sites of oxygen anions.

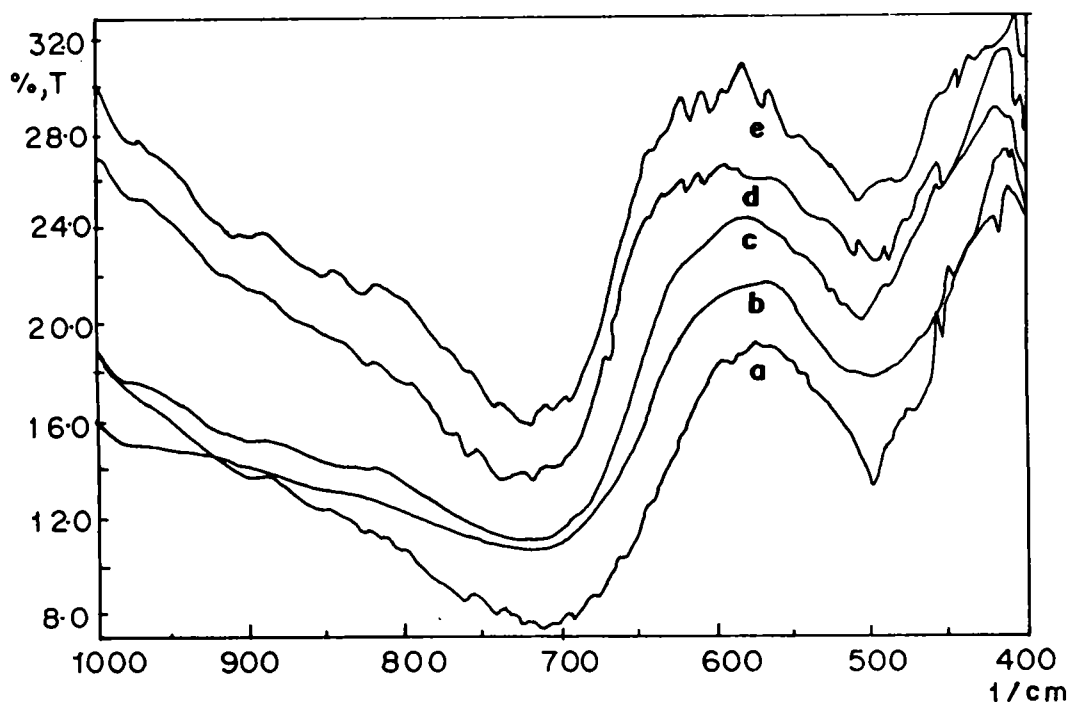


Fig. 3.1.6. DR-IR spectra of (a) $ZnFe_2O_4$ (b) $Zn_{0.8}Co_{0.2}Fe_2O_4$ (c) $Zn_{0.5}Co_{0.5}Fe_2O_4$ (d) $Zn_{0.2}Co_{0.8}Fe_2O_4$ (e) $CoFe_2O_4$.

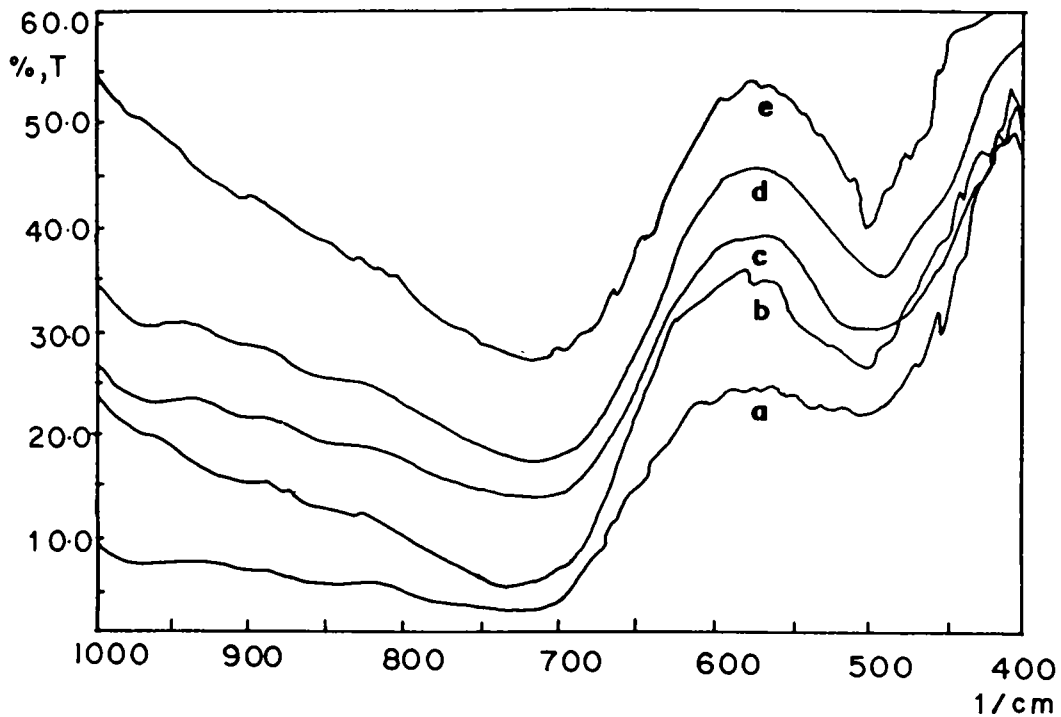


Fig. 3.1.7. DR-IR spectra of (a) CoFe_2O_4 (b) $\text{Co}_{0.8}\text{Ni}_{0.2}\text{Fe}_2\text{O}_4$ (c) $\text{Co}_{0.5}\text{Ni}_{0.5}\text{Fe}_2\text{O}_4$ (d) $\text{Co}_{0.2}\text{Ni}_{0.8}\text{Fe}_2\text{O}_4$ (e) NiFe_2O_4 .

3.1.4. Thermal Analysis:

TGA-DTA curves for ZnFe_2O_4 and CoFe_2O_4 were presented in Fig: 3.1.8 and Fig. 3.1.9 respectively. As shown in the figures, in the TG curve, the % weight loss against temperature is plotted. For all samples there is a distinct weight loss from room temperature to 100°C . The weight loss of the catalysts below 100°C is due to desorption of physically adsorbed water. However, all catalysts displayed good thermal stability after 150°C , as indicated by the fairly horizontal portions of the TGA curves. In some cases, however, there is a small hump around 350°C both in TGA and DTA curves. Since the materials were precipitated from the aqueous solutions of the respective metal nitrates, some amount of nitrate may exist in the adsorbed form. Decomposition of nitrate at 400°C is responsible for the hump in the TGA-DTA curves.

These results indicate that ferrite systems are thermally stable in the temperature range 150 to 1000 °C without creating major weight loss, decomposition or phase transformations.

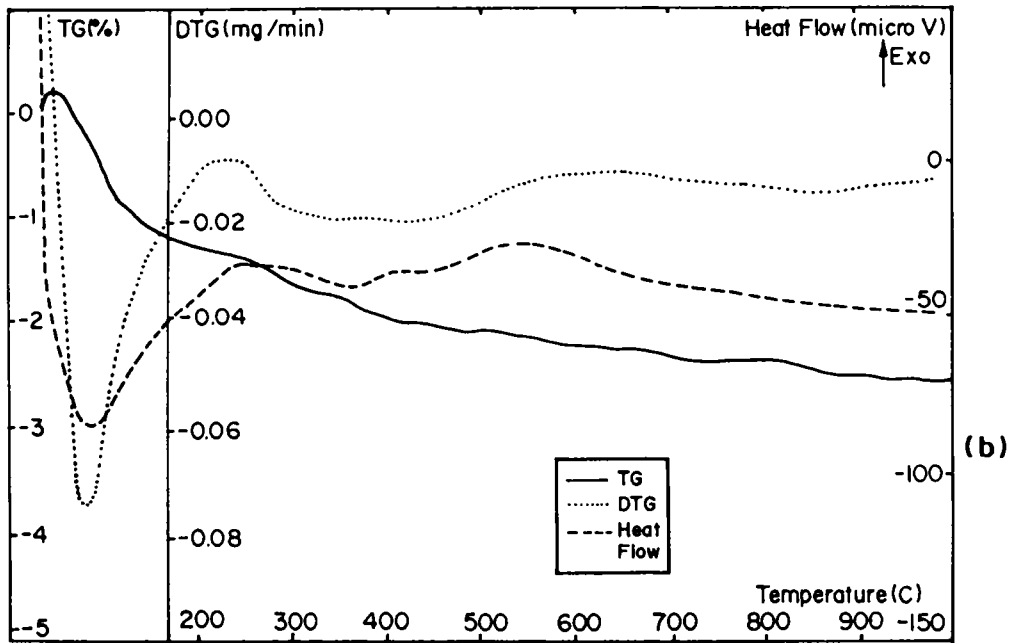


Fig. 3.1.8. TG-DTA curves of ZnFe₂O₄.

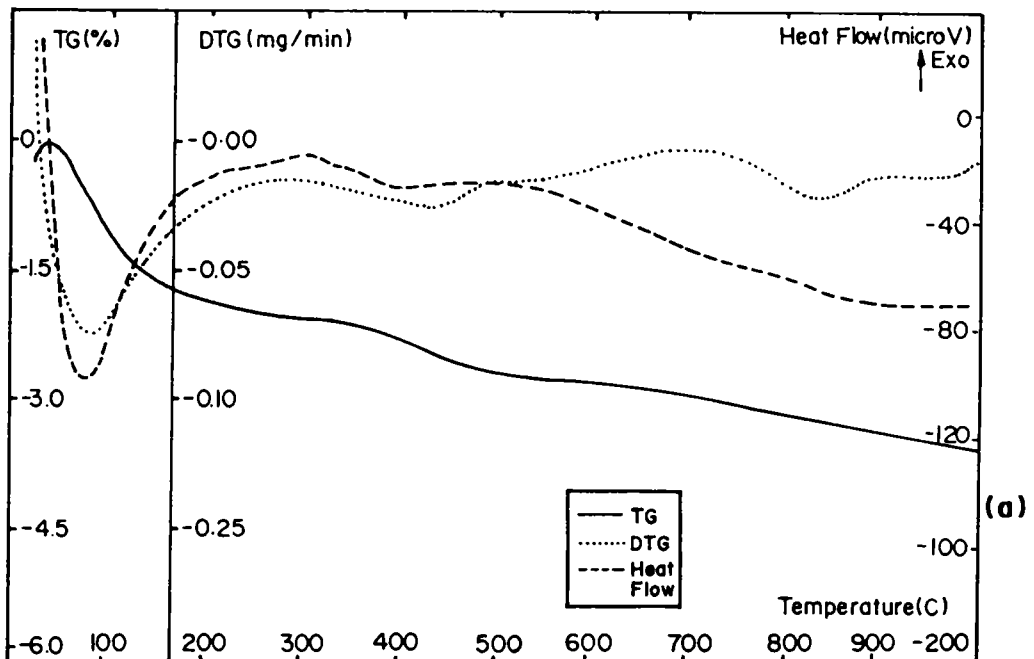


Fig. 3.1.9. TG-DTA curves of CoFe₂O₄.

3.1.5. Surface area and pore volume distribution:

The BET surface areas of the different compositions of the samples calcined at 300 and 500 °C were measured using an OMNISORP 100 CX instrument. The data are presented in Table 3.1.2. Increase in calcination temperature decreased the surface area. This can be due to the increase in particle size and higher crystallinity at higher calcination temperature.

The pore volumes of the systems were calculated using a Quantachrome mercury porosimeter. The pore volumes obtained were summarised in Table 3.1.2. The differential pore volume curves of ZnFe₂O₄ and CoFe₂O₄ are presented in figure (Fig. 3.1.9). This samples have a very sharp volume distribution from 50 Å to 180 Å. A major part of the pore volumes being present in pores in this range.

Catalyst composition	BET surface area(m ² /g)		Pore volume(cm ³ /g)
	300 ^o C	500 ^o C	
Zn_{1-x}Co_xFe₂O₄-- series			
ZnFe ₂ O ₄	85.78	30.01	0.3823
Zn _{0.8} Co _{0.2} Fe ₂ O ₄	91.21	33.57	0.3852
Zn _{0.5} Co _{0.5} Fe ₂ O ₄	100.07	39.46	0.3879
Zn _{0.2} Co _{0.8} Fe ₂ O ₄	112.64	39.82	0.4333
CoFe ₂ O ₄	121.21	40.06	0.4353
Zn_{1-x}Ni_xFe₂O₄-- series			
ZnFe ₂ O ₄	85.78	30.01	0.3823
Zn _{0.8} Ni _{0.2} Fe ₂ O ₄	102.31	37.71	0.3831
Zn _{0.5} Ni _{0.5} Fe ₂ O ₄	124.47	47.64	0.3156
Zn _{0.2} Ni _{0.8} Fe ₂ O ₄	133.03	57.72	0.3994
NiFe ₂ O ₄	150.90	60.91	0.4550
Co_{1-x}Ni_xFe₂O₄-- series			
CoFe ₂ O ₄	121.21	40.06	0.4353
Co _{0.8} Ni _{0.2} Fe ₂ O ₄	133.30	35.67	0.4659
Co _{0.5} Ni _{0.5} Fe ₂ O ₄	137.21	38.89	0.4440
Co _{0.2} Ni _{0.8} Fe ₂ O ₄	144.10	58.25	0.4694
NiFe ₂ O ₄	150.90	60.91	0.4554

Table 3.1.2. Surface areas and pore volumes of the catalysts.

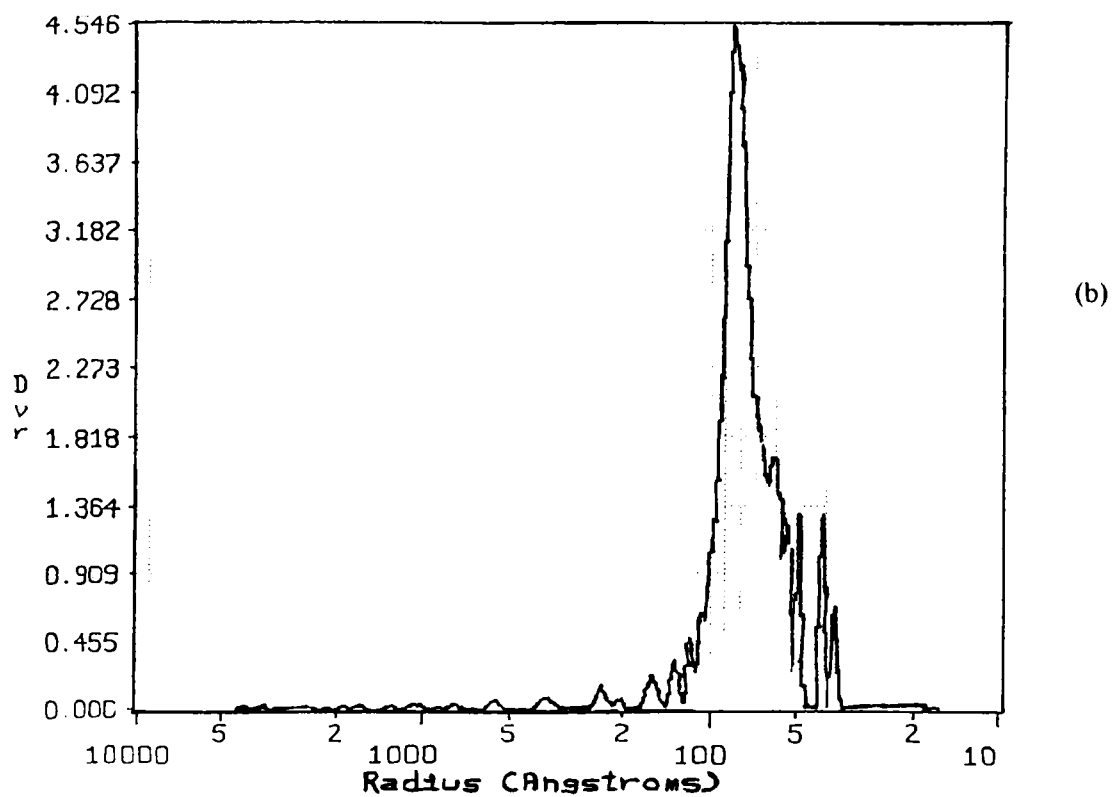
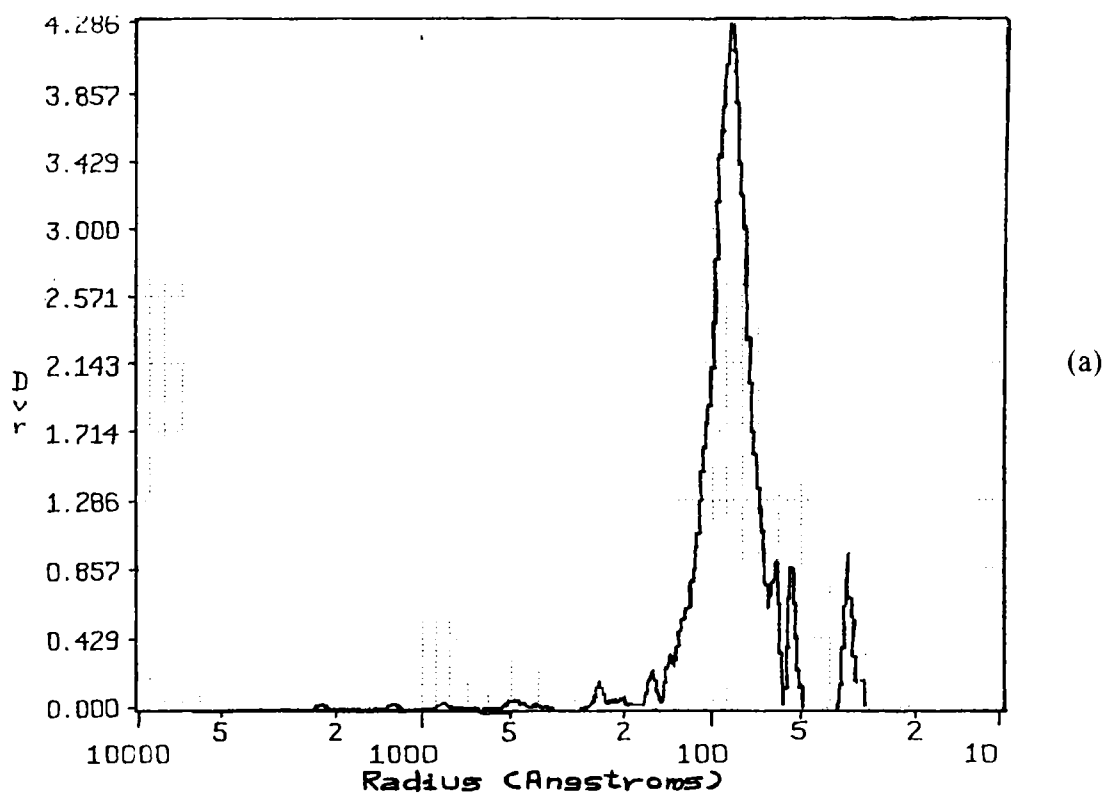


Fig. 3.1.9. Pore volume distribution curves of (a) ZnFe_2O_4 and (b) CoFe_2O_4 , calcined at 500°C

3.2. SURFACE PROPERTIES--ACIDITY / BASICITY

According to the concept of solid acids and bases, surface of many oxides possesses acid base properties. In a number of reactions, catalyzed by heterogeneous systems, these surface acid base properties play an important role in determining catalytic activity and selectivity to a particular reaction. Surface acid-base properties vary with composition. In the present series of systems, since composition varies with 'x' value, evaluation of surface acidity and basicity for each composition is of utmost importance.

Two independent methods were adopted to evaluate the surface basicity and acidity of the systems. For the determination of basicity of the systems, adsorption studies of electron acceptors having different electron affinity values were performed. Dehydration of alcohol is a very good test reaction for evaluating surface acidity. In the present case two such experiments using isopropanol and cyclohexanol as the substrates have been performed.

3.2.1. Surface electron donating properties (Evaluation of Lewis basicity):

Investigation of strength and distribution of electron donor sites on oxide surface using electron acceptors having different electron affinity values have been well established. The limiting amount of electron acceptors adsorbed depends on two factors: (1) strength and distribution of donor sites (Lewis basic sites) on the surface and (2) the electron affinity values of the electron acceptors used. Thus, a comparison of limiting concentration of electron acceptors adsorbed and the electron affinity values of the respective electron acceptors used, valuable information regarding the strength and distribution of donor sites can be obtained. So, in this part of the thesis, an attempt has been done to establish the donor properties of various ferrite surfaces and their variation with composition in each series of ferros spinels.

The electron acceptors used for adsorption study are given in Table 3.2.1.

Electron Acceptors used (EA)	Electron Affinity values
7,7,8,8-tetracyanoquinodimethane (TCNQ)	2.84
2,3,5,6-tetrachloro-p-benzoquinone (Chloranil)	2.40
p-dinitrobenzene	1.77

Table 3.2.1. List of electron acceptors used for the adsorption study.

Solution of EAs in acetonitrile was used for the study.

Adsorption experiments were performed at three different activation temperatures; 300, 500 and 700 °C. However, since the catalytic activity studies (*i.e.* both aniline and phenol alkylation reactions, chapter 4 and 5 respectively) were performed with systems activated at 500 °C, special emphasis has been made while studying and explaining the donor properties of the systems calcined at 500 °C. The limiting concentrations were expressed in m²/g; the surface areas being determined using BET method for each sample.

The limiting amount adsorbed for TCNQ and Chloranil on different Zn-Ni, Zn-Co and Co-Ni systems are presented in Tables 3.2.2 and 3.2.3. The adsorption of PDNB was so negligible that the amount adsorbed was hardly estimated. Langmuir type of adsorption isotherms obtained for TCNQ and Chloranil (activation temperature 500 °C) were shown in figures (Fig. 3.2.1 to Fig. 3.2.6).

Catalyst Composition	Limiting amount adsorbed ($\times 10^{-5}$ mol m ⁻²)		
	300 °C	500 °C	700 °C
<u>Zn_{1-x}Ni_xFe₂O₄</u>			
ZnFe ₂ O ₄	2.06	1.66	0.30
Zn _{0.8} Ni _{0.2} Fe ₂ O ₄	2.54	1.76	0.30
Zn _{0.5} Ni _{0.5} Fe ₂ O ₄	3.33	1.91	0.33
Zn _{0.2} Ni _{0.8} Fe ₂ O ₄	4.07	2.19	0.51
NiFe ₂ O ₄	5.62	2.38	0.87
<u>Zn_{1-x}Co_xFe₂O₄</u>			
ZnFe ₂ O ₄	2.06	1.66	0.30
Zn _{0.8} Co _{0.2} Fe ₂ O ₄	2.00	1.56	Nil
Zn _{0.5} Co _{0.5} Fe ₂ O ₄	1.90	1.55	Nil
Zn _{0.2} Co _{0.8} Fe ₂ O ₄	1.79	1.52	Nil
CoFe ₂ O ₄	1.67	1.53	Nil
<u>Co_{1-x}Ni_xFe₂O₄</u>			
CoFe ₂ O ₄	1.67	1.53	Nil
Co _{0.8} Ni _{0.2} Fe ₂ O ₄	2.37	1.90	0.30
Co _{0.5} Ni _{0.5} Fe ₂ O ₄	3.50	1.92	0.44
Co _{0.2} Ni _{0.8} Fe ₂ O ₄	4.31	2.00	0.58
NiFe ₂ O ₄	5.62	2.38	0.87

Table 3.2.2. Adsorption data of TCNQ over different ferrite series at different activation temperatures.

Catalyst Composition	Limiting amount adsorbed($\times 10^{-5}$ mol m ⁻²)		
	300 °C	500 °C	700 °C
<u>Zn_{1-x}Ni_xFe₂O₄</u>			
ZnFe ₂ O ₄	1.88	0.66	Nil
Zn _{0.8} Ni _{0.2} Fe ₂ O ₄	1.97	0.73	Nil
Zn _{0.5} Ni _{0.5} Fe ₂ O ₄	1.99	0.84	0.11
Zn _{0.2} Ni _{0.8} Fe ₂ O ₄	2.17	1.02	0.17
NiFe ₂ O ₄	2.31	1.06	0.21
<u>Zn_{1-x}Co_xFe₂O₄</u>			
ZnFe ₂ O ₄	1.88	0.66	Nil
Zn _{0.8} Co _{0.2} Fe ₂ O ₄	1.77	0.48	Nil
Zn _{0.5} Co _{0.5} Fe ₂ O ₄	1.53	0.43	Nil
Zn _{0.2} Co _{0.8} Fe ₂ O ₄	1.43	0.37	Nil
CoFe ₂ O ₄	1.41	0.31	Nil
<u>Co_{1-x}Ni_xFe₂O₄</u>			
CoFe ₂ O ₄	1.41	0.31	Nil
Co _{0.8} Ni _{0.2} Fe ₂ O ₄	1.83	0.71	Nil
Co _{0.5} Ni _{0.5} Fe ₂ O ₄	2.53	0.87	Nil
Co _{0.2} Ni _{0.8} Fe ₂ O ₄	3.05	0.97	0.10
NiFe ₂ O ₄	3.31	1.06	0.21

Table 3.2.3. Adsorption data of chloranil over different ferrite series at different activation temperatures.

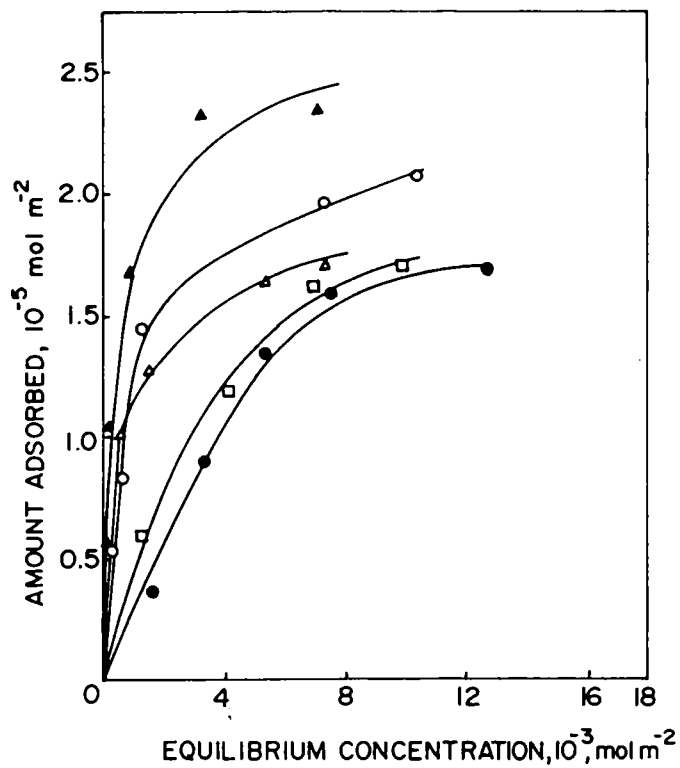


Fig. 3.2.1. Adsorption isotherms of TCNQ in acetonitrile over different Zn-Ni ferrite systems calcined at 500 °C. ● ZnFe₂O₄; □ Zn_{0.8}Ni_{0.2}Fe₂O₄; △ Zn_{0.5}Ni_{0.5}Fe₂O₄; ○ Zn_{0.2}Ni_{0.8}Fe₂O₄; ▲ NiFe₂O₄.

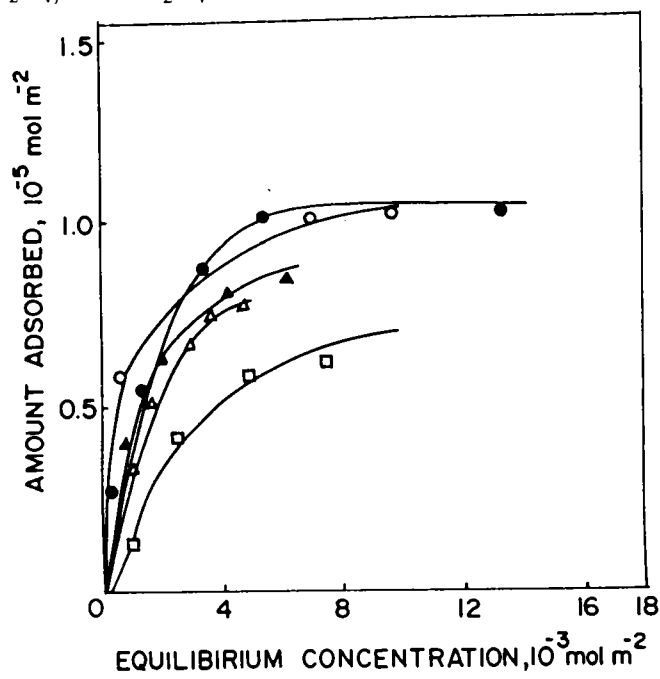


Fig. 3.2.2. Adsorption isotherms of chloranil in acetonitrile over different Zn-Ni ferrite systems calcined at 500 °C. □ ZnFe₂O₄; △ Zn_{0.8}Ni_{0.2}Fe₂O₄; ▲ Zn_{0.5}Ni_{0.5}Fe₂O₄; ○ Zn_{0.2}Ni_{0.8}Fe₂O₄; ● NiFe₂O₄.

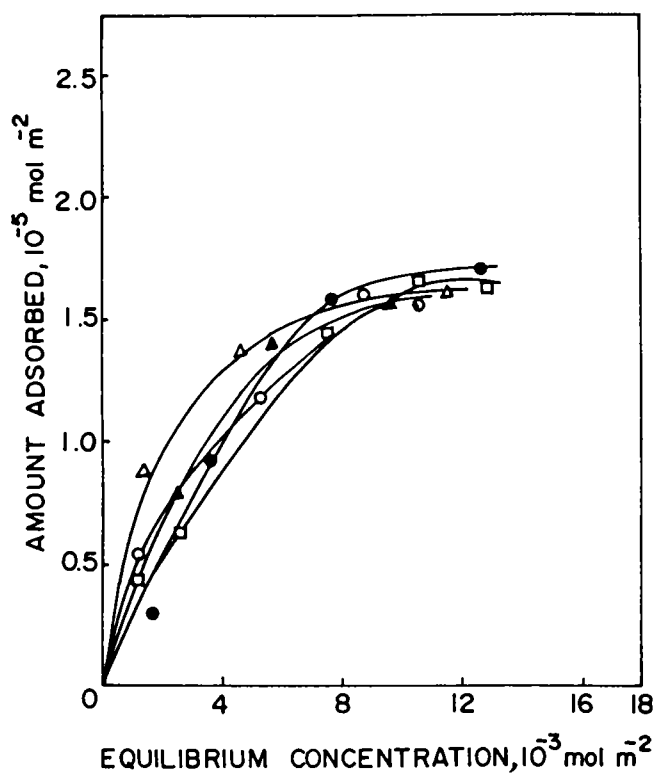


Fig. 3.2.3. Adsorption isotherms of TCNQ in acetonitrile over different Zn-Co ferrite systems calcined at 500 °C. ● ZnFe₂O₄; ▲ Zn_{0.8}Co_{0.2}Fe₂O₄; □ Zn_{0.5}Co_{0.5}Fe₂O₄; ○ Zn_{0.2}Co_{0.8}Fe₂O₄; △ CoFe₂O₄.

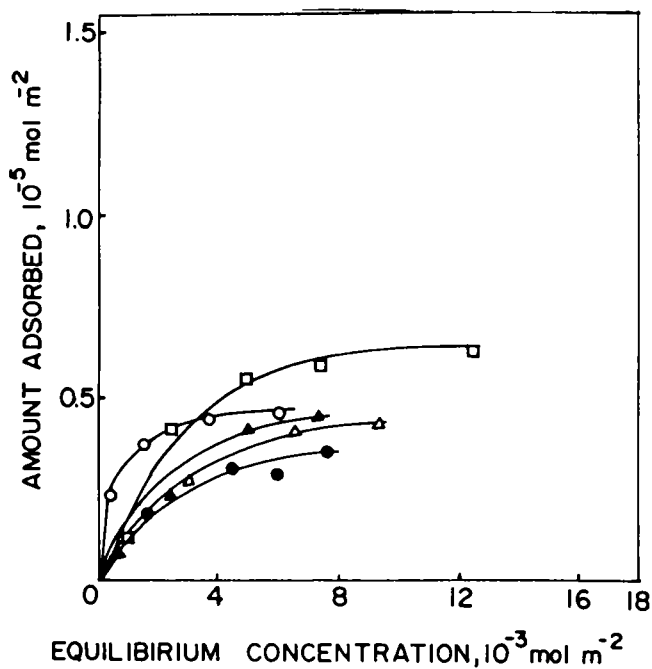


Fig. 3.2.4. Adsorption isotherms of chloranil in acetonitrile over different Zn-Co ferrite systems calcined at 500 °C. □ ZnFe₂O₄; ○ Zn_{0.8}Co_{0.2}Fe₂O₄; ▲ Zn_{0.5}Co_{0.5}Fe₂O₄; △ Zn_{0.2}Co_{0.8}Fe₂O₄; ● CoFe₂O₄.

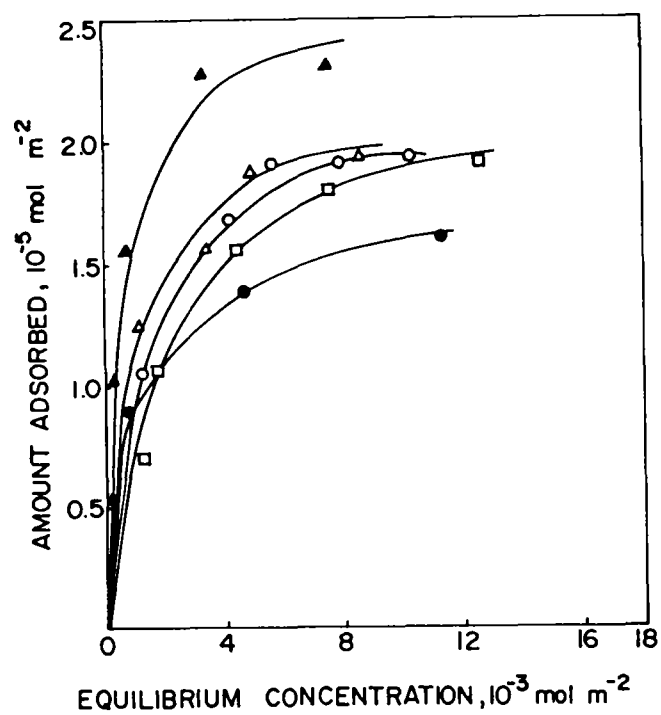


Fig. 3.2.5. Adsorption isotherms of TCNQ in acetonitrile over different Co-Ni ferrite systems calcined at 500 °C. • CoFe_2O_4 ; \square $\text{Co}_{0.8}\text{Ni}_{0.2}\text{Fe}_2\text{O}_4$; \circ $\text{Co}_{0.5}\text{Ni}_{0.5}\text{Fe}_2\text{O}_4$; Δ $\text{Co}_{0.2}\text{Ni}_{0.8}\text{Fe}_2\text{O}_4$; \blacktriangle NiFe_2O_4 .

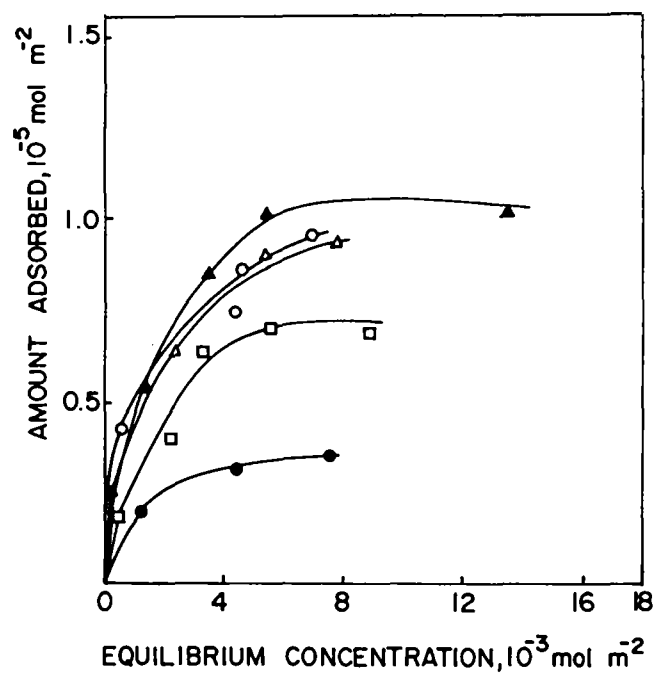


Fig. 3.2.6. Adsorption isotherms of chloranil in acetonitrile over different Co-Ni ferrite systems calcined at 500 °C. • CoFe_2O_4 ; \square $\text{Co}_{0.8}\text{Ni}_{0.2}\text{Fe}_2\text{O}_4$; Δ $\text{Co}_{0.5}\text{Ni}_{0.5}\text{Fe}_2\text{O}_4$; \circ $\text{Co}_{0.2}\text{Ni}_{0.8}\text{Fe}_2\text{O}_4$; \blacktriangle NiFe_2O_4 .

A strong EA like TCNQ can accept electrons from both strong and weak donor sites, whereas a weak EA like PDNB can accept electrons from strong donor sites only. Negligible adsorption of PDNB in all cases indicates the absence of very strong basic sites, and hence the limiting amount of TCNQ and chloranil would be an estimate of weak or moderately strong donor sites. From the tables it is clearly evident that increase in temperature significantly diminished basicity in all series of systems.

A survey of the results presented so far has enabled us to achieve some conclusions:

(a) Zn_{1-x}Ni_xFe₂O₄-type systems:

In this case, the basicity of the systems follows the order: NiFe₂O₄ > Zn_{0.2}Ni_{0.8}Fe₂O₄ > Zn_{0.5}Ni_{0.5}Fe₂O₄ > Zn_{0.8}Ni_{0.2}Fe₂O₄ > ZnFe₂O₄, indicating that basicity shows an increasing trend with progressive substitution of Zn by Ni. ZnFe₂O₄ is a typical normal spinel, in which all Zn²⁺ ions are in the tetrahedral sites and all Fe³⁺ ions are in the octahedral sites. Jacobs *et al.*[5] in a study based on Low Energy Ion Scattering (LEIS, a technique which is highly sensitive for determining surface atomic layer) have reported that in a spinel the surface layer is mainly octahedral and tetrahedral sites are not easily accessible. Hence, it is reasonable to conclude that adsorption of EAs occurs mainly at the octahedral sites. Also, due to the lower covalency of tetrahedral cations, the M-O (where 'M' is the cation) bond strength will be stronger in the tetrahedral sites than in the octahedral sites [6,7]. In other words the octahedral M-O bond will be more polar. From these it is clear that the octahedral cation plays a significant role in determining the acido-basic properties of the system. As 'x' increases Ni²⁺ ions replace Fe³⁺ ions isomorphically from the octahedral sites. This leads to a progressive increase in the concentration of Ni²⁺ ions in the octahedral sites and a corresponding increase of Fe³⁺ ions in the tetrahedral sublattice. Replacement of more acidic Fe³⁺ ions from the octahedral sites and occupancy of less acidic Ni²⁺ ions in the same positions is responsible for the increase in the basicity during Ni substitution.. When 'x' becomes 1, we get NiFe₂O₄, a typical inverse spinel, where half of the Fe³⁺ is the tetrahedral sites and the other half together with whole Ni²⁺ ions in the octahedral sites. This system is found to be the most basic one.

(b) Zn_{1-x}Co_xFe₂O₄-type systems

Structurally Zn-Co systems are similar to the corresponding Zn-Ni systems. This means that, as Co²⁺ concentration increases, the system progressively changes from a normal (*i.e.* ZnFe₂O₄) to a completely inverse form (*i.e.* CoFe₂O₄). However, unlike the corresponding nickel systems, cobalt substitution decreased the basicity of the systems. This decrease is very slow, as evident from the nearly close limiting amount values for the neighbouring members. Basicity follows the order ZnFe₂O₄ ≈ Zn_{0.8}Co_{0.2}Fe₂O₄ > Zn_{0.5}Co_{0.5}Fe₂O₄ > Zn_{0.2}Co_{0.8}Fe₂O₄ ≈ CoFe₂O₄.

(c) Co_{1-x}Ni_xFe₂O₄-type systems.

Unlike the above mentioned two systems, all members of Co-Ni ferrite series are inverse in nature. Here Fe³⁺ ion concentration in the tetrahedral as well as octahedral sublattices remain unaltered (*i.e.* half of the Fe³⁺ is distributed in the tetrahedral and the other half in the octahedral holes) and only the Co-Ni ratio in the octahedral site varies. Hence the Co²⁺/Ni²⁺ ratio plays a decisive role in determining the donor properties of the system. From the tables 3.2.2 and 3.2.3 it is clear that basicity showed an increasing trend as Co²⁺ is being substituted by Ni²⁺ ions. The order of basicity can be represented as NiFe₂O₄ > Co_{0.2}Ni_{0.8}Fe₂O₄ > Co_{0.5}Ni_{0.5}Fe₂O₄ > Co_{0.8}Ni_{0.2}Fe₂O₄ > CoFe₂O₄.

From these observations it is clear that Ni²⁺ addition significantly enhanced the basicity values in both Zn-Ni and Co-Ni ferrite systems. Zn-Co ferrites showed close basicity values, even though Co²⁺ doping slightly decreased the basicity. Two possible electron sources exist on oxide surface responsible for electron transfer. One of these has electron trapped in intrinsic defects and other has surface hydroxyl ions [8]. At lower temperatures surface sites may be associated with the presence of unsolvated hydroxyl ions and at higher temperature these hydroxyl groups will vanish. Strong dependence of limiting values with the activation temperature supports the fact that in ferrosinels basicity mainly appear due to the presence of surface hydroxyl groups.

The limiting amount value is higher for TCNQ than for chloranil. Since TCNQ is a strong electron acceptor (electron affinity value 2.84 eV) it forms anion radicals

adsorbed from strong as well as weak donor sites. In other words, the limiting amount of TCNQ adsorbed will give a measure of strong as well as weak donor sites on the catalyst surface. However, chloranil (electron affinity value 2.40 eV) can accept electrons from strong and moderately strong donor sites. Negligible adsorption of PDNB in all systems indicates absence of very strong electron donor sites. This suggests that adsorption sites on Zn-Ni, Zn-Co and Co-Ni ferros spinels act as electron donors to the adsorbed molecule with electron affinity values less than 2.40 but greater than 1.77 eV in acetonitrile. Accordingly the limit of electron transfer from electron donor sites of ferros spinels to the electron acceptor molecule is located between 2.40 and 1.77 eV.

3.3. ALCOHOL DECOMPOSITION REACTIONS.

Most of the transition metal oxides behave as dual function catalysts. They promote both dehydration and dehydrogenation of alcohols depending on the physical nature and acidity of the surface. According to the widely accepted concept, dehydration is mainly influenced by the acidity of the surface, whereas dehydrogenation is favoured by a combined interaction of both acidic and basic sites on the surface. This means that the multipathway conversion of alcohol can be used as a test reaction to study the surface acidity of heterogeneous systems.

The present part of the work is an attempt to characterize surface acidity of various ferros spinels by studying the dehydration and dehydrogenation of isopropanol and cyclohexanol in a down flow vapour phase silica reactor.

3.3.1. Isopropyl alcohol decomposition:

The results obtained for the decomposition of isopropanol at 280 °C over different Zn-Ni, Zn-Co and Co-Ni ferros spinels are summarized in Tables 3.3.1 to 3.3.3. Contact time (*i.e.* W/F, where W is the weight of catalyst in grams and F the feed flow rate in gram per hour) was maintained 1.3 h in all cases. Liquid products were condensed using a cold trap. Liquid and gaseous products were separately analyzed using Shimadzu GC-15A gas chromatograph fitted with TCD. Mass balance was measured and product distribution was accordingly calculated in each case.

$Zn_{1-x}Ni_xFe_2O_4$	x = 0	x = 0.2	x = 0.5	x = 0.8	x = 1.0
Product Distribution, Wt. %					
Propene	33.66	30.77	24.63	17.21	16.50
Acetone	16.69	17.44	21.22	22.38	24.70
Water	12.60	12.01	8.67	8.54	4.87
Others	1.50	1.47	1.77	2.52	3.20
Isopropanol Conversion	64.45	61.69	56.29	50.65	49.27
Selectivity					
Propene	52.23	49.87	43.75	33.97	33.48
Acetone	25.89	28.27	37.70	44.18	50.13

Table 3.3.1. Product distribution data of isopropanol reaction over Zn-Ni ferrites. Reaction temperature 280 °C, contact time 1.3 h and TOS 2 h.

$Zn_{1-x}Co_xFe_2O_4$	x = 0	x = 0.2	x = 0.5	x = 0.8	x = 1.0
Product Distribution, Wt. %					
Propene	33.66	37.20	37.76	38.21	44.68
Acetone	16.69	16.60	15.94	15.44	13.66
Water	12.60	15.20	14.93	15.71	19.21
Others	1.50	0.87	0.54	0.75	1.73
Isopropanol Conversion	64.45	69.87	69.17	70.11	79.28
Selectivity					
Propene	52.23	53.24	54.59	54.50	56.35
Acetone	25.89	23.75	29.20	22.02	17.23

Fig. 3.3.2. Product distribution data of isopropanol reaction over Zn-Co ferromagnetic oxides. Reaction temperature 280 °C, contact time 1.3 h and TOS 2 h.

$\text{Co}_{1-x}\text{Ni}_x\text{Fe}_2\text{O}_4$	$x = 0$	$x = 0.2$	$x = 0.5$	$x = 0.8$	$x = 1.0$
Product Distribution, Wt. %					
Propene	44.68	36.52	33.26	20.46	16.50
Acetone	13.66	15.20	18.49	19.74	24.70
Water	19.21	13.20	8.36	6.78	4.87
Others	1.73	1.81	1.93	2.43	3.20
Isopropanol Conversion	79.28	66.73	62.04	49.41	49.28
Selectivity					
Propene	56.35	54.75	53.61	41.41	33.48
Acetone	17.23	22.78	29.80	39.95	50.12

Fig. 3.3.3. Product distribution data of isopropanol reaction over Co-Ni ferrites. Reaction temperature 280 °C, contact time 1.3 h and TOS 2 h.

The effect of contact time on dehydration-dehydrogenation activities was studied using CoFe_2O_4 as a specific example. The result is shown in Fig.3.3.1. Amount of propene was maximum in the high contact time regions and declined as the flow rate was increased. At high flow rate (*i.e.* low contact time) the vapour will move so rapidly that only insufficient interaction with the catalyst surface will occur. The rate of formation of acetone (dehydrogenation product) was higher at intermediate contact time regions. As could be seen from the figure only lesser amount of acetone was detected in the high contact time regions. As reported by V.Krishnasamy *et al.*[9] at high contact time, a part of the adsorbed acetone may be oxidized to CO_2 by the lattice oxygen. This was evident from the evolution of CO_2 during the reaction. The formation of CO_2 has been further confirmed by carrying out runs with acetone alone over CoFe_2O_4 .

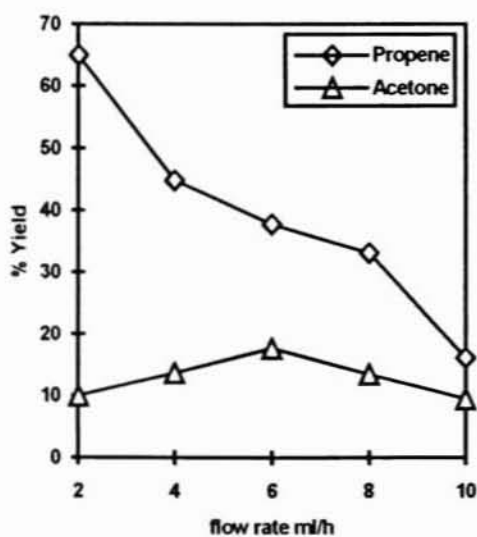


Fig. 3.3.1. Effect of feed flow-rate on dehydration and dehydrogenation activities over CoFe_2O_4 .

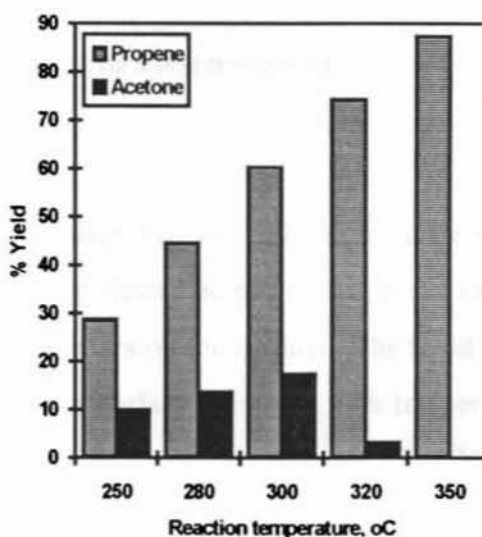


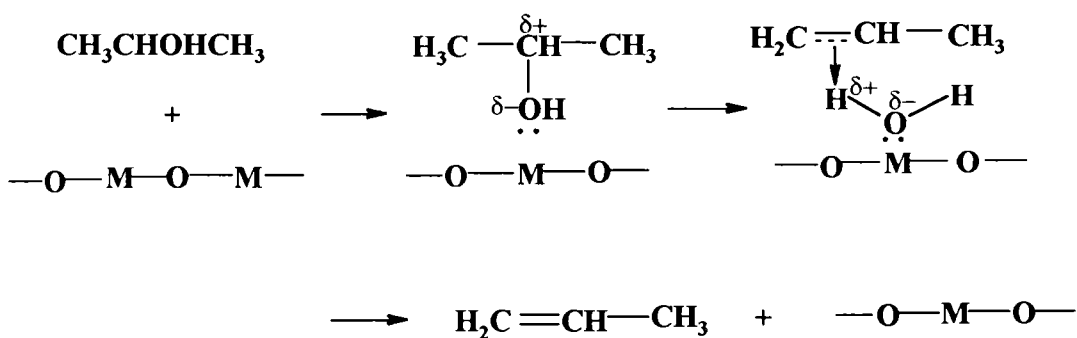
Fig. 3.3.2. Effect of reaction temperature on dehydration and dehydrogenation activities over CoFe_2O_4 .

In a similar way, the effect of reaction temperature on dehydration and dehydrogenation activities was studied using CoFe_2O_4 . It has been observed that at a contact time of 1.30 h, increase in the reaction temperature increased both dehydration and dehydrogenation in the lower temperature range upto 320°C (Fig.3.3.2). With further increase in temperature dehydration again increased, while a fall in the dehydrogenation activity was observed. Daniel *et al.* [10] while studying the dehydrogenation of isopropanol over chromia-alumina catalyst and Garcia de La Banda [11] while studying the same reaction with chromia catalyst were also investigated a similar behaviour. A probable reason, as suggested by them, is due to the change in the electronic nature of the material (i.e. a change from p-type to an n-type semiconductor). Many ferrites are exhibiting strong temperature sensitivity on their electronic properties [12,13]. Transformation from p-type to n-type creates excess electrons in the catalyst. Usually, dehydrogenation of isopropyl alcohol is associated with a transfer of electron from acetone to the catalyst surface. But due to the change in the electronic nature at high temperature the surface will become electron rich. This will affect the smooth transfer of electron from acetone to the surface. Hence, the desorption of acetone must be the rate controlling step [14].

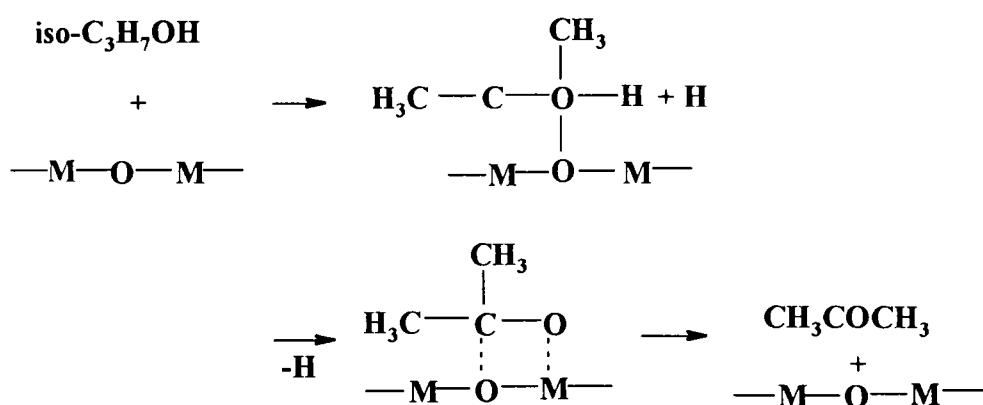
When acetone is desorbed rapidly, the surface reaction may proceed beyond the equilibrium value, but when the acetone can stay longer on the surface equilibrium for the reaction on the surface may be attained leading to a lesser amount of acetone in the gas phase.

However, a linear variation in the dehydration activity with temperature shows this reaction is independent of the variation in the electronic properties of the catalyst system. Dehydration is catalyzed by the acidic centers on the surface. The trend in the dehydration activity implies that the acidity of the surface increases with temperature. As suggested by Wolkenstein [15], the ability of the catalyst to break the C-OH bond during the chemisorption itself by polarizing the C-O bond leaving O-H bond intact may be important in catalyzing the dehydration reaction. This is facilitated by the presence of acidic groups on the surface. It is possible that for dehydration on ferrites a mechanism similar to the one proposed by Wolkenstein is prevalent.

(a) Mechanism of dehydration of isopropanol:

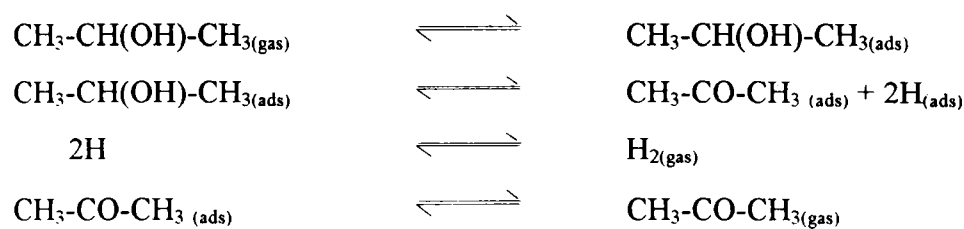


(b) Mechanism of dehydrogenation of isopropanol:



When the catalyst was poisoned with pyridine, the dehydration activity was significantly affected, whereas the dehydrogenation activity was slightly affected. The suppression of dehydrogenation by pyridine is due to the neutralization of the acidic groups on the surface that are responsible for the dehydration.

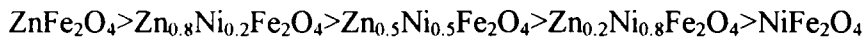
In order to determine the rate determining step of dehydrogenation, product inhibition studies were performed. The various steps of dehydrogenation reaction are:



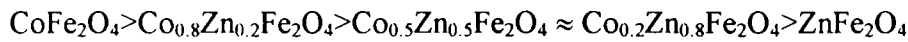
When the reaction was carried out under controlled hydrogen current, dehydrogenation activity remained more or less unaffected. However, addition of acetone in the feed significantly affected the dehydrogenation activity, indicating that the desorption of acetone is the rate determining step.

Thus, we can classify each series of ferrites according to their acid strength, as follows:

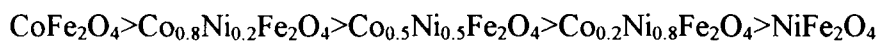
(a) Zn_{1-x}Ni_xFe₂O₄-type systems:



(b) Zn_{1-x}Co_xFe₂O₄-type systems:



(c) Co_{1-x}Ni_xFe₂O₄-type systems:



It has been observed that NiFe₂O₄ exhibits only poor dehydration activity, and the activity was found to be increased by substituting Ni²⁺ by Co²⁺ or by Zn²⁺. Incorporation of Zn²⁺ ions into NiFe₂O₄ matrix replaces an equivalent amount of Fe³⁺ ions from the tetrahedral site and the replaced Fe³⁺ ions occupy in the octahedral sublattice. When 'x' becomes 0, the spinel structure changes from inverse to normal, where all Fe³⁺ ions lie in the octahedral interstices. Zn²⁺ being a d¹⁰ system (filled d-shell) and also due to its occupancy in the less accessible tetrahedral sites, it is considered that Fe³⁺ ions in the octahedral site act as a possible active site for dehydrogenation. Thus, the concentration of Fe³⁺ ions in the octahedral sites act as a major factor influencing the acidity of Zn_{1-x}Ni_xFe₂O₄-type systems.

Though Zn-Co systems are structurally similar to the corresponding Zn-Ni systems, in the Zn-Co system, Co substitution enhanced the acidity of the system. This indicates that exposure of Co²⁺ ions creates stronger acid sites than due to Fe³⁺ ions. Supplementary evidence for this is obtained if we consider Co-Ni ferrite series, where Fe³⁺ ion concentration remained unaltered as the composition varies (both tetrahedral and octahedral sites contain equal amount (50 % each) of Fe³⁺ ions). Here only the Co²⁺/Ni²⁺ ratio varies from one member to the other. Large variation in the dehydrogenation activity clearly implies the creation of strong acid sites due to Co²⁺ ions.

Creation of acidic sites by octahedral ions can also be explained in another way. Due to the lower coordination number of the tetrahedral cations, the effective attractive force for a single tetrahedral M-O bond will be strong [6]. Since each octahedral cation is surrounded by more number of anions, the octahedral M-O bonds will be weaker, and, hence will be more polar. As suggested by Narasimhan *et al.* [7], weak octahedral M-O bonds act as strong alcohol adsorption centers. When Fe^{3+} ions are available in both tetrahedral and octahedral sites, the Fe^{3+} -O bond distance will be more when Fe^{3+} is in octahedral symmetry than when it is in tetrahedral symmetry. Hence, Fe^{3+} will be more readily available for adsorption of alcohol when it is in an octahedral site than in a tetrahedral site.

Thus, acidity of different systems shows a trend just opposite to their basicity. This indicates that, replacement of basic sites is associated with a concomitant generation of acid centers.

3.3.2. Cyclohexanol conversion--as a test of acid-base properties of ferrite catalysts:

Cyclohexanol conversion on oxide catalysts is recommended as another best model reaction for the acid-base properties of oxide catalysts. The amphoteric character of cyclohexanol permits their interaction with acid and base centers. Dehydration leads to cyclohexene whereas dehydrogenation gives cyclohexanone. Cyclohexene formation results from the reaction of cyclohexanol with Brønsted acid sites. The mechanism of dehydrogenation of cyclohexanol is given below (Fig. 3.3.3):

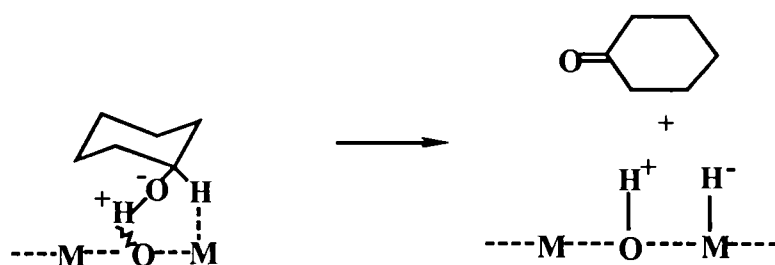


Fig. 3.3.3. Mechanism of dehydrogenation of cyclohexanol on oxide systems.

In addition to cyclohexene and cyclohexanone, trace amount of phenol, benzene and cyclohexane were also detected. Benzene and cyclohexane were formed via the disproportionation of cyclohexene formed as a result of dehydration of cyclohexanol [16]. Phenol formation was detected only at high contact times. It was reported that cyclohexanone (the dehydrogenation product) undergoes further transformation to phenol at high contact time [17]. Since the present work is carried out with an objective to evaluate the nature of acidity variation with composition of the systems, we have not taken any effort to understand the formation of products other than cyclohexene and cyclohexanone. Reactions were performed in a similar type of gas-phase set up used for the isopropanol decomposition studies. G.C was fitted with a $6' \times \frac{1}{8}$ " stainless steel column packed with 5 % NPQSB + 1 % H₃PO₄ on anachrom A 80/100 mesh.

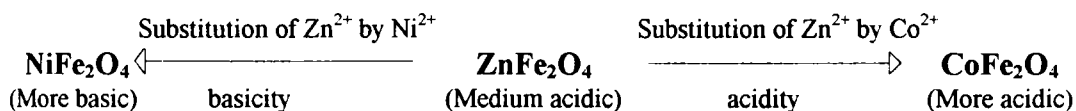
Product distribution	Cyclohexene	Cyclohexanone
Zn_{1-x}Ni_xFe₂O₄--series		
ZnFe ₂ O ₄	39.72	20.67
Zn _{0.8} Ni _{0.2} Fe ₂ O ₄	35.28	17.30
Zn _{0.5} Ni _{0.5} Fe ₂ O ₄	29.57	21.50
Zn _{0.2} Ni _{0.8} Fe ₂ O ₄	19.17	25.89
NiFe ₂ O ₄	12.03	31.11
Co_{1-x}Ni_xFe₂O₄--series		
CoFe ₂ O ₄	55.30	20.30
Co _{0.8} Ni _{0.2} Fe ₂ O ₄	37.27	22.30
Co _{0.5} Ni _{0.5} Fe ₂ O ₄	24.66	25.18
Co _{0.2} Ni _{0.8} Fe ₂ O ₄	16.70	28.22
NiFe ₂ O ₄	12.03	31.11
Zn_{1-x}Co_xFe₂O₄--series		
ZnFe ₂ O ₄	39.72	20.67
Zn _{0.8} Co _{0.2} Fe ₂ O ₄	40.40	36.81
Zn _{0.5} Co _{0.5} Fe ₂ O ₄	49.80	30.54
Zn _{0.2} Co _{0.8} Fe ₂ O ₄	52.40	25.35
CoFe ₂ O ₄	55.30	20.30

Table 3.3.4. Dehydration and dehydrogenation activities of ferrites. Reaction temperature 325 °C, contact time 1.3 h and TOS 2 h.

To correlate the acidity variation on substitution in each series, the dehydration and dehydrogenation activity at 325 °C and contact time 1.3 h are considered (Table: 3.3.4). From the table it is evident that Ni²⁺ substitution has a decreasing effect on dehydration activity on both Zn-ferrite and Co-ferrite, indicating removal of acidic sites originally present in these systems. Zn-Co systems did not show sharp variation in the acidity at low 'x' values, however, acidity significantly improved after x = 0.5. This leads to an appreciable difference in the acidity values of pure zinc-ferrite (*i.e.* ZnFe₂O₄) and pure cobalt-ferrite (*i.e.* CoFe₂O₄). Following conclusions can be drawn from the results:

1. NiFe₂O₄ is found to be least acidic. Ni addition substantially decreased the acidity in both Zn and Co-ferrites.
2. CoFe₂O₄ is found to be most acidic. ZnFe₂O₄ is moderately acidic. Co substitution increased the acidity of the Zn system.

The acidity change can be represented as:



Increase in temperature increased the dehydration activity of all the systems. However, dehydrogenation activity does not show any gradual change with rise in temperature. Increase in temperature will decompose surface hydroxyl ions and subsequently will create more Lewis acid centers. However, since the dehydrogenation, being a concerted reaction involving the participation of both acidic and basic centers on the surface, the dehydrogenation activity will depend on the relative amount of both type of sites. Since, in most cases, the creation of new acidic centers is usually associated with the destruction of some basic centers, the dehydrogenation activity will depend on both these factors. Additionally, as mentioned in the previous section, dehydrogenation activity will depend also on the electronic

nature of the material. Since most of the ferrite systems are reported to show temperature dependent conductivity variations, the change in dehydrogenation activity with temperature will depend, upto some extent, on the variation of the electronic nature of the surface in the temperature range studied. A typical activity profile diagram, obtained using $\text{Co}_{0.8}\text{Zn}_{0.2}\text{Fe}_2\text{O}_4$, is presented in the following figure (Fig. 3.3.4).

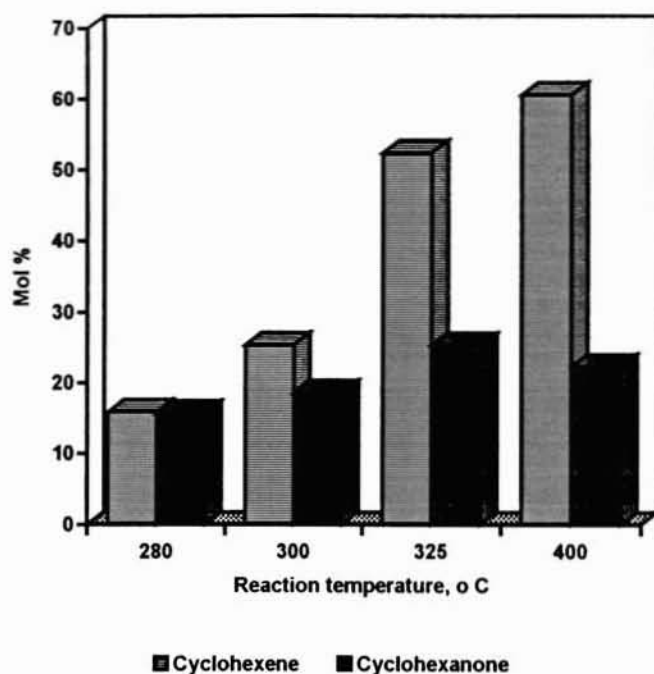


Fig. 3.3.4. Variation of dehydration and dehydrogenation reaction of cyclohexanol over $\text{Co}_{0.8}\text{Zn}_{0.2}\text{Fe}_2\text{O}_4$ as a function of reaction temperature.(Contact time 1.3 h & TOS 2 hours).

3.4. Oxidative dehydrogenation of ethylbenzene:

It has been reported that ethylbenzene may be dehydrogenated to styrene over some oxide catalysts either in the presence or absence of oxygen. In the absence of gas phase oxygen, lattice oxygen directly participates in this reaction, resulting in the bulk reduction of the catalyst. It is generally considered that ethylbenzene oxidative dehydrogenation reactions over metal oxides, including ferrites, proceed via a redox cycle, involving the reduction of at least one metal cation to a lower oxidation state by reaction with ethylbenzene and subsequent reoxidation back to the higher oxidation state by oxygen from gas phase. With a view to understand the influence of metal

cations in the spinel matrix, we carried out the oxidative dehydrogenation reaction of ethylbenzene.

The reactions were performed in a vapour-phase down-flow silica reactor, by passing 10 ml of air/minute alongwith ethyl benzene in the temperature range 350 - 500 °C. Products were analyzed using a Shimadzu GC-15A gas chromatograph fitted with a xylene-master capillary column and FID.

The results obtained using the various ferrite series at 500 °C and WHSV 1.2 h⁻¹ are presented in Tables 3.4.1, 3.4.2 and 3.4.3. In the Zn_{1-x}Co_xFe₂O₄ type systems, ZnFe₂O₄ exhibited good styrene selectivity. Both styrene yield and its selectivity decreased upto x = 0.5. Further increase in Co²⁺ ion concentration increased the yield and selectivity of styrene. Toluene was detected as a major side product when the spinel matrix contains more Zn²⁺ ions, whereas upon substituting Zn²⁺ by Co²⁺ toluene concentration decreased and benzene concentration increased. Both ethylbenzene conversion and styrene selectivity were maximum for CoFe₂O₄. Ni²⁺ substitution in Co as well as Zn systems decreased styrene selectivity. However, unlike the previous case, here toluene was detected as a major product and only poor yield of styrene was obtained. Significantly large amount of benzene was also detected, especially in the systems possessing high Ni²⁺ concentration. Since, large amount of ethylbenzene is undergoing disproportionation over Ni-containing systems, oxidative dehydrogenation activity is almost completely suppressed in the highly Ni-substituted systems.

$Zn_{1-x}Co_xFe_2O_4$	$x = 0$	$x = 0.2$	$x = 0.5$	$x = 0.8$	$x = 1.0$
Product distribution, wt. %					
Toluene	4.18	3.00	2.17	1.02	0.10
Benzene	0.47	1.61	2.01	2.74	3.83
Unreacted ethylbenzene	80.03	86.00	86.50	84.90	79.75
Others	0.59	Nil	0.50	Nil	0.02
Styrene	14.73	9.43	8.82	11.34	16.30
E.B conversion	19.97	14.04	13.50	15.1	20.23
Selectivity					
Toluene	21.56	21.36	16.07	7.03	0.49
Benzene	2.35	11.46	14.88	18.15	18.93
Styrene	76.00	67.16	65.33	75.09	80.57

Table 3.4.1. Product distribution and selectivity data of the oxidative dehydrogenation of ethyl benzene over Zn-Co ferrites. Reaction temperature 500 °C, WHSV 1.2 h⁻¹ and TOS 2 h.

$Co_{1-x}Ni_xFe_2O_4$	$x = 0$	$x = 0.2$	$x = 0.5$	$x = 0.8$	$x = 1.0$
Product distribution, wt. %					
Toluene	0.10	4.88	15.32	34.67	45.00
Benzene	3.83	0.43	3.50	10.05	13.34
Unreacted ethylbenzene	79.75	89.16	77.64	53.22	40.78
Others	0.02	0.21	0.21	0.94	Nil
Styrene	16.30	5.32	3.33	1.12	0.87
E.B conversion	20.23	10.84	22.36	46.78	59.22
Selectivity					
Toluene	0.49	45.02	68.51	74.11	75.98
Benzene	18.93	3.96	15.65	21.48	22.53
Styrene	80.57	49.07	14.89	2.39	1.46

Table 3.4.2. Product distribution and selectivity data of the oxidative dehydrogenation of ethyl benzene over Co-Ni ferrites. Reaction temperature 500 °C, WHSV 1.2 h⁻¹ and TOS 2 h.

$Zn_{1-x}Ni_xFe_2O_4$	x = 0	x = 0.2	x = 0.5	x = 0.8	x = 1.0
Product distribution, wt %					
Toluene	4.18	5.76	16.50	35.30	45
Benzene	0.47	0.51	4.28	10.74	13.34
Unreacted ethylbenzene	80.03	81.28	73.85	53.09	40.78
Others	0.59	Nil	Nil	Nil	Nil
Styrene	14.73	12.48	5.37	0.87	0.87
E.B conversion	19.97	18.72	26.15	46.91	59.22
Selectivity					
Toluene	21.56	30.72	63.09	75.25	75.98
Benzene	2.35	2.74	16.36	22.89	22.53
Styrene	76.00	66.56	20.53	1.85	1.46

Table 3.4.3. Product distribution and selectivity data of the oxidative dehydrogenation of ethyl benzene over Zn-Ni ferrites. Reaction temperature 500 °C, WHSV 1.2 h⁻¹ and TOS 2 h.

The formation of toluene and benzene is caused by the interaction of acid-base centers on the catalyst surface, as reported by Wang *et al.* [18] and by Krouse *et al.* [19]. We have already noticed that, cobalt addition created acidic centers on the system. According to Wang *et al.*, strong acidic sites can abstract α -hydrogen of ethylbenzene and, thus, facilitating the cleavage of phenyl-C bond, resulting higher yield of benzene. Hence, catalysts $Zn_{0.2}Co_{0.8}Fe_2O_4$ and $CoFe_2O_4$, owing to their high acidity, abstracts α -hydrogen of ethylbenzene, and the subsequent bond cleavage afforded more amount of benzene. In a similar way, Krouse *et al.* [19] have suggested that strong basic sites can abstract the β -hydrogen of ethylbenzene which facilitates the cleavage of side chain C-C bond resulting in the formation of toluene. From the adsorption experiments using electron acceptors, we have clearly identified the strong basic centers created during Ni substitution in both Co and Zn systems. Hence, the increased yield of toluene on Ni containing systems can be attributed to their increased basicity upon Ni-substitution, which facilitates β -hydrogen abstraction of ethylbenzene resulting in the cleavage of side chain C-C bond. Also, the increase in toluene yield is

associated with a concomitant increase in benzene yield. When toluene alone was passed over these systems at 500 °C, appreciable amount of benzene was detected. This indicates that toluene formed from ethylbenzene further undergoing disproportionation, and giving more amount of benzene. The following figures (Figs. 3.4.1 and 3.4.2) represent the conversion and selectivity data over $Zn_{1-x}Co_xFe_2O_4$ and $Co_{1-x}Ni_xFe_2O_4$ type systems.

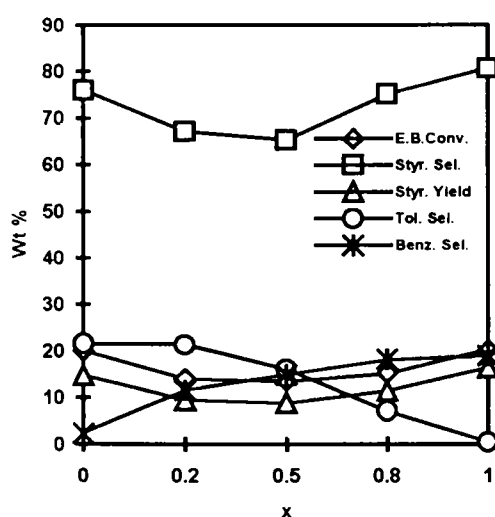


Fig. 3.4.1 Ethylbenzene conversion and product distribution in presence of air over $Zn_{1-x}Co_xFe_2O_4$.

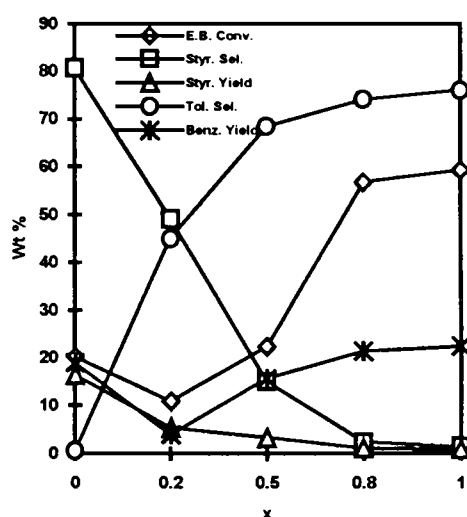


Fig. 3.4.2 Ethylbenzene conversion and product distribution in presence of air over $Co_{1-x}Ni_xFe_2O_4$.

The results of dehydrogenation over $ZnFe_2O_4$, as a function of temperature are presented in Fig.3.4.3, which show an increasing trend for styrene yield and ethylbenzene conversion. The reaction of ethylbenzene to styrene is endothermic with $\Delta H = 124.9$ kJ/mol [20]. Hence an increase in temperature will always favour the reaction. However, styrene selectivity increased first in the temperature range of 350 to 450 °C and thereafter it decreased due to the higher rate of disproportionation reactions at high temperature. Higher amount of benzene and toluene formed at 500 °C supports this conclusion.

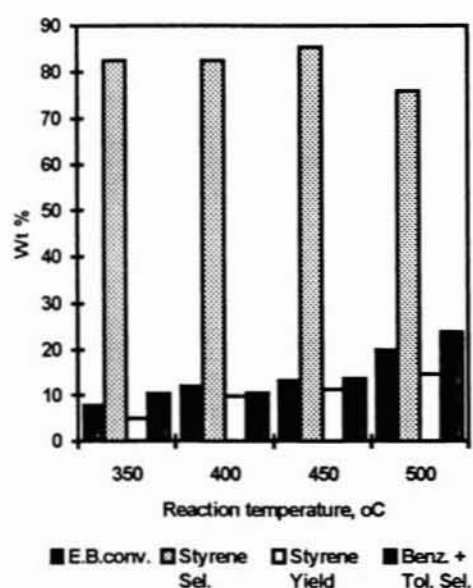


Fig. 3.4.3. Effect of reaction temperature on product distribution of ethylbenzene dehydrogenation over $ZnFe_2O_4$.

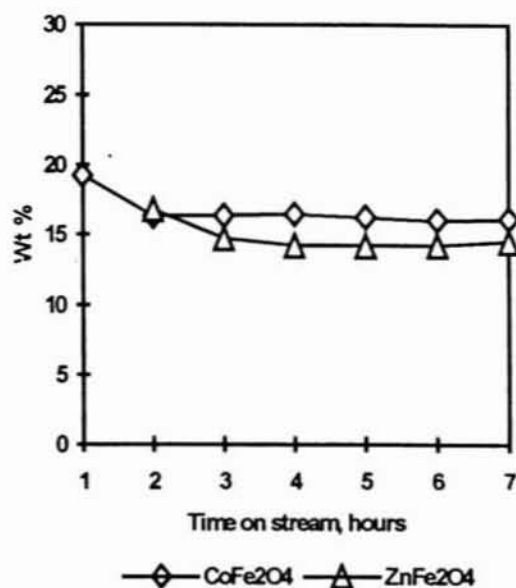
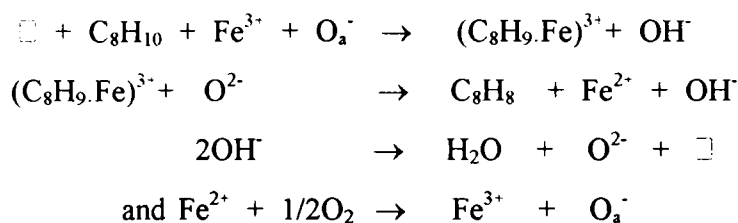


Fig. 3.4.4. Effect of time on stream on ethylbenzene oxidative dehydrogenation over $ZnFe_2O_4$ and $CoFe_2O_4$.

Another set of experiments were carried out to evaluate the stability of the systems. A typical activity profile for $ZnFe_2O_4$ and $CoFe_2O_4$ as a function of time on stream is shown in Fig.3.4.4. From the figure it is clear that, even in the presence of gaseous oxygen, styrene yield initially decreased with time on stream. This indicates that the catalyst oxygen has a major effect on the reaction rates, whereas the gas-phase oxygen may serve only in reoxidising the catalyst itself.

To understand the nature of the active sites for oxidative dehydrogenation, Jabarathinam *et al.* [21] carried out some oxygen chemisorption experiments over Zn-Fe-Cr ternary spinel systems. They observed that, the amount of oxygen chemisorbed was high on the spent catalysts than on the fresh ones. The high oxygen chemisorption of spent systems indicates reoxidation of Fe^{2+} and Fe^0 to the original Fe^{3+} form. It is reasonable to accept a similar type of redox cycle involving $Fe^{3+} \rightleftharpoons Fe^{2+}$ as an active process for the present systems also. Hence the mechanism suggested by Jabarathinam *et al.* and Rennard *et al.* [22] can be applied for the present case.



where \square is an anion vacancy adjacent to an Fe^{3+} , O_a^- is an adsorbed oxygen ion, O^{2-} is a lattice oxygen and $(\text{C}_8\text{H}_9\text{Fe})^{3+}$ is a complex. The relative high yield of styrene over ZnFe_2O_4 and CoFe_2O_4 is due to the presence of stable $\text{Fe}^{3+}/\text{Fe}^{2+}$ redox couple on the catalyst. However, in the absence of gas-phase oxygen styrene will be formed only until the adsorbed oxygen is consumed. This results in a sharp decline in the activity. The spinel structure itself is not a sufficient criterion for catalytic activity and that the presence of a reducible cation is necessary for oxidation. In ZnFe_2O_4 , Zn^{2+} is not easily reducible, whereas Fe^{3+} can be readily reduced to Fe^{2+} . Greater reducibility of Co ion relative to the Ni ion may be the reason for the large difference in the activity of the Co-Ni systems.

In order to understand the nature of the catalyst after the reaction we have taken the Mössbauer spectra of CoFe_2O_4 and ZnFe_2O_4 before and after the reaction. The room temperature spectra of fresh ZnFe_2O_4 and CoFe_2O_4 are shown in Fig. 3.4.5 and Fig. 3.4.6 respectively. It has been shown that [23] for well characterized ferric ions, the isomer shift is approximately 0.5 mm/sec, and on this basis it is clear from the figures that, the iron is present as Fe^{3+} in both catalysts. The quadrupole splitting data shown in figures were calculated from the central line which correspond to a phase in which the energy levels are not subjected to Zeeman splitting. CoFe_2O_4 is a ferrimagnetic spinel, in which the inter-sublattice magnetic interaction is stronger than either of the intra-sublattice interactions. The hyperfine pattern of CoFe_2O_4 is also shown (Fig. 3.4.7). ZnFe_2O_4 is a normal spinel with Zn^{2+} ion in the A site and both the Fe^{3+} ions occupying the B sites. There can be neither A-B interaction nor A-A interaction since Zn^{2+} is a non-magnetic ion. The only prevalent magnetic interaction is B-B interaction between Fe^{3+} ions, which is antiferromagnetic. ZnFe_2O_4 does not show any hyperfine pattern at room temperature due to its low magnetic phase component, while in CoFe_2O_4 it is a major component and iron nuclei are located in two different types of sites.

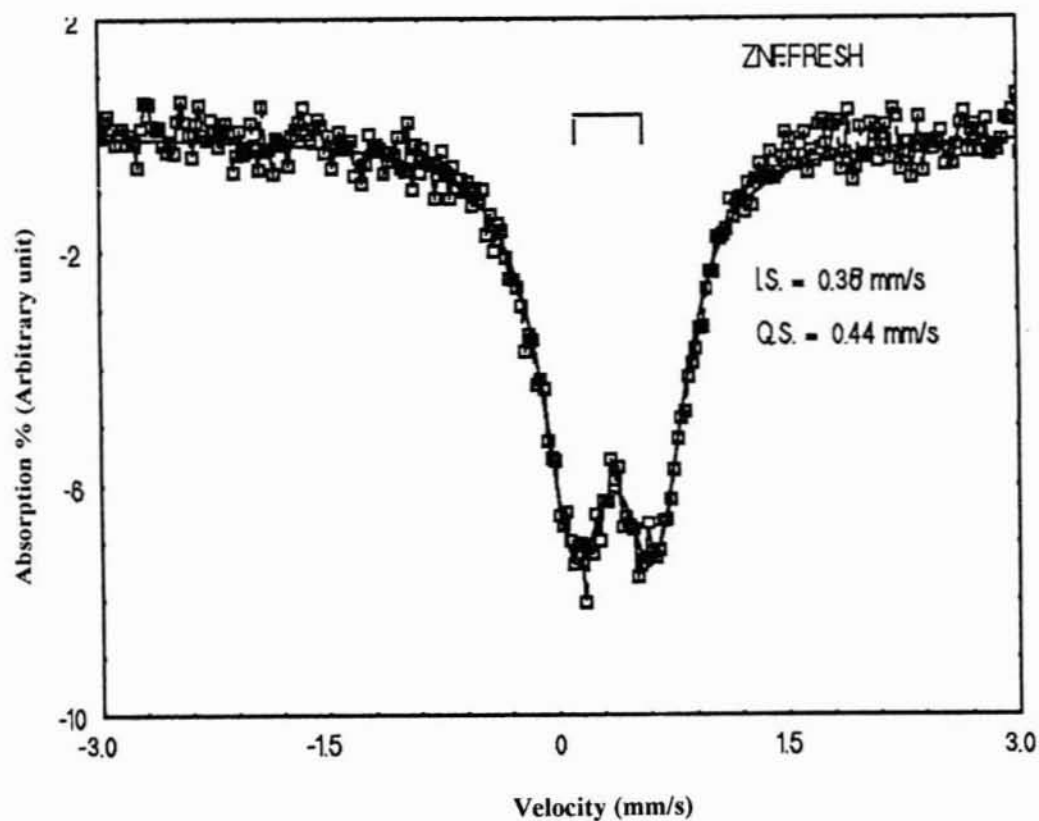


Fig. 3.4.5 Room temperature Mössbauer spectrum of fresh ZnFe_2O_4 .

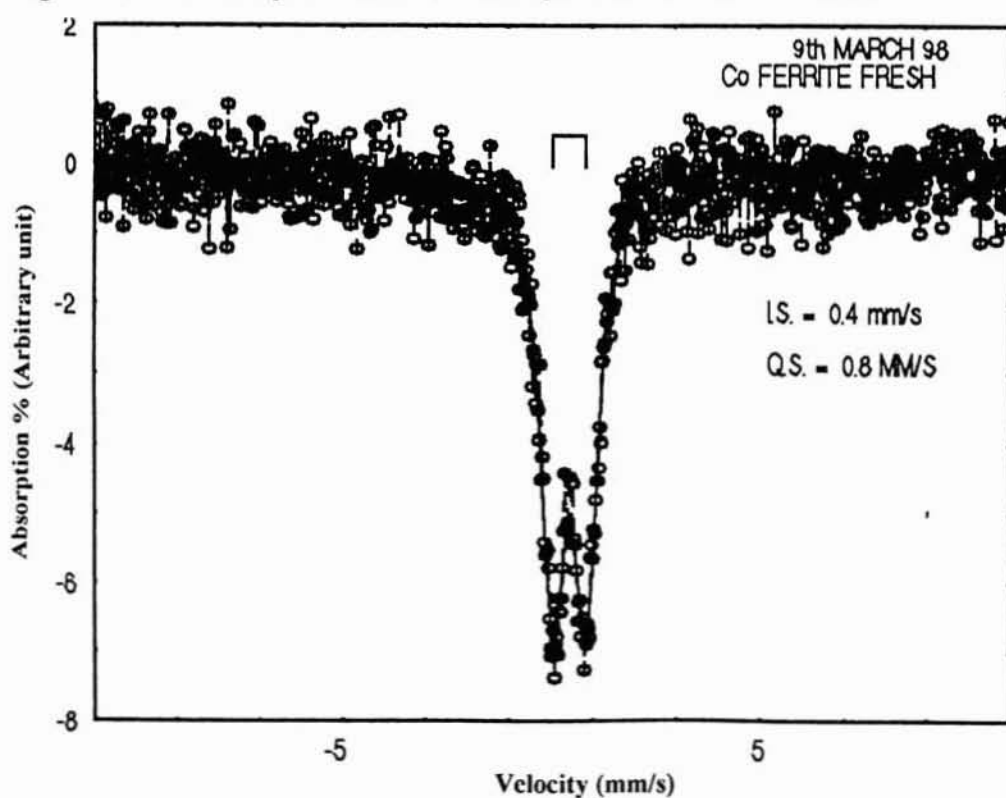


Fig. 3.4.6 Room temperature Mössbauer spectrum of fresh CoFe_2O_4 .

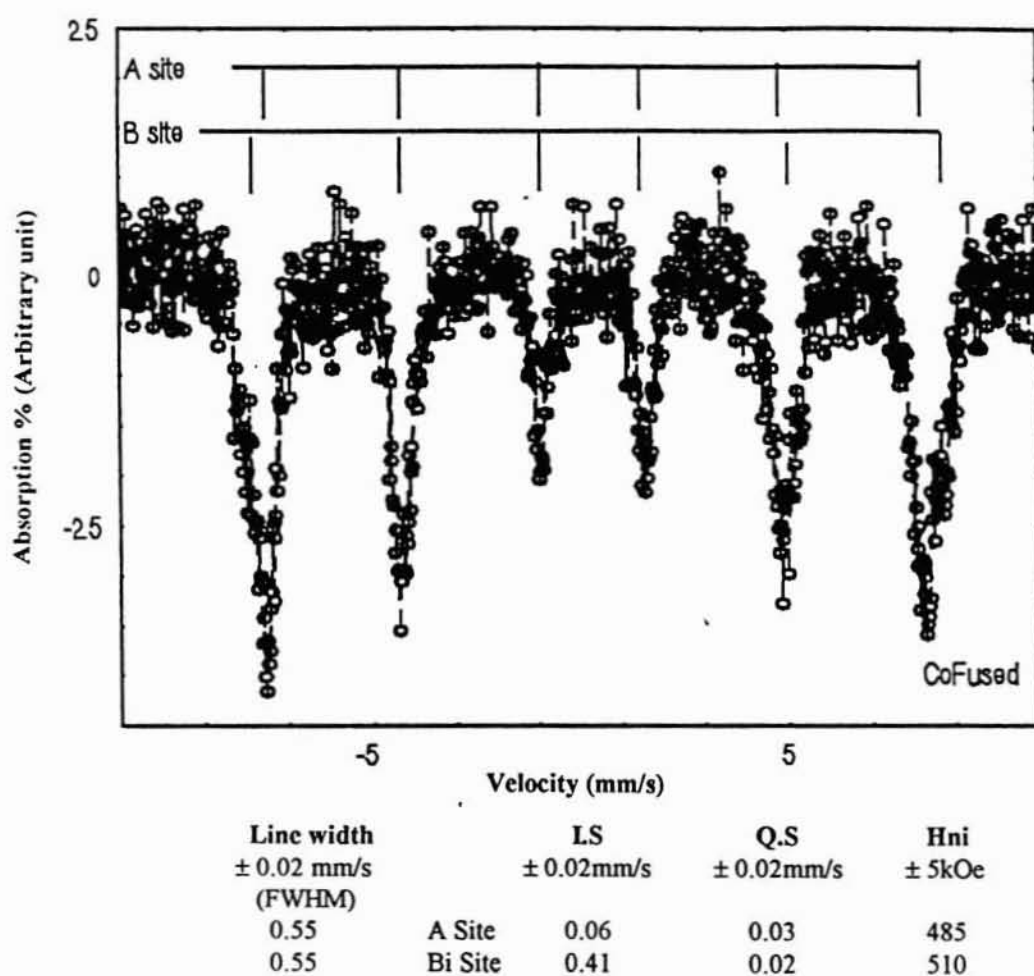


Fig. 3.4.7 Hyperfine pattern of CoFe_2O_4 .

The room temperature spectra of ZnFe_2O_4 and CoFe_2O_4 after use for the oxidative dehydrogenation of ethyl benzene are shown in Fig. 3.4.6 and Fig.3.4.7 respectively. Mössbauer isomer shift is a parameter by which the nature of different cationic oxidation states in a catalyst may be monitored. The isomer shift values of used systems are nearly identical with the fresh ones. Thus, the similarity and nature of the spectra for fresh and used systems suggest that no major bulk reduction has happened after the reaction.

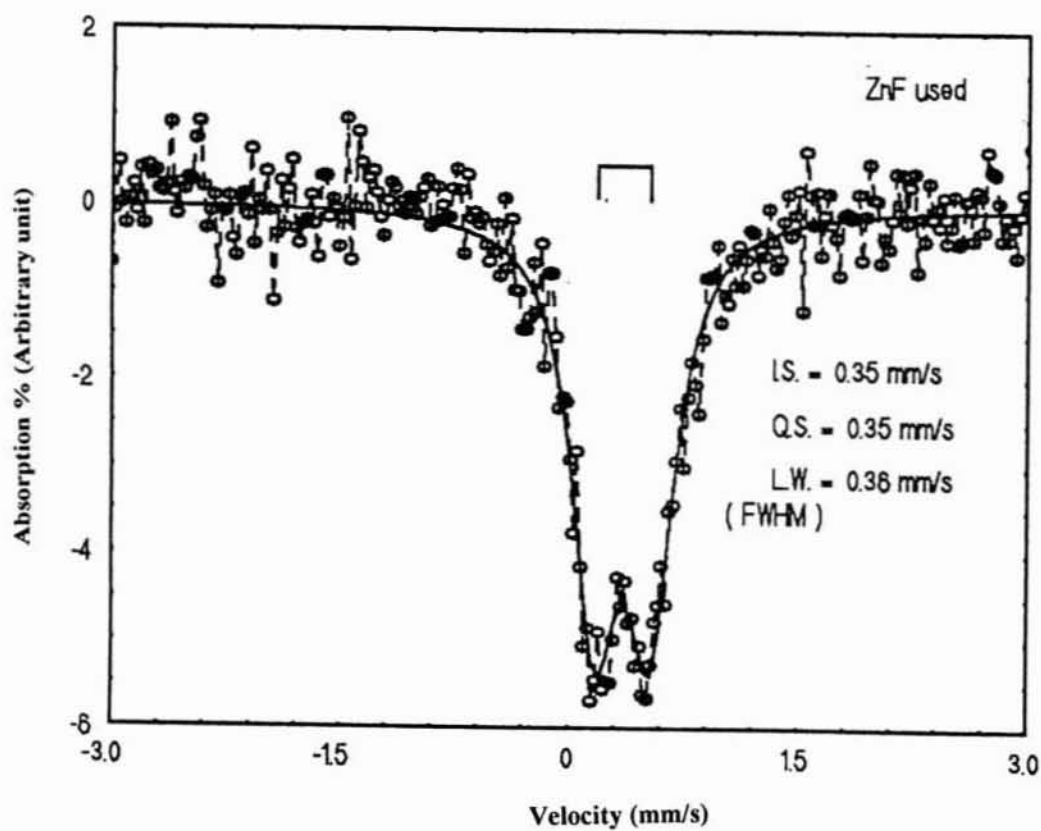


Fig. 3.4.8 Room temperature Mössbauer spectrum of used ZnFe_2O_4 .

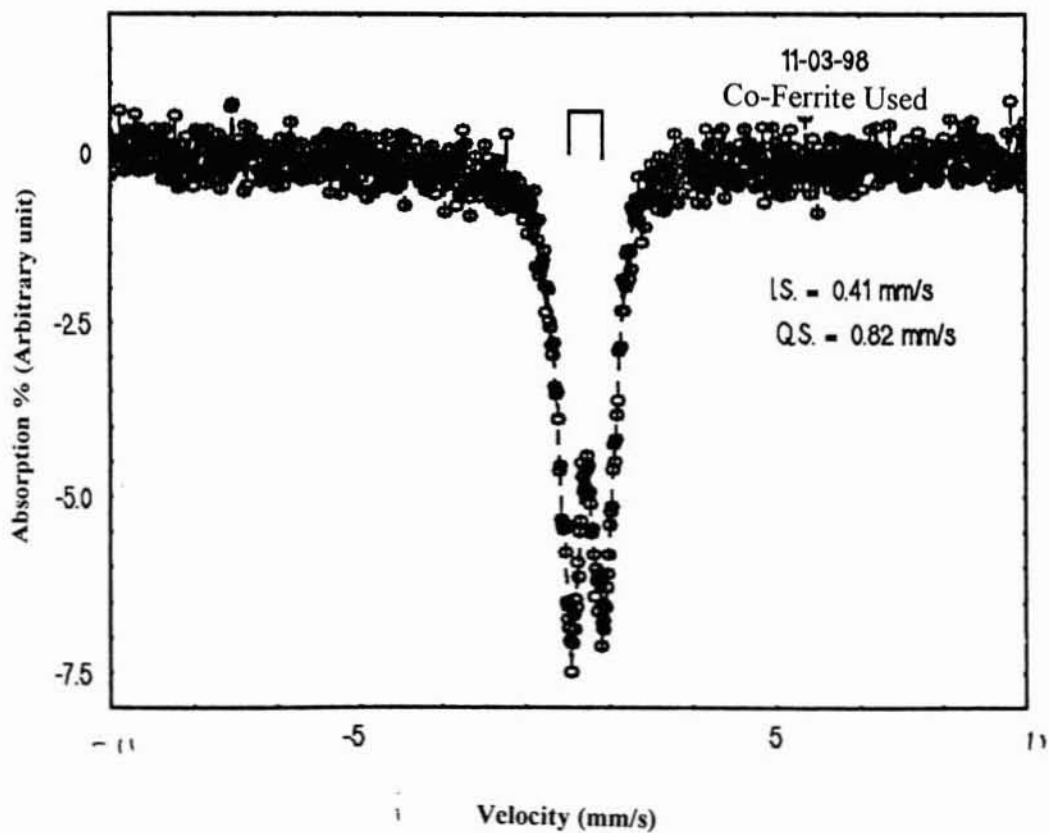


Fig. 3.4.9 Room temperature Mössbauer spectrum of used CoFe_2O_4 .

REFERENCES

- [1] P.S. Anil Kumar, J.J. Shotri, S.D. Kulkarni, C.E. Deshpande, S.K. Date; *Materials Letters* 27 (1996) 293.
- [2] R.D. Waldron; *Phy. Rev.*, 99 (1955) 1727.
- [3] W.B. White and B.A. De Angelis; *Spectrochim Acta A*, 23 (1967) 985.
- [4] J. Preudhomme and P. Tarte; *Spectrochim Acta*, 27 (1971) 961.
- [5] J.P. Jacobs, A. Maltha, J.R.H. Reintjes, T. Dimal, V. Ponec and H.H. Brogersma; *J. Catal.*, 147 (1994) 294.
- [6] F.C. Romeijin; *Phil. Res. Rep.*, 8 (1953) 304.
- [7] C.S. Narasimhan, C.S. Swamy; *Appl. Catal.*, 2 (1982) 315.
- [8] K. Meguro and K. Isumi; *J. Colloid Interface Sci.*, 59 (1973) 93.
- [9] V. Krishnasamy and S. Chokkalingam; *J. Indian Chem. Soc.*, Vol LIX, May 1982, 641.
- [10] C. Daniel and J.C. Kuriacose; *Ind. J. Chem*; 6 (1968) 136.
- [11] J.F. Garcia De La Banda; *J. Catal.*, 1 (1962) 136.
- [12] P. Manjula; in: *Ferrite Materials*, Edited by B. Viswanathan and V.R.K. Murthy, Narosha Publishing House, p. 26-35 (1990).
- [13] T. Seshagiri Rao; in: *Ferrite Materials*, Edited by B. Viswanathan and V.R.K. Murthy, Narosha Publishing House, p. 38-55 (1990).
- [14] E. Wicke; *Z. Electrochem*, 52 (1948) 86; 53 (1949) 279.
- [15] Th. Wolkenstein; *Adv. Catalysis*, 12 (1960) 189.
- [16] M. Dobrovosky, P. Tenyi and Z. Paal; *J. Catal.*, 74 (1982) 31.
- [17] N.J. Jabarathinam and V. Krishnasamy; In: *Intermediate Series on Chemical Engineering - Catalysis: Present and Future*, Editors: P. Kanta Rao and B.S. Benwal, Publication and Information Directorate, New Delhi and Wiley Eastern Ltd. New Delhi, p. 288.
- [18] I. Wang, W.F. Chang, R.J. Shieu, J.C. Wu and C.S. Chang; *J. Catal.*, 83 (1983) 438.
- [19] A. Krause; *Sci. Pharm.*, 38 (1970) 266.
- [20] E.H. Lee; *Catal. Rev.*, 8 (1973) 285.
- [21] N.J. Jabarathinam, M. Eswaramoorthy and V. Krishnasamy; *Appl. Catal. A*,

145 (1996) 57.

[22] R.J. Rennard and W.L. Kehl; *J. Catal.*, 21 (1971) 282.

CHAPTER IV
ALKYLATION OF ANILINE

4.1. INTRODUCTION

Methylation of aniline is industrially important owing to the numerous uses of various substituted anilines like N-methylaniline (NMA), N,N-dimethylaniline (NNDMA), toluidines, N-methyltoluidines and Xylidines [1]. A schematic representation of the various pathways of aniline methylation using methanol as the alkylating agent is presented below (Fig: 4.1).

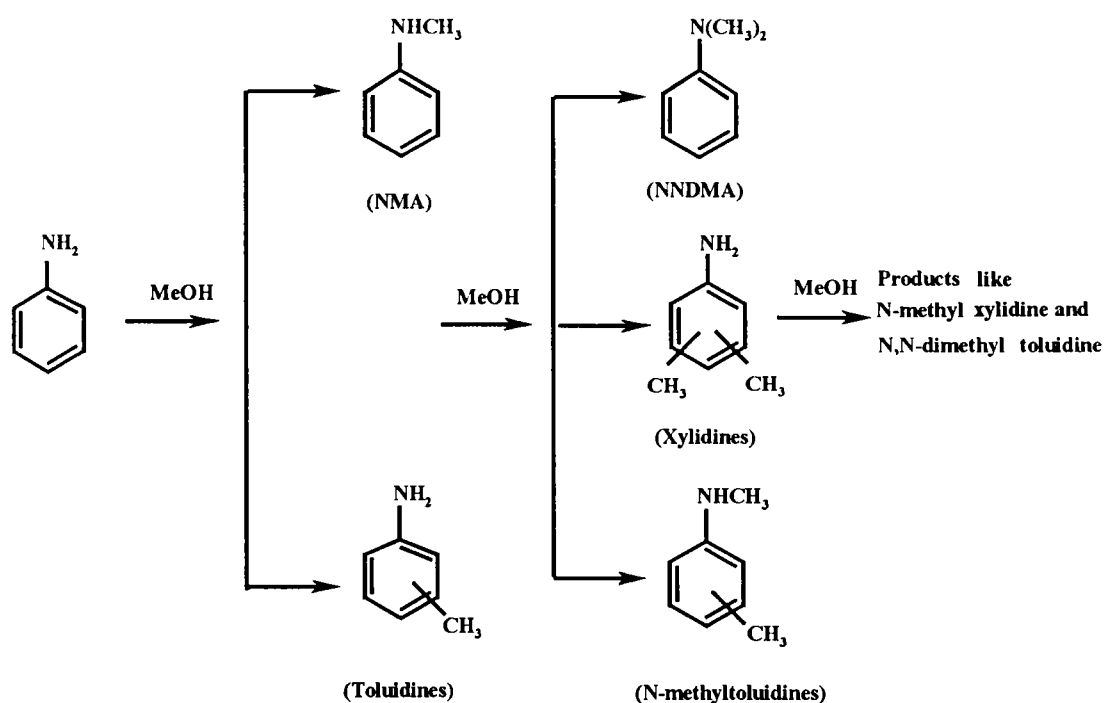


Fig. 4.1. Reaction scheme of aniline alkylation using methanol as the alkylating agent.

Many of these aniline derivatives are important in synthetic organic chemistry. Many of these compounds are acting as building blocks in various aniline based products, including dyes, pharmaceuticals, explosives and agrochemicals.

Initially aniline was alkylated with methanol in the liquid phase at high pressure using acid or halide as catalysts [2]. The use of aluminum alkoxides and strong acids as catalyst has also been reported [3,4]. Another common method of alkylation use dimethyl sulfate or alkyl halides as the alkylating agents [5]. There are, however, significant disadvantages in carrying out alkylation with these agents:

1. Dimethyl sulphate and methyl halides are toxic and also corrosive. Therefore, acid-resistant materials must be used for the reactors.

2. Since the reaction proceeds in basic media, stoichiometric amounts of bases are required to neutralize the acid (HCl) that is formed. This results in the stoichiometric formation of inorganic solids (NaCl), which have to be disposed of properly.

3. Reactions in the liquid-phase usually require tedious and expensive procedures for separating solvents from products.

To avoid these disadvantages, solid acids or bases are introduced as the catalysts and toxic alkylating agents are replaced by non-toxic alkylating agents such as methanol and dimethyl carbonate. By performing alkylations in vapour-phase reactors, the tedious and expensive procedures associated with liquid-phase reactions can also be avoided.

Thus, a broad range of solid acid systems have been introduced, due to their eco-friendly nature and their potential to replace the conventional Friedel-Crafts type systems. In this connection several alkylation reactions have been tried over zeolites [6,7], oxides [8,9], supported oxides [10] and clays [11,12]. However, in the reaction using solid acid catalysts, formation of the primary product, *i.e.* NMA is always associated with the formation of N,N-dialkylated and C-alkylated products. Though metal oxides were reported to show better selectivity for N-alkylation over C-alkylation, usually many such systems afford both mono and di-substitution on nitrogen, leading to poor selectivity for the synthetically more important mono-substituted product. Many reported systems were found to be active at sufficiently high reaction temperatures. Moreover, in many cases, large methanol to aniline molar ratio was maintained, which leads to large loss of methanol due to decomposition. The present part of the thesis deals with the detailed investigation of $Zn_{1-x}Co_xFe_2O_4$, $Zn_{1-x}Ni_xFe_2O_4$ and $Co_{1-x}Ni_xFe_2O_4$ -type ferrosphenel systems for aniline alkylation using methanol as the alkylating agent. The objectives are to investigate the reaction pathways and associated mechanism and to correlate the activity with acid-base

properties and composition of the catalysts. In addition, the influence of various reaction parameters such as methanol to aniline molar ratio, time-on-stream, reaction temperature and contact time are studied. Interestingly, while performing the alkylation reactions with ferrite systems, we observed that these systems, particularly $Zn_{1-x}Co_xFe_2O_4$ and $Zn_{1-x}Ni_xFe_2O_4$, were highly selective for N-monomethylation of aniline. High NMA yield was observed even at comparatively low methanol to aniline molar ratio.

Reaction runs were carried out in a fixed-bed, down-flow silica reactor at 300-400 °C under atmospheric pressure. The catalyst was placed at the centre of the reactor; it was activated at 500 °C in flowing air, and brought down to the corresponding reaction temperatures by cooling under a current of nitrogen gas of high purity. The mixture of aniline and methanol was fed by a syringe pump. Liquid products were analyzed by a Shimadzu GC-15 A gas chromatograph using FID and 2 M, 2% carbowax 20M + 5% KOH on a chromosorb W column. The gaseous products were analyzed using a porapak -Q column with TCD. A blank run without any catalyst indicated negligible thermal reaction.

The chapter is divided into two chapters. The effect of various reaction parameters on product distribution over the three series of ferrite catalyst is discussed in the first section. A detailed discussion regarding the catalytic pathway and the influence of factors such as catalyst composition, their acidity and basicity is presented in the second section. Catalytic activity is correlated with acid-base properties determined by alcohol decomposition reactions and electron acceptor adsorption studies. Selectivities of the products were calculated using the following equation:

$$\text{Selectivity of the product 'i'} = \frac{\text{Wt. \% of the product 'i'}}{\text{Wt. \% of aniline converted}} \times 100$$

SECTION I -- PROCESS OPTIMIZATION.

4.2. $Zn_{1-x}Co_xFe_2O_4$ ($x = 0, 0.2, 0.5, 0.8$ and 1.0)-TYPE SYSTEMS

4.2.1 Effect of methanol to aniline molar ratio: In order to understand the optimum feed-mix ratio, a series of experiments were performed at 350°C with different molar ratios of methanol to aniline over $Zn_{0.8}Co_{0.2}Fe_2O_4$ (Fig. 4.2.1). In all cases N-methylaniline has been detected as the major product. Slight amount of aniline was detected at higher feed-mix ratios and no toluidines were detected throughout the experiments. Even at a methanol to aniline molar ratio of 2, the catalyst showed excellent NMA yield, whereas its yield significantly improved upto a molar ratio of 5. However, on further increasing the molar ratio NMA yield decreased, and correspondingly more amount of NNDMA was produced, indicating consecutive methylation of NMA in the presence of sufficiently large amount of the alkylating agent.

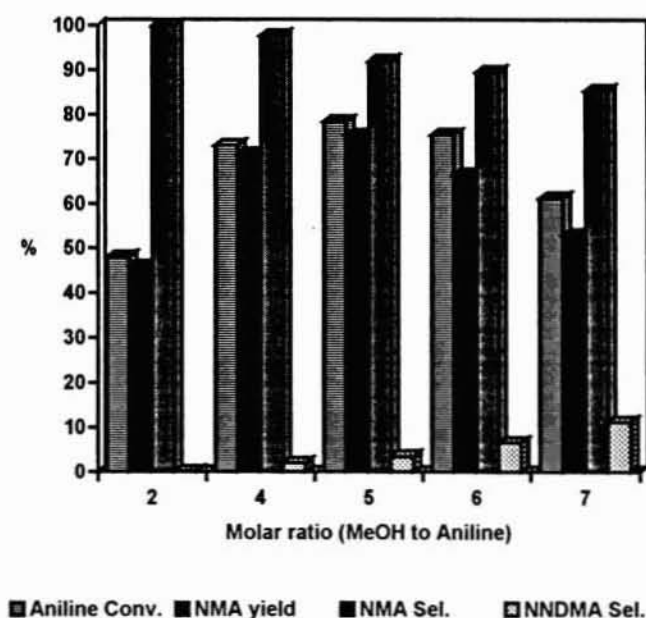


Fig. 4.2.1. Effect of methanol to aniline molar ratio on aniline conversion, NMA yield and NMA, NNDMA selectivities over $Zn_{0.8}Co_{0.2}Fe_2O_4$. WHSV 1.3 h^{-1} ; reaction temperature 350°C ; TOS 1 h.

4.2.2 Effect of time-on-stream: Stability studies of different catalysts were performed by observing NMA yield over a period of six hours. Reactions were carried out at 350 °C and product analysis was done at regular intervals of 60 minutes; data are presented in Fig. 4.2.2. All catalysts except ZnFe₂O₄ showed prolonged stability, and with ZnFe₂O₄ also selectivity was much less affected. Poor stability of ZnFe₂O₄ is probably due to the reduction of Fe³⁺ ions in the reducing atmosphere, and the normal spinel structure of the system prevents fast redistribution of electrons and thus to regain their original oxidation states quickly. Zn_{0.8}Co_{0.2}Fe₂O₄, a system possessing inverse spinel lattice, showed excellent activity and stability over a long period of time.

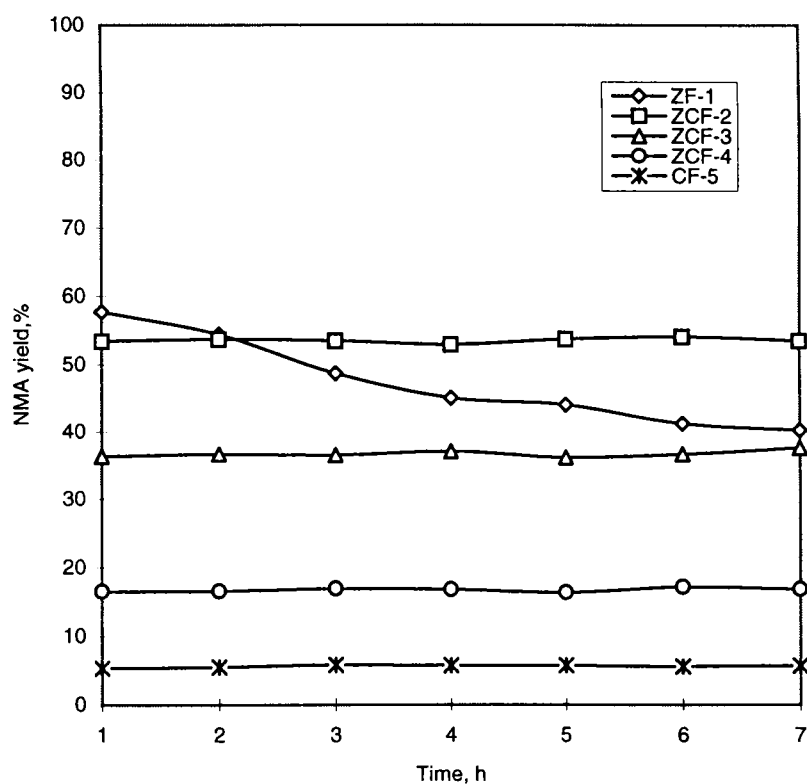


Fig. 4.2.2. Effect of time on stream: Concentration of N-methylaniline (Wt %) is plotted as a function of reaction time in hours over different Zn-Co ferros spinels. Reaction temperature 350°C, feed molar ratio (methanol to aniline) 2. ZF-1 (ZnFe₂O₄); ZCF-2 (Zn_{0.8}Co_{0.2}Fe₂O₄); ZCF-3 (Zn_{0.5}Co_{0.5}Fe₂O₄); ZCF-4 (Zn_{0.2}Co_{0.8}Fe₂O₄); CF-5 (CoFe₂O₄).

4.2.3 Effect of catalyst composition: The effect of catalyst composition on activity and selectivity is shown in Fig: 4.2.3. An examination of the figure reveals that zinc-cobalt ratio in the spinel lattice is a decisive factor greatly affecting product selectivity and conversion. At low 'x' values the selectivity for NMA is increased; $ZnFe_2O_4$, $Zn_{0.8}Co_{0.2}Fe_2O_4$ and $Zn_{0.5}Co_{0.5}Fe_2O_4$ showed nearly 99 % NMA selectivity. The influence of 'x' on NMA yield was much more pronounced. Even at a methanol to aniline molar ratio of 2 both $ZnFe_2O_4$ and $Zn_{0.8}Co_{0.2}Fe_2O_4$ exhibited very high activity for the N-monoalkylation of aniline (NMA yield nearly 51 and 44 % respectively). However with pure cobalt ferrite, where $x = 1$, selectivity for NMA was only 10 %. Large amount of secondary products viz. benzene and toluene, as a result of deamination of aniline, were also detected on this system.

4.2.4 Effect of reaction temperature and feed flow rate: Catalyst runs have been performed over all systems in the temperature range between 250-400 °C. The results are presented in Table 4.2.1. The data were obtained by analyzing the samples 60 minutes after the commencement of the reaction. Temperature has a marked influence on aniline conversion. Alkylation of aniline takes place effectively at temperatures above 250 °C. It is clear from the table that, for systems having 'x' values 0 and 0.2, hardly any ring alkylated products were formed and only N-alkylation takes place with NMA selectivity always greater than 90% in the temperature range between 300 to 350 °C. Upto 350 °C, both aniline conversion and NMA yield improved with rise in temperature. Maximum yield of NMA was observed at 350 °C, with selectivity more than 91%. The temperature range providing maximum yield of NNDMA was 350-370°C; however its yield was within 7 %. Further increase in temperature did not improve alkylation activity, but at higher temperature methanol decomposed in greater extent giving products like CO, CO₂, and traces of C₁ and C₂ hydrocarbons. The high self-decomposition rate of methanol over the catalysts above 350 °C was further clarified by passing methanol alone in the temperature range selected for alkylation experiments. Thus it indicates that the optimum temperature range for selective NMA formation is 300-350 °C.

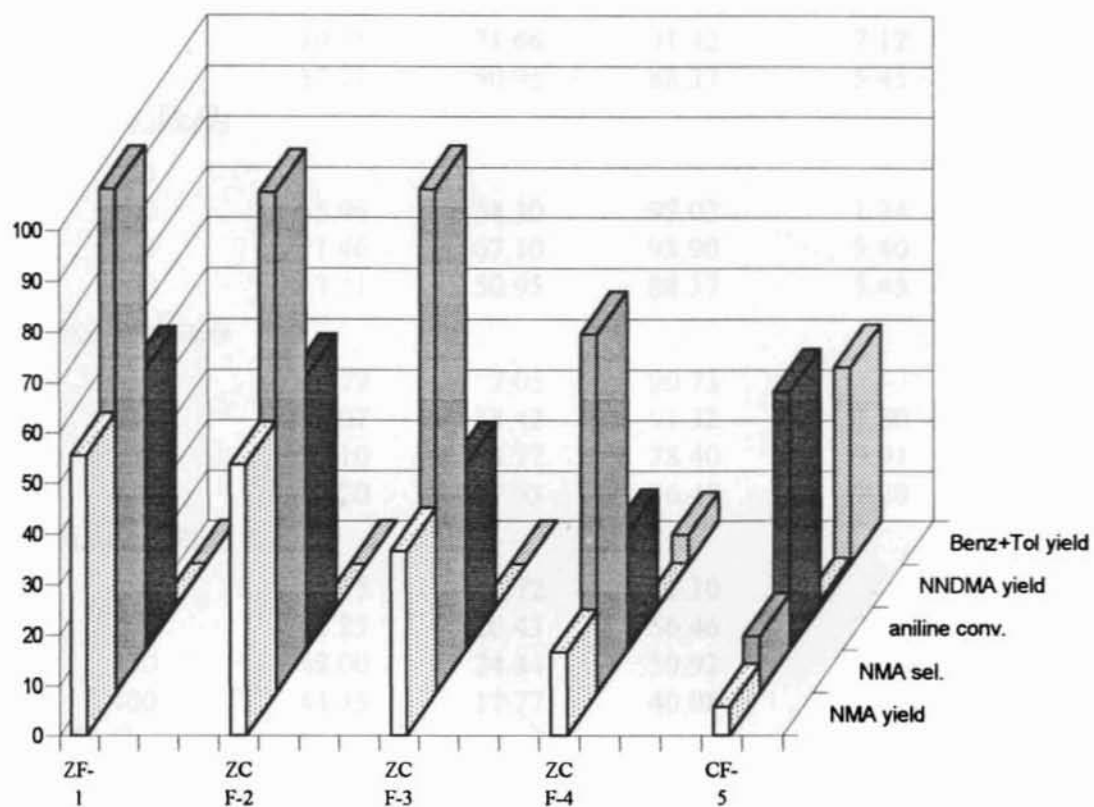


Fig.4.2.3. Product distribution and selectivity pattern of aniline alkylation over different Zn-Co ferrite systems. (Catalyst amount 3g, reaction temperature 350 °C, TOS 2 h, feed flow rate 6 ml/h, MeOH-aniline molar ratio2:1).

Catalyst designation: ZF-1 ($ZnFe_2O_4$); ZCF-2 ($Zn_{0.8}Co_{0.2}Fe_2O_4$); ZCF-3 ($Zn_{0.5}Co_{0.5}Fe_2O_4$); ZCF-4 ($Zn_{0.2}Co_{0.8}Fe_2O_4$); CF-5 ($CoFe_2O_4$).

Reaction temperature, °C	Aniline conversion	NMA yield %	NMA selectivity, %	NNDMA yield, %	Benz. + Tol. yield, %
<u>ZnFe₂O₄</u>					
250	14.35	14.05	97.90	--	--
300	55.96	55.10	98.46	--	0.45
350	79.55	71.66	91.42	7.12	1.00
400	57.71	50.95	88.37	5.45	1.80
<u>Zn_{0.8}Co_{0.2}Fe₂O₄</u>					
250					
300	55.96	54.30	97.03	1.34	0.73
350	71.46	67.10	93.90	5.40	1.28
400	57.71	50.95	88.37	5.45	3.00
<u>Zn_{0.5}Co_{0.5}Fe₂O₄</u>					
250	7.77	7.05	90.73	--	0.50
300	42.07	38.42	91.32	1.80	1.21
350	57.10	44.77	78.40	9.91	2.17
400	49.20	37.63	76.48	7.20	3.40
<u>Zn_{0.2}Co_{0.8}Fe₂O₄</u>					
250	11.15	5.72	51.30	--	5.42
300	36.25	20.43	56.46	2.00	13.63
350	48.00	24.44	50.92	4.17	19.20
400	44.33	17.77	40.08	5.77	20.21
<u>CoFe₂O₄</u>					
250	23.80	3.03	12.73	0.54	20.20
300	49.20	8.08	16.42	2.02	38.98
350	53.47	7.42	13.87	4.02	42.00
400	54.10	4.37	8.07	4.14	45.50

Table 4.2.1. Effect of reaction temperature on aniline alkylation using Zn_{1-x}Co_xFe₂O₄ type systems. Methanol to aniline molar ratio 6, flow rate 6 ml/minute, catalyst amount 3 g.

Figure 4.2.4. shows the effect of flow rate on aniline conversion and NMA selectivity. Selectivity and conversion first increased and reached a maximum at a flow rate of 6 ml/hour, and then declined. The feed rate alters the contact time and the reason for the optimum velocity for NMA formation is apparently that, above this value, contact time becomes insufficient for NMA formation.

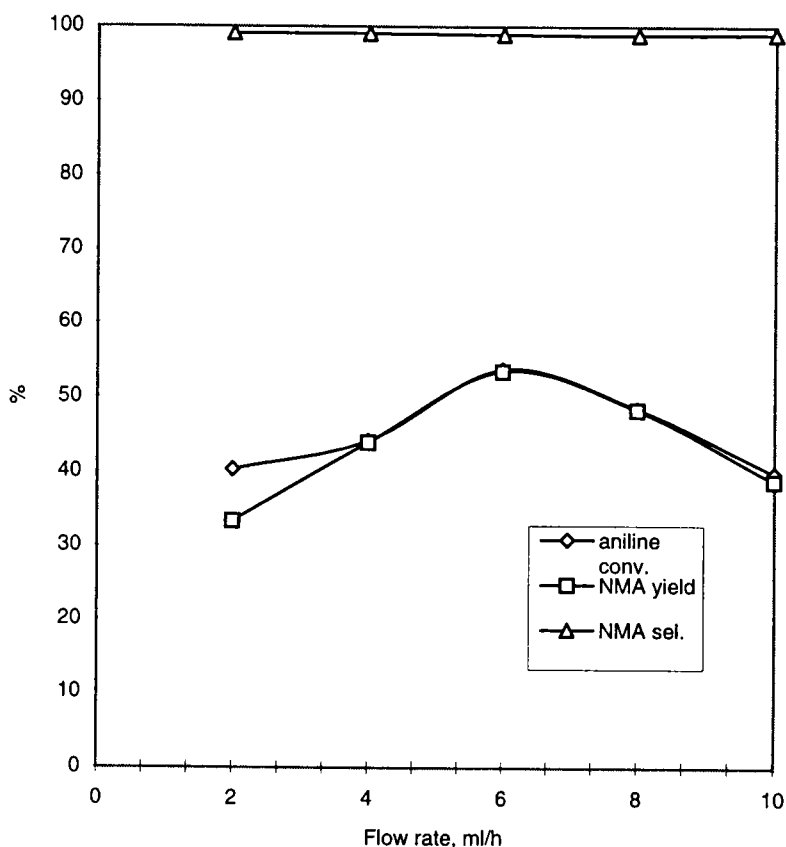


Fig. 4.2.4. Effect of feed flow rate on aniline conversion and product selectivities. Catalyst $Zn_{0.8}Co_{0.2}Fe_2O_4$, reaction temperature $350\text{ }^{\circ}C$, MeOH-aniline molar ratio 2:1, TOS 1 h.

4.3. $Zn_{1-x}Ni_xFe_2O_4$ ($x = 0, 0.2, 0.5, 0.8$ and 1.0)-TYPE SYSTEMS

4.3.1. Effect of methanol to aniline molar ratio: Figure 4.3.1 shows the influence of molar ratio of the reactants over $Zn_{0.8}Ni_{0.2}Fe_2O_4$ ($x = 0$). NMA has been detected as the major product. Both NMA yield and aniline conversion increased with methanol to aniline molar ratio and at the molar ratio of 7, the yield of NMA was maximized (38.9%). Highest amount of NNDMA (3.2 %) has also been detected at this stage. This result clearly indicates that the increase in methanol to aniline molar ratio does not significantly increase the N,N-dialkylation rate and thereby decrease NMA selectivity.

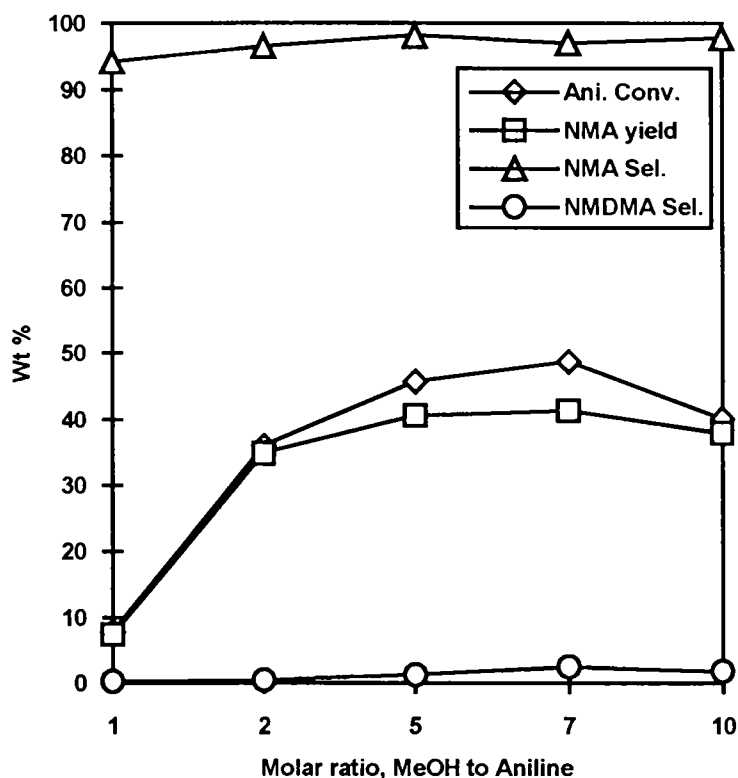


Fig. 4.3.1. Effect of feed molar ratio (methanol to aniline) on conversion and selectivities over $Zn_{0.8}Ni_{0.2}Fe_2O_4$. Reaction temperature $350\text{ }^{\circ}\text{C}$, WHSV 2 h^{-1} , TOS 2 h.

4.3.2. Effect of contact time: In another series of experiments, the effect of contact time on the activity was studied. A typical activity profile of aniline methylation as a function of feed rate (Weight Hourly Space Velocity, WHSV, varies from 0.67 h^{-1} to 3.3 h^{-1}) over $Zn_{0.8}Ni_{0.2}Fe_2O_4$ is shown in Fig. 4.3.2. The yield of NMA was maximized at the flow rate 6 ml/hour (WHSV, 2 h^{-1}). The selectivity of NMA was found to be about 97.5 % at this stage. But, as shown in the figure, aniline conversion reached a maximum and then decreased by increasing flow rate. The low aniline conversion rate at high contact time on can be attributed to the increased rate of methanol decomposition as a side reaction. Since the methanol to aniline molar ratio is only 2, such side reactions of methanol will seriously affect aniline conversion. As contact time decreases, the rate of side reaction also decreases, resulting in more aniline conversion and NMA yield.

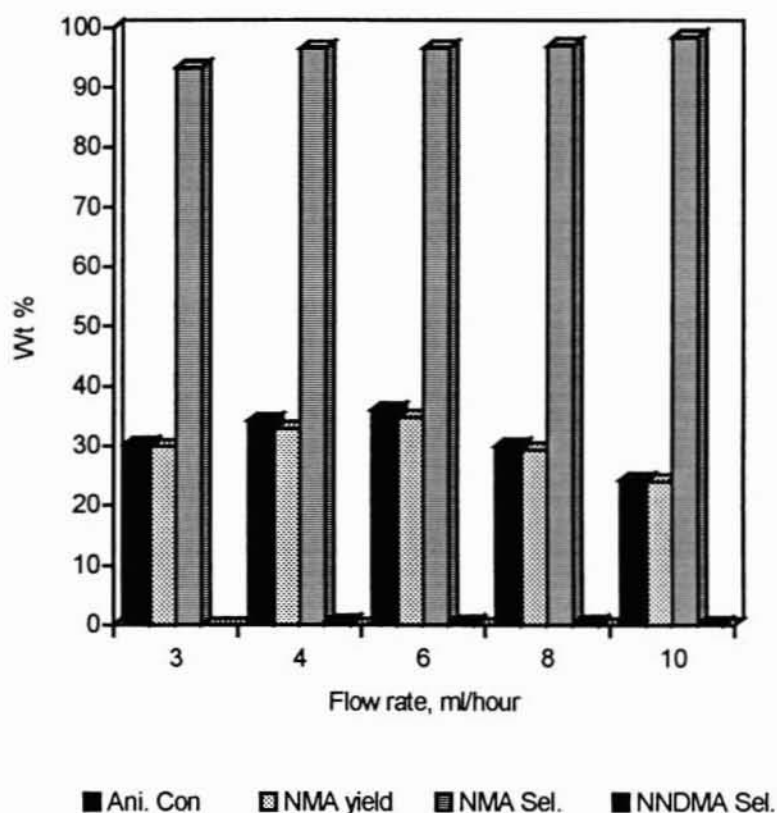


Fig. 4.3.2. Effect of contact time on aniline conversion and product selectivities over $Zn_{0.8}Ni_{0.2}Fe_2O_4$. Catalyst amount 3 g, feed molar ratio (methanol to aniline) 2, reaction temperature $350\text{ }^{\circ}C$ and TOS 2 h.

4.3.3. Effect of reaction temperature: The alkylation experiments were performed in the temperature range of 300 to $400\text{ }^{\circ}C$ over $ZnFe_2O_4$. Table 4.3.1 shows the influence of temperature on product distribution. Optimum temperature for maximum NMA yield and aniline conversion was 340 - $350\text{ }^{\circ}C$. As is evident from the table, there was a slight enhancement in the selectivity of NNDMA as temperature was increased from 300 to $400\text{ }^{\circ}C$. However, beyond $350\text{ }^{\circ}C$ the aniline conversion declined and lesser amount of NMA was formed. Methanol decomposition rate seemed to enhance at this stage. Analysis of the gaseous products indicates the presence of considerable amount of formaldehyde, C_1 and C_2 hydrocarbons and oxides of carbon.

Product distribution, Wt %	Temperature, °C			
	280	300	350	400
Benzene	Nil	Nil	0.02	0.73
Toluene	Nil	Nil	Nil	0.33
Unreacted aniline	83.39	60.32	48.41	72.71
NMA	16.20	39.00	50.49	25.58
NNDMA	Nil	0.03	0.09	0.17
Others	0.40	0.62	1.00	0.20
Aniline conversion	16.61	39.68	51.59	27.29
Selectivity				
NMA	98.00	98.28	97.84	94.70
NNDMA	--	0.08	0.11	0.62

Table. 4.3.1. Product distribution and selectivity data of aniline alkylation using methanol over $ZnFe_2O_4$ as a function of reaction temperature. WHSV 2 h^{-1} , feed molar ratio (MeOH to aniline) 2, TOS 1 h.

4.3.4. Effect of time-on-stream: Another set of experiments was carried out to establish the stability of the systems. In Fig. 4.3.3 the yield of NMA is plotted as a function of time-on-stream (TOS). All catalysts except $ZnFe_2O_4$ displayed excellent stability even after 10 hours. $ZnFe_2O_4$ showed deactivation in the initial period of the run (upto 4 hours) and thereafter it maintained a steady value of activity. As explained earlier, the deactivation of $ZnFe_2O_4$ can be explained if one considers the normal spinel lattice of $ZnFe_2O_4$, where electron hopping is constrained due to the non-availability of Fe^{3+} ions in the tetrahedral sites. Others are inverse in nature and all such systems showed prolonged stability.

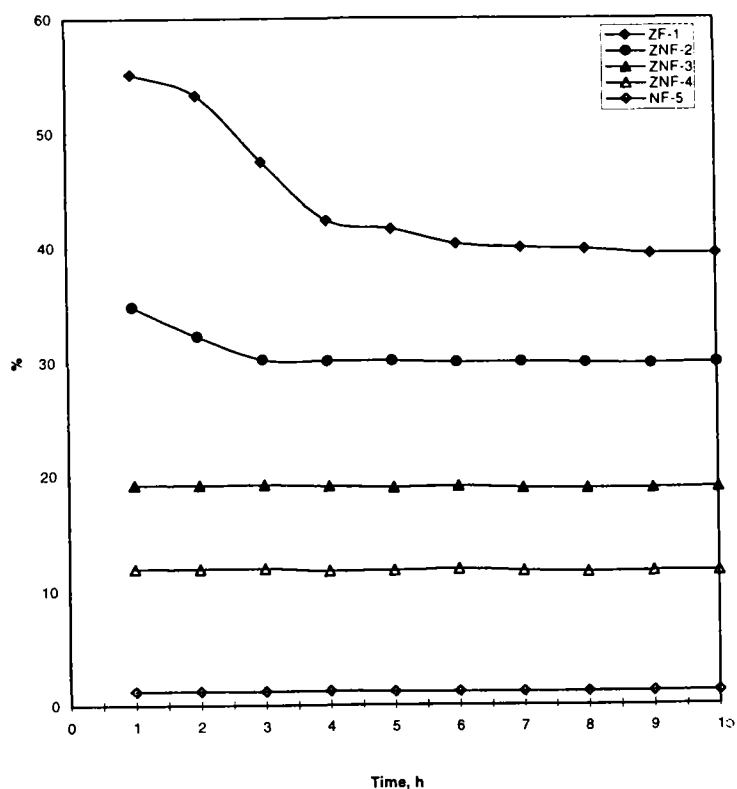


Fig. 4.3.3. Effect of time on stream: Concentration of N-methyl aniline (Wt. %) is plotted as a function of reaction time in hours over different Zn-Ni ferrite systems. Reaction temperature 350 °C, WHSV 2 h⁻¹ and TOS 1 h. Catalyst designation: ZF-1 (ZnFe₂O₄); ZNF-2 (Zn_{0.8}Ni_{0.2}Fe₂O₄); ZNF-3 (Zn_{0.5}Ni_{0.5}Fe₂O₄); ZNF-4 (Zn_{0.2}Ni_{0.8}Fe₂O₄); NF-5 (NiFe₂O₄).

4.3.5. Effect of catalyst composition: The effect of catalyst composition on activity and selectivity is shown in Fig. 4.3.4. Catalytic activity follows the order: ZnFe₂O₄ > Zn_{0.8}Ni_{0.2}Fe₂O₄ > Zn_{0.5}Ni_{0.5}Fe₂O₄ > Zn_{0.2}Ni_{0.8}Fe₂O₄ > NiFe₂O₄. Since acidity values of the systems were also found to follow the same order, the gradation in activity can be explained by considering factors like variation of acidity with Ni²⁺ substitution and its direct influence on the distribution of active Fe³⁺ ions in the spinel lattice.

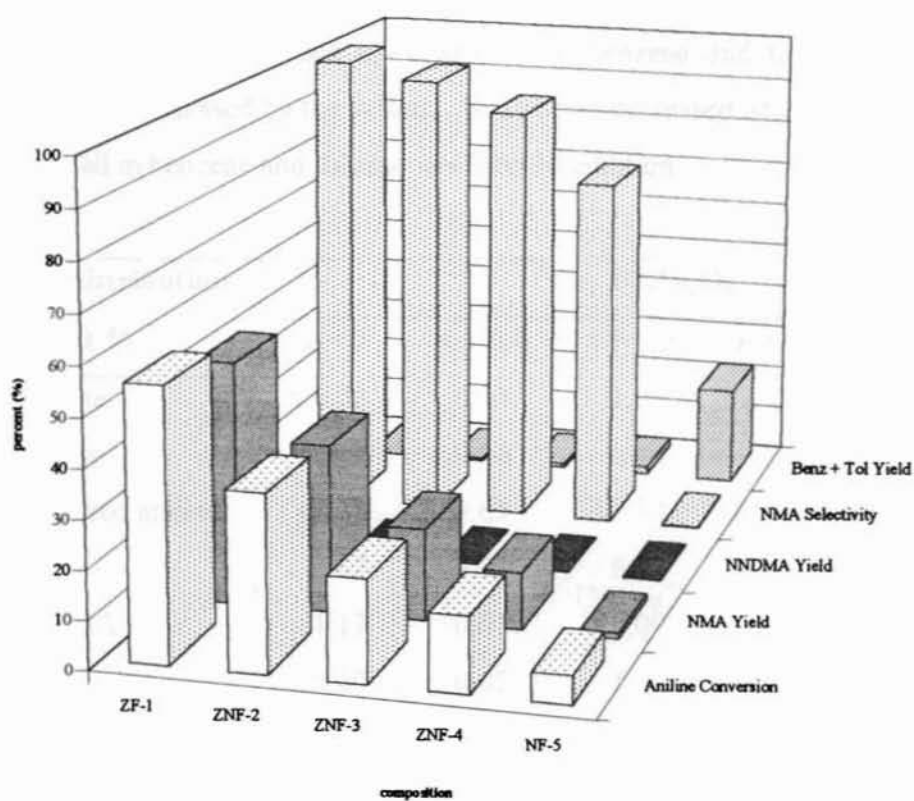


Fig. 4.3.4. Product distribution and selectivity pattern of aniline alkylation using methanol over different Zn-Ni-ferrite systems. Catalyst amount 3 g, reaction temperature 350 °C, TOS 2 h, feed flow rate 6 ml/h and methanol-aniline molar ratio 2:1.

Catalyst designation: ZF-1 (ZnFe_2O_4); ZNF-2 ($\text{Zn}_{0.8}\text{Ni}_{0.2}\text{Fe}_2\text{O}_4$); ZNF-3 ($\text{Zn}_{0.5}\text{Ni}_{0.5}\text{Fe}_2\text{O}_4$); ZNF-4 ($\text{Zn}_{0.2}\text{Ni}_{0.8}\text{Fe}_2\text{O}_4$); NF-5 (NiFe_2O_4).

4.4. $\text{Co}_{1-x}\text{Ni}_x\text{Fe}_2\text{O}_4$ ($x = 0, 0.2, 0.5, 0.8$ and 1.0)-TYPE SYSTEMS

4.4.1 Effect of catalyst composition: The product distribution over different Co-Ni systems is presented in the table (Table 4.4.1). Runs were performed at 350°C over 3 g catalyst and methanol to aniline molar ratio was maintained at 2:1. All compositions showed poor activity, even though selectivity varies considerably with composition. CoFe_2O_4 afforded more amount of benzene and toluene, due to the inherent acidity possessed by the system. Ni addition decreased acidity, as reflected by the sudden fall in benzene and toluene yields on Ni addition.

Product distribution, Wt %	$\text{Co}_{1-x}\text{Ni}_x\text{Fe}_2\text{O}_4$				
	$x = 0$	$x = 0.2$	$x = 0.5$	$x = 0.8$	$x = 1.0$
Benzene	26.02	0.50	1.06	2.78	3.3
Toluene	12.96	0.06	0.16	0.52	0.7
Unreacted aniline	48.74	89.63	90.54	93.30	94.2
NMA	5.07	9.73	6.66	3.25	1.2
NNDMA	1.17	0.01	0.09	0.1	0.2
Others	6.00	0.02	1.5	0.2	Nil
Aniline conversion	51.26	10.37	9.46	6.00	5.8
Selectivity					
NMA	9.89	93.73	70.40	748.50	21.43
NNDMA	2.28	0.10	0.10	0.10	0.20

Table. 4.4.1. Product distribution and selectivity data of aniline methylation over $\text{Co}_{1-x}\text{Ni}_x\text{Fe}_2\text{O}_4$ type systems. Reaction temperature 350°C , WHSV 1.3 h^{-1} , TOS 1 h.

4.4.2. Effect of reaction temperature: Table. 4.4.2 indicates the influence of reaction temperature on the product distribution and selectivities over $\text{Co}_{0.8}\text{Ni}_{0.2}\text{Fe}_2\text{O}_4$. As the temperature was increased from 250 to 400°C the conversion of aniline and the yield of NMA increased. Unlike the mentioned two systems above, maximum NMA yield was observed at 400°C . However maximum NMA yield was only 13.4 % even though selectivity always exceeded 90 %.

Reaction temperature, °C	Aniline conversion	NMA yield	NMA selectivity	Benzene + Toluene
250	3.20	3.20	100	Nil
300	7.43	7.23	96.26	Nil
350	10.37	9.72	93.73	0.10
400	15.28	13.42	90.17	1.30

Table. 4.4.2. Effect of the reaction temperature on the product distribution of aniline methylation over $\text{Co}_{0.8}\text{Ni}_{0.2}\text{Fe}_2\text{O}_4$. WHSV 1.3 h^{-1} , TOS 1 h.

4.4.3. Effect of feed flow-rate and time on stream: In another series of experiments the effect of feed flow-rate was studied. NMA yield was maximum in the feed flow-rate range 4-6 ml/hour. At still high flow rate N-alkylation decreased, but selectivity increased. At sufficiently high contact time (low flow-rate) NNDMA was a major product. Following figure represents the reaction pattern.

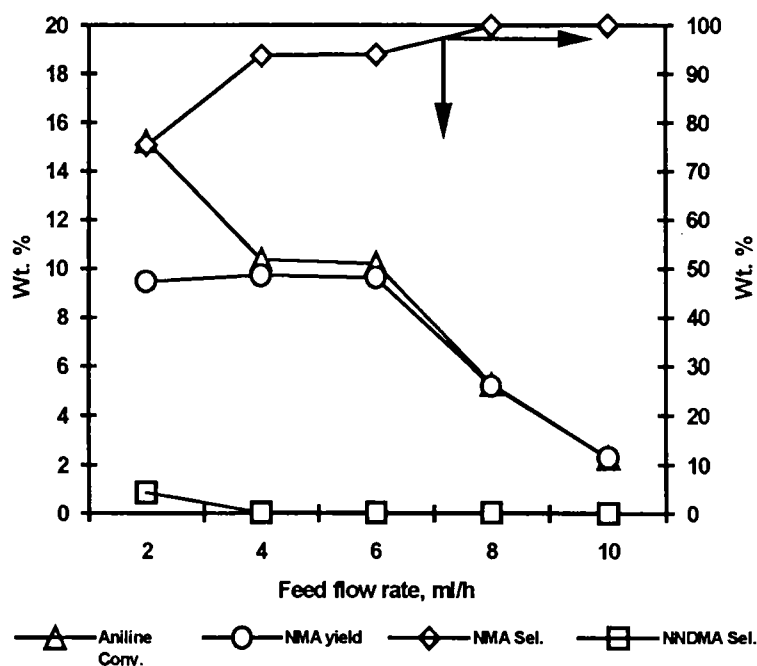


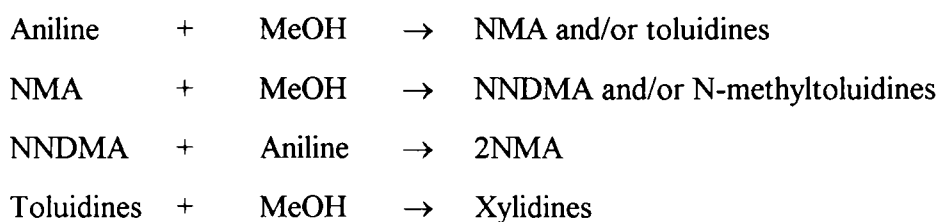
Fig. 4.4.1. Effect of feed flow rate (or contact time) on aniline conversion, NMA yield and selectivities of NMA and NNDMA over $\text{Co}_{0.8}\text{Ni}_{0.2}\text{Fe}_2\text{O}_4$. Catalyst amount 3 g, reaction temperature $350 \text{ }^\circ\text{C}$, molar ratio (methanol to aniline) 2 and TOS 1 h.

All systems were found to be stable for a sufficiently long period. However, at high methanol to aniline molar ratio, $\text{Co}_{0.2}\text{Fe}_2\text{O}_4$ and NiFe_2O_4 were found to be deactivated owing to the deposition of carbonaceous products on the catalyst surface, which inhibited the interaction between the catalyst and the reactants.

SECTION II-REACTION NETWORK AND ASSOCIATED MECHANISM

4.5 GENERAL CATALYTIC PATHWAY

Methylation of aniline is a multistep sequential reaction; the main reaction scheme can be represented as follows:



It is considered that alkylation of aniline is a concerted reaction involving simultaneous participation of both acidic and basic centers on the catalyst surface. Optimum concentration of acidic and basic sites are required for this reaction. Aniline conversion usually increases with acidity of the surface. However, the selectivity strongly depends on the experimental conditions (temperature, WHSV etc.) and on the nature of the catalyst, more specifically on the acido-basicity of the catalysts. A wide range of systems have been studied so far by various groups. A survey of these works indicates that strong Bronsted acid sites are responsible for C-alkylation[13-15] and N-alkylation is generally favoured on active centers such as basic and/or Lewis acid sites[16,17]. Rao *et al.* [18] while comparing the catalytic activity of H-Beta zeolite with Cs and K exchanged Beta, observed that Cs-Beta yields exclusively the N-alkylated product. (NMA), whereas H-Beta favoured more C-alkylation. The acidity of the systems decreases in the order H-Beta > K-Beta > Cs-Beta since the strong acid sites of the protonic H-Beta are suppressed due to the K and Cs exchange. As basicity

increased in the samples selectivity towards N-alkylation also increased and C-alkylation decreased. It was suggested that, the increase in N-selectivity in the cation exchange of zeolites is partially due to the suppression of the strong acid sites which favours C-alkylation, and partially due to the conjugate basicity and acidity associated with the samples. Narayanan *et al.* [17] studied a comparative study on aniline alkylation over silica and vanadia supported silica. Silica, as such, showed low acidity and activity. They reported that addition of 10 Wt.% vanadia increased acidity as well as activity. Aniline alkylation is an electrophilic substitution reaction. A catalyst system containing acid and base sites seems to favour the formation of NMA. The Brønsted sites help in the formation of carbocation from alcohol and Lewis sites help in the electrophilic substitution of the proton on aniline with the alkyl carbocation.

4.6 ACTIVITY AND SURFACE PROPERTIES OF THE PRESENT SYSTEMS

The above discussion clearly revealed that, in aniline alkylation reaction the number and strength of acidic and basic sites play a decisive role in determining product patterns. The mechanism of aniline alkylation reaction was well established by An Nanko *et al.* [18], according to which Lewis acid sites of the metal oxide system interact with the methoxy species and the hydrogen atom of the undissociated hydroxyl group interact with the Lewis basic site (Fig. 4.6.1). Thus aniline and methanol are adsorbed undissociately on the oxide surface (step 'a' and 'b'). The electrophilic attack of the methyl group of methanol on the nitrogen atom of aniline yields N-methylaniline. Adsorption behaviour of N-methylaniline also follows a similar pattern. N,N-dimethylaniline is produced in a similar way by the subsequent methylation of N-methyl aniline. Thus the mechanism accounts for the need of moderate amounts of both acidic and basic Lewis sites for the system. However, this mechanism differs from the one suggested by Rao *et al.* [19] for ALPO and SAPO, since in the latter case adsorption and subsequent polarization of the substrates is mainly caused by Brønsted acidity on the surface. Any factor that alters either acidity or basicity of the system will significantly influence the selectivity of the products and the activity of the system. A detailed discussion on the catalytic activity of different spinel series with surface acid-base properties and spinel structure is made in the following sections

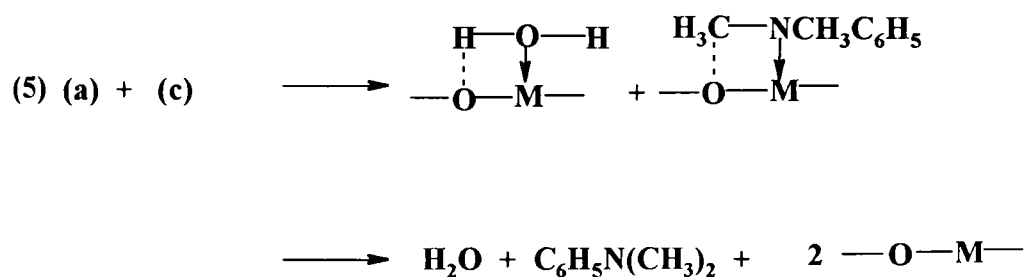
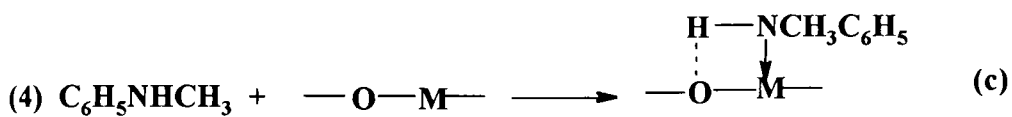
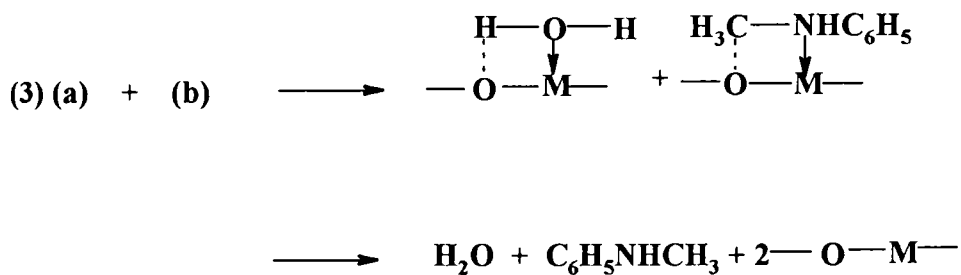
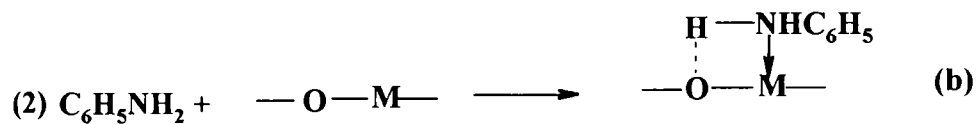
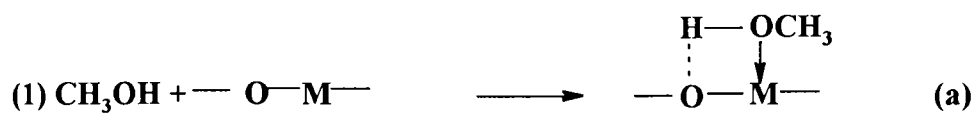


Fig. 4.6.1. The mechanism of N-methylation of aniline over oxide surface.

4.6.1 Zn_{1-x}Co_xFe₂O₄-type systems: From the adsorption study of electron acceptors and their dehydration activity, we could understand the trend in the acid-base site distribution with composition. We have observed that, for Zn_{1-x}Co_xFe₂O₄-type systems, as 'x' increased the dehydration activity increased, whereas the limiting concentration of electron acceptors adsorbed decreased. In other words, replacement of Zn²⁺ by Co²⁺ increased acidity with a concomitant decrease in basicity. Activity of the systems for N-alkylation follows the order ZnFe₂O₄ > Zn_{0.8}Co_{0.2}Fe₂O₄ > Zn_{0.5}Co_{0.5}Fe₂O₄ > Zn_{0.2}Co_{0.8}Fe₂O₄ > CoFe₂O₄. This indicates that the alkylation activity shows a trend not commensurating with their dehydration property. In this sense, unlike other typical acid-base reactions, acidity cannot be considered as the sole factor determining catalytic activity. Since aniline itself is a strong base, even the weak Lewis sites on the catalyst surface can effectively co-ordinate with this molecule. So the effective adsorption of alcohol and its subsequent reactions on the catalyst surface, which depends mainly on the cation distribution in the oxide lattice as reported by earlier workers [20-21], also should be considered to evaluate the catalytic properties of the systems.

Most interesting feature of the spinel systems in catalytic activity is the site preference occupancy of metal ions in tetrahedral (Tet.) and octahedral (Oct.) sites of coordinated oxygen atoms. ZnFe₂O₄ is a typical normal spinel. Substitution of Zn by cobalt isomorphically replaces Fe (III) ions from octahedral to tetrahedral sites.

x	Composition	Cation distribution	
	Zn _{1-x} Co _x Fe ₂ O ₄	Tetrahedral sites	Octahedral sites
0	ZnFe ₂ O ₄	Zn _{1.0} ²⁺	Fe ₂ ³⁺
0.2	Zn _{0.8} Co _{0.2} Fe ₂ O ₄	Zn _{0.8} ²⁺ Fe _{0.2} ³⁺	Fe _{1.8} ³⁺ Co _{0.2} ²⁺
0.5	Zn _{0.5} Co _{0.5} Fe ₂ O ₄	Zn _{0.5} ²⁺ Fe _{0.5} ³⁺	Fe _{1.5} ³⁺ Co _{0.5} ²⁺
0.8	Zn _{0.2} Co _{0.8} Fe ₂ O ₄	Zn _{0.2} ²⁺ Fe _{0.8} ³⁺	Fe _{1.2} ³⁺ Co _{0.8} ²⁺
1.0	CoFe ₂ O ₄	Fe _{1.0} ³⁺	Fe _{1.0} ³⁺ Co _{1.0} ²⁺

Table 4.6.1. Catalyst composition and cation distribution of Zn_{1-x}Co_xFe₂O₄-type systems.

Such changes in the spinel matrix affects the acid-base properties of the systems. The spinel compositions and their cation distributions are summarized in Table 4.6.1. Dehydration activities and the limiting amounts of electron acceptors adsorbed for Zn-Co systems are presented in the following table (Table 4.6.2) along with the NMA yields.

Catalyst composition	Dehydration	Activity	Limiting	Amount	NMA yield Wt%
	Wt %	%	$\times 10^{-5}$	mol m^{-2}	
$\text{Zn}_{1-x}\text{Co}_x\text{Fe}_2\text{O}_4$	Cyclohexene	Propene	TCNQ	Chloranil	
ZnFe_2O_4	39.72	33.66	1.66	0.66	50.50
$\text{Zn}_{0.8}\text{Co}_{0.2}\text{Fe}_2\text{O}_4$	40.40	37.20	1.60	0.48	44.00
$\text{Zn}_{0.5}\text{Co}_{0.5}\text{Fe}_2\text{O}_4$	49.80	37.76	1.55	0.43	36.12
$\text{Zn}_{0.2}\text{Co}_{0.8}\text{Fe}_2\text{O}_4$	52.40	38.21	1.54	0.37	14.66
CoFe_2O_4	55.30	44.68	1.50	0.31	5.07

Table 4.6.2. Dehydration activities and limiting concentration of electron acceptors adsorbed over different compositions in the $\text{Zn}_{1-x}\text{Co}_x\text{Fe}_2\text{O}_4$ series.

The results indicate that catalytic activity decreases linearly with increase in the $\text{Fe}^{3+}_{\text{Tet.}}/\text{Fe}^{3+}_{\text{Oct.}}$ ratio. In a spinel lattice, due to the lower covalency of the tetrahedral cation, the effective attractive force for a single Tet. metal-oxygen pair will be stronger than the corresponding Oct. metal-oxygen pair. In other words the octahedral metal oxygen bonds are weaker and hence will be more polar [22, 23]. This leads to a comparatively higher activity for the octahedral cations. Additionally, Jacobs *et al.* after some experiments [24], based on LEIS measurement (Low Energy Ion Scattering, a technique which is sensitive to the outermost atomic layer), reported that spinel surface sites are octahedral and the tetrahedral sites are not easily accessible to the reactants. However, electrons can easily hop between sites and, therefore, tetrahedral ions can also influence in the overall activity of the system. It is believed that the high strength Lewis acid sites are provided by octahedral ions (either Fe^{3+} in ZnFe_2O_4 or Fe^{3+} and Co^{2+} in the substituted spinels). In ferrites Fe^{3+} -O bond distance is more when Fe^{3+} is in octahedral symmetry than when it is in tetrahedral symmetry. Hence such Fe^{3+} ions will be readily available for adsorption of alcohol. The

involvement of Fe^{3+} ions in the octahedral sites as the alcohol adsorbing centers in ferrite systems have already been reported [22]. Among these spinel series, ZnFe_2O_4 possessed all Fe^{3+} in the octahedral sublattice. Hence the high NMA yield of the system can be due to the moderate acidity created by surface Fe^{3+} ions. Activity decreases with Co^{2+} substitution. The systems possessing highest 'x' values ($\text{Zn}_{0.2}\text{Co}_{0.8}\text{Fe}_2\text{O}_4$ and CoFe_2O_4) were found to be only less selective and active for the alkylation reaction, and both these systems afford significantly large amount of deaminated products viz. benzene and toluene. We have noticed that substitution of zinc by cobalt creates strong acidic sites in the system. The high deamination rate is probably due to the creation of strong acid sites created by Co^{2+} ions. This is further confirmed by passing aniline alone over the system at $350\text{ }^\circ\text{C}$, where benzene was noted as a major product as a result of deamination. But as far as aniline alkylation reaction is concerned, a favourable condition with respect to both activity and selectivity is obtained when $x = 0.8$, *i.e.* $\text{Zn}_{0.8}\text{Co}_{0.2}\text{Fe}_2\text{O}_4$, a system possessing inverse spinel lattice and moderate acid-base strength.

From Fig.4.3.3 it is clear that ZnFe_2O_4 , even though executing excellent activity in the initial period of the run, deactivates quickly. Cobalt addition surprisingly stabilized the system. The stability of the systems can be explained by considering the above-mentioned structural features of the systems and the ease with which such systems can undergo oxidative migration after alcohol adsorption. Adsorption of alcohol leads to electron transfer from adsorbate to catalyst, which changes the oxidation state of iron. However, if Fe^{3+} ions are available in the neighbouring tetrahedral sites, reduced Fe^{3+} ions can regain their original state by electron exchange. ZnFe_2O_4 being a normal spinel, these types of electron exchanges are not possible and hence in the reducing atmosphere such systems deactivate at a faster rate than the corresponding inverse systems. In order to understand the nature of the catalyst after reaction the Diffuse Reflectance Infrared (DR-IR) spectra of the used ZnFe_2O_4 and $\text{Zn}_{0.8}\text{Co}_{0.2}\text{Fe}_2\text{O}_4$ were taken. Fig. 4.6.2 represents the DR-IR spectra of pure and used ZnFe_2O_4 and Fig. 4.6.3 represents DR-IR spectra of pure and used $\text{Zn}_{0.8}\text{Co}_{0.2}\text{Fe}_2\text{O}_4$. Used ZnFe_2O_4 showed merging of two distinct peaks originally present in the pure ZnFe_2O_4 , indicating partial destruction of spinel matrix.

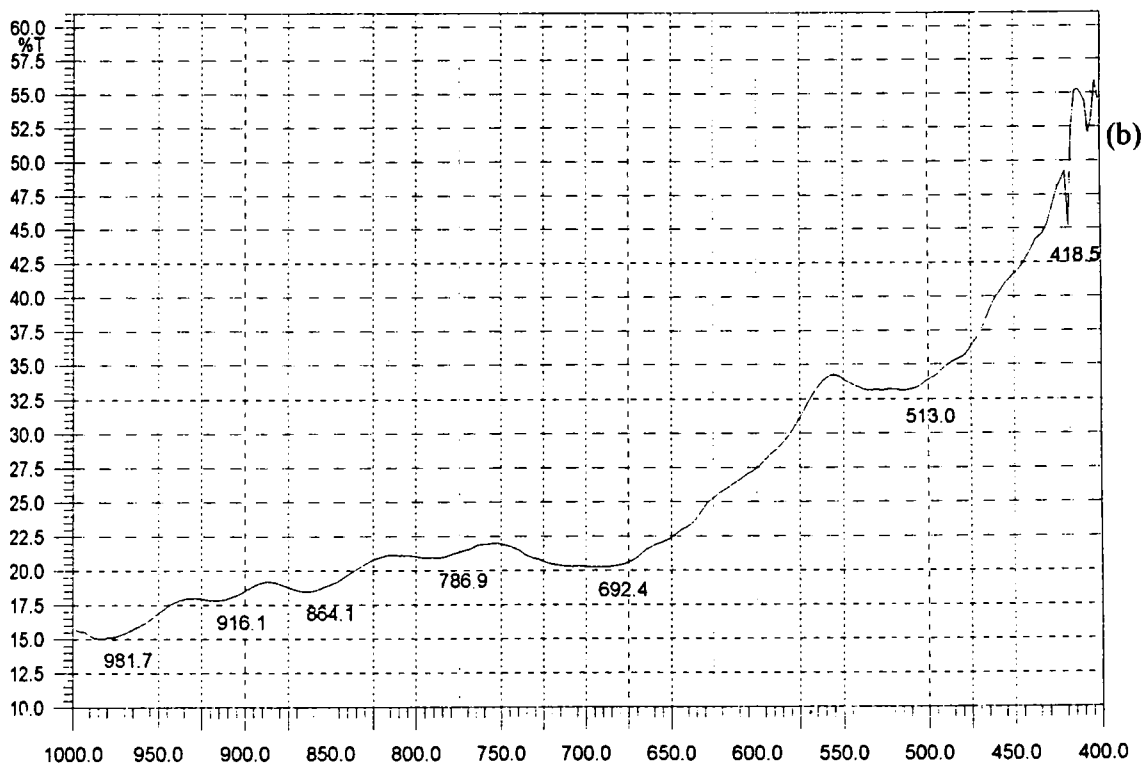
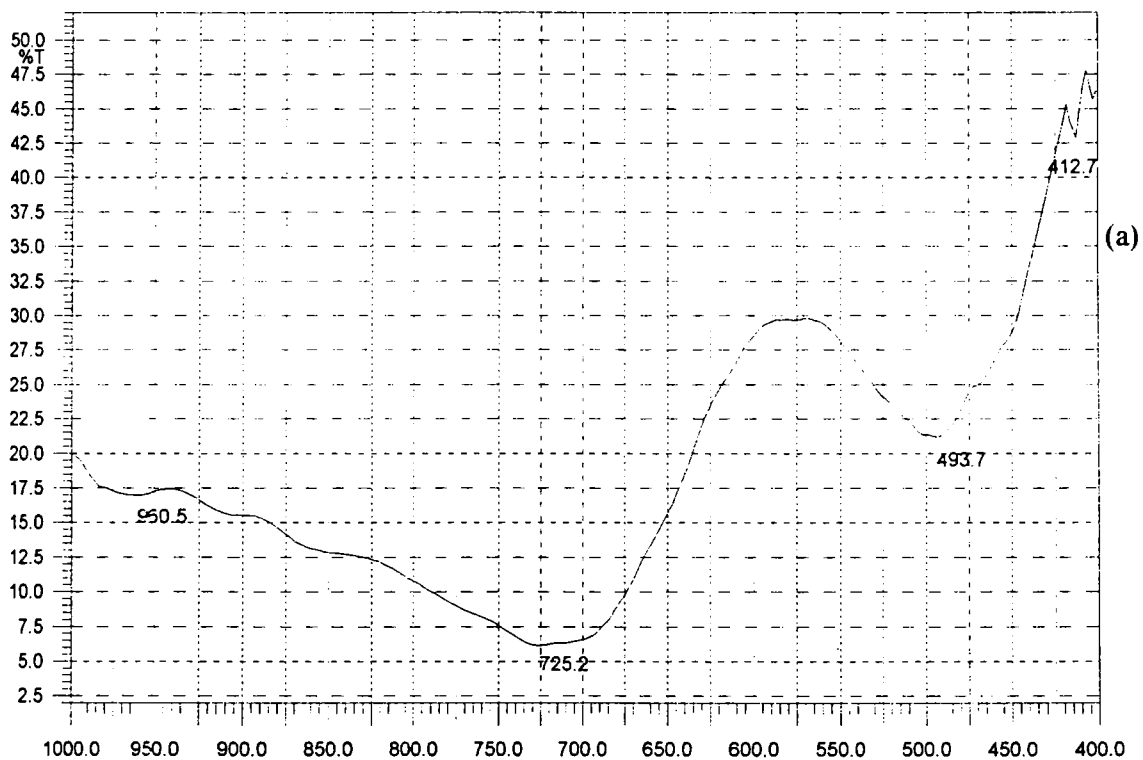


Fig. 4.6.2. Diffuse reflectance infrared (DR-IR) spectra of (a) fresh ZnFe₂O₄ (b) used ZnFe₂O₄. Used system shows merging of the two broad peaks originally present in the fresh system, indicating partial destruction of spinel structure.

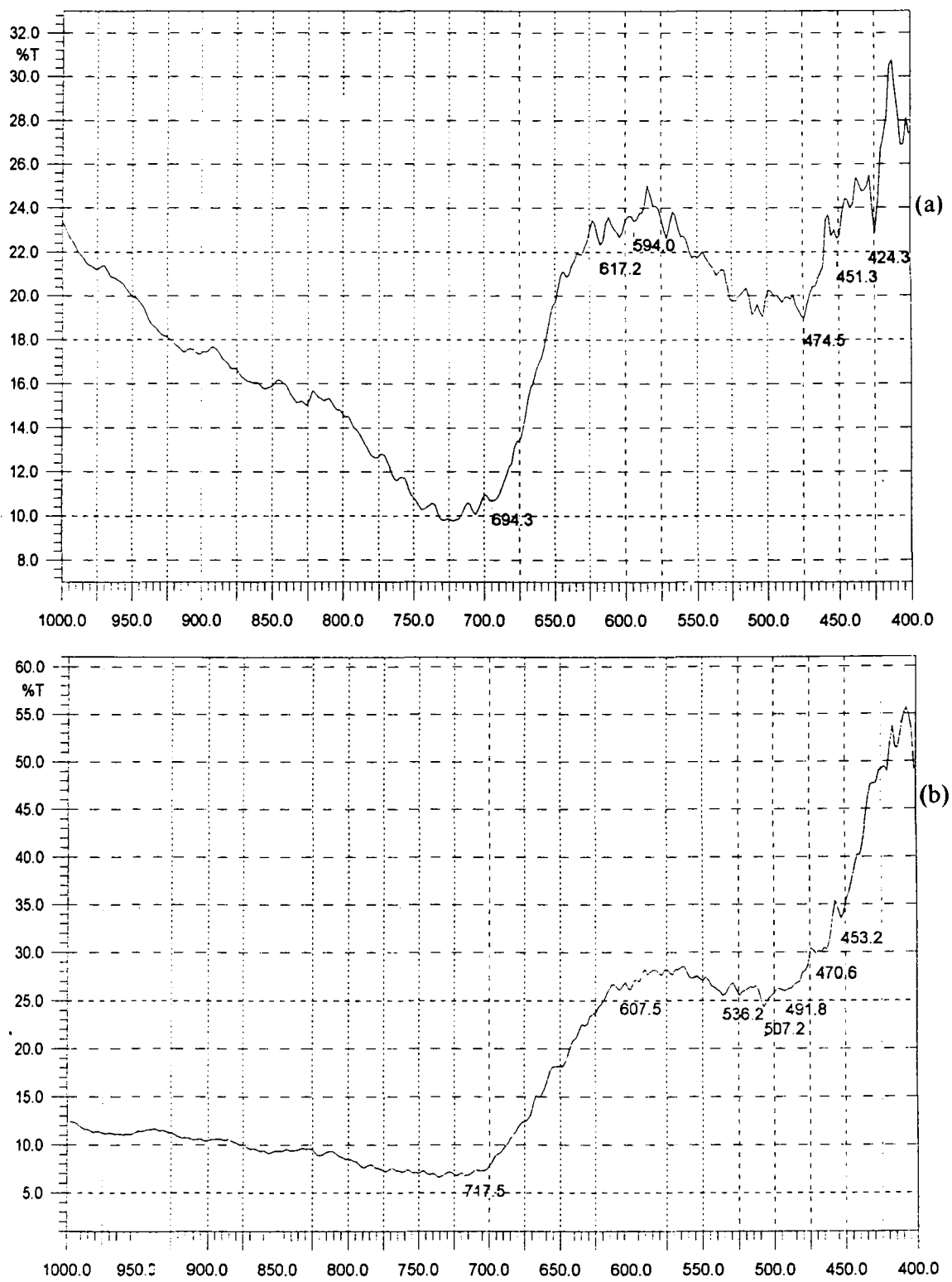


Fig. 4.6.3. Diffuse reflectance infrared (DR-IR) spectra of (a) fresh $Zn_{0.8}Co_{0.2}Fe_2O_4$ (b) used $Zn_{0.8}Co_{0.2}Fe_2O_4$. Even after reaction the catalyst retained the spinel structure indicating the stabilization effect due to cobalt addition in Zn-ferrite matrix.

4.6.2. $Zn_{1-x}Ni_xFe_2O_4$ -type systems: The spinel composition and the cation distributions in the two types of coordinated environments are presented below (Table 4.6.3). As in the previous case, here Ni^{2+} ions progressively substitute for Fe^{3+} ions in the octahedral sublattice. In other words, as 'x' increases the concentration of Ni^{2+} ions in the octahedral sites increases whereas Fe^{3+} ion concentration in the tetrahedral sites also increases.

x	Composition	Cation distribution	
	$Zn_{1-x}Ni_xFe_2O_4$	Tetrahedral sites	Octahedral sites
0	$ZnFe_2O_4$	$Zn_{1.0}^{2+}$	Fe_2^{3+}
0.2	$Zn_{0.8}Ni_{0.2}Fe_2O_4$	$Zn_{0.8}^{2+}Fe_{0.2}^{3+}$	$Fe_{1.8}^{3+}Ni_{0.2}^{2+}$
0.5	$Zn_{0.5}Ni_{0.5}Fe_2O_4$	$Zn_{0.5}^{2+}Fe_{0.5}^{3+}$	$Fe_{1.5}^{3+}Ni_{0.5}^{2+}$
0.8	$Zn_{0.2}Ni_{0.8}Fe_2O_4$	$Zn_{0.2}^{2+}Fe_{0.8}^{3+}$	$Fe_{1.2}^{3+}Ni_{0.8}^{2+}$
1.0	$NiFe_2O_4$	$Fe_{1.0}^{3+}$	$Fe_{1.0}^{3+}Ni_{1.0}^{2+}$

Table: 4.6.3. Cation distribution in $Zn_{1-x}Ni_xFe_2O_4$ -type spinel series.

From the adsorption experiments using electron acceptors and from their dehydration activities, it is clear that Ni substitution in the Zn-ferrite matrix significantly increased

Catalyst composition	Dehydration	Activity	Limiting	Amount	NMAyield
	Wt	%	$\times 10^{-5}$	mol m^{-2}	
$Zn_{1-x}Co_xFe_2O_4$	Cyclohexene	Propene	TCNQ	Chloranil	Wt%
$ZnFe_2O_4$	39.72	33.66	1.66	0.66	50.50
$Zn_{0.8}Ni_{0.2}Fe_2O_4$	35.28	30.77	1.76	0.73	34.81
$Zn_{0.5}Ni_{0.5}Fe_2O_4$	29.57	24.63	1.91	0.84	19.16
$Zn_{0.2}Ni_{0.8}Fe_2O_4$	19.17	17.21	2.19	1.02	11.90
$NiFe_2O_4$	12.03	16.50	2.38	1.06	1.20

Table: 4.6.4. Dehydration activities and limiting amount values of electron acceptors adsorbed over different compositions of $Zn_{1-x}Ni_xFe_2O_4$ series.

the basicity of the system with a concomitant decrease in the acidity. Catalytic activity, together with their acid-base strength (*i.e.* the limiting concentration of electron acceptors adsorbed and dehydration activities) is summarised in Table 4.6.4. Both acidity and catalytic activity of the systems follow the order: $\text{ZnFe}_2\text{O}_4 > \text{Zn}_{0.8}\text{Ni}_{0.2}\text{Fe}_2\text{O}_4 > \text{Zn}_{0.5}\text{Ni}_{0.5}\text{Fe}_2\text{O}_4 > \text{Zn}_{0.2}\text{Ni}_{0.8}\text{Fe}_2\text{O}_4 > \text{NiFe}_2\text{O}_4$. The high strength Lewis acidity can probably be due to the Fe^{3+} ions in the octahedral sites because of the stable nature of Zn^{2+} ions (d^{10} configuration) and also due to their occupancy in the less accessible tetrahedral sites. A similar conclusion regarding acidity was reported by Dixit *et al.*[25] for Cu-Cr-Fe ternary spinel systems, since they observed a progressive decrease in the activation energy for Friedel-Crafts benzylation reaction as the iron content of the system increases. As 'x' increases, Ni^{2+} ions replace Fe^{3+} ions isomorphically from octahedral sites to tetrahedral sites, leading to a decrease in the activity of the systems. In other words, the low activity can be accounted for by the replacement of acidic sites by basic sites during Ni^{2+} substitution. We have already seen that, since aniline is a strong base even weak Lewis acid sites can effectively coordinate with aniline and, therefore, the liability of the systems towards alcohol adsorption becomes more important. This means that, a large decrease in acidity due to Ni-substitution may not significantly affect aniline adsorption capacity, but will have a major influence on the adsorption and subsequent bond polarization of methanol.

4.6.3 $\text{Co}_{1-x}\text{Ni}_x\text{Fe}_2\text{O}_4$ -type systems: In the present case, all systems are inverse in nature. Hence Fe^{3+} ion concentration in the octahedral sites is the same in all compositions. The spinel compositions and the cation distributions are presented in the following table (Table 4.6.5). Thus it is clear that, it is the $\text{Co}^{2+}/\text{Ni}^{2+}$ ratio that plays a major role in determining the overall activity towards alkylation reaction. The acidity-basicity and catalytic activity data is summarised in Table 4.6.6. Unlike the previously discussed two systems, all members in the Co-Ni series executed very poor activity towards N-alkylation, even though some members showed excellent selectivity. Large quantities of benzene and toluene were formed over CoFe_2O_4 , owing to the presence of strong acidic centers on the system. A sharp decrease in acidity is observed during Ni substitution,

x	Composition	Cation distribution	
	$\text{Co}_{1-x}\text{Ni}_x\text{Fe}_2\text{O}_4$	Tetrahedral sites	Octahedral sites
0	CoFe_2O_4	$\text{Fe}_{1.0}^{3+}$	$\text{Fe}_{1.0}^{3+}\text{Co}_{1.0}^{2+}$
0.2	$\text{Co}_{0.8}\text{Ni}_{0.2}\text{Fe}_2\text{O}_4$	$\text{Fe}_{1.0}^{3+}$	$\text{Fe}_{1.0}^{3+}\text{Co}_{0.8}^{2+}\text{Ni}_{0.2}^{2+}$
0.5	$\text{Co}_{0.5}\text{Ni}_{0.5}\text{Fe}_2\text{O}_4$	$\text{Fe}_{1.0}^{3+}$	$\text{Fe}_{1.0}^{3+}\text{Co}_{0.5}^{2+}\text{Ni}_{0.5}^{2+}$
0.8	$\text{Co}_{0.2}\text{Ni}_{0.8}\text{Fe}_2\text{O}_4$	$\text{Fe}_{1.0}^{3+}$	$\text{Fe}_{1.0}^{3+}\text{Co}_{0.2}^{2+}\text{Ni}_{0.8}^{2+}$
1.0	NiFe_2O_4	$\text{Fe}_{1.0}^{3+}$	$\text{Fe}_{1.0}^{3+}\text{Ni}_{1.0}^{2+}$

Table 4.6.5. Cation distribution in $\text{Co}_{1-x}\text{Ni}_x\text{Fe}_2\text{O}_4$ -type systems.

and it is reflected in the product distribution also since the deamination reaction (both benzene and toluene formation) is almost completely suppressed on Ni-containing systems. Thus if we compare the Co-Ni systems with Zn-Co and Zn-Ni systems it can be readily realized that active systems always contain more Fe^{3+} ions in the octahedral lattice.

Catalyst composition	Dehydration	Activity	Limiting $\times 10^{-5}$	Amount mol m^{-2}	NMA yield Wt%
	Wt %	%			
$\text{Co}_{1-x}\text{Ni}_x\text{Fe}_2\text{O}_4$	Cyclohexene	Propene	TCNQ	Chloranil	
CoFe_2O_4	55.30	44.68	1.90	0.31	5.07
$\text{Co}_{0.8}\text{Ni}_{0.2}\text{Fe}_2\text{O}_4$	37.27	36.52	1.92	0.71	9.73
$\text{Co}_{0.5}\text{Ni}_{0.5}\text{Fe}_2\text{O}_4$	24.66	33.26	2.00	0.97	6.66
$\text{Co}_{0.2}\text{Ni}_{0.8}\text{Fe}_2\text{O}_4$	16.70	20.46	2.00	0.97	3.25
NiFe_2O_4	12.03	16.50	2.38	1.06	1.20

Table 4.6.6. Dehydration activities and limiting concentration of electron acceptors adsorbed over different compositions of $\text{Zn}_{1-x}\text{Ni}_x\text{Fe}_2\text{O}_4$ -type systems.

4.7. DIMETHYL CARBONATE FOR ENVIRONMENTALLY BENIGN REACTIONS

Alkylation using methanol has been extensively studied. Recently it was shown that on fujasite catalysts, dimethyl carbonate (DMC) is very selective for the alkylation of aniline to N-methylaniline [26]. DMC has two carbon centers at which a nucleophile may attack; the carbonyl and the methyl group. When a nucleophile attacks carbonyl carbon of DMC, the cleavage of acyl-oxygen bond results in a methoxy carbonyl product. When the attack is on the methyl carbon of DMC, the methylation product is produced by the alkyl-oxygen bond cleavage [27]. An important advantage of DMC is that it is non toxic in nature. Totta *et al.* [28] reported that the reaction of aniline with DMC gave 60.5 % of N-methyl aniline at 91.4% aniline conversion (DMC/aniline = 10) using α -alumina coated with potassium carbonate and polyethylene glycol as the catalyst. Later, the methylation of aniline with DMC was studied in detail by Fu and Uno [29]. Two possible routes of alkylation using DMC are represented below (Fig.4.7.1):

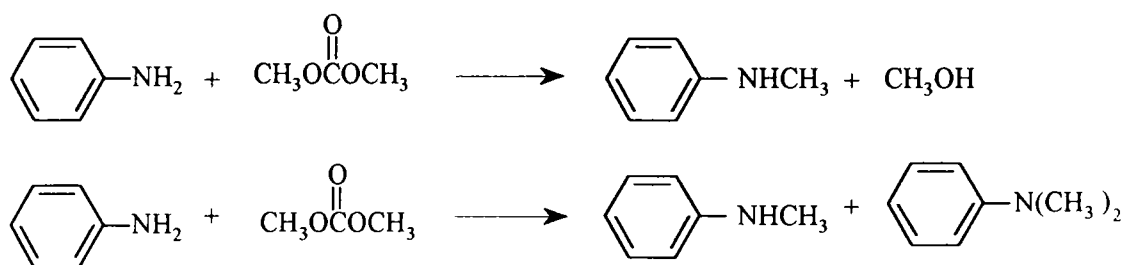


Fig. 4.7.1. Two possible routes of aniline alkylation using DMC.

From the detailed study of aniline alkylation using methanol as the alkylating agent, we have seen that $Zn_{1-x}Co_xFe_2O_4$ and $Zn_{1-x}Ni_xFe_2O_4$ systems can selectively alkylate aniline in the nitrogen atom leading to N-monomethylated product selectively, even though activity varies with composition. High NMA selectivity, high activity even at a significantly low methanol to aniline molar ratio and prolonged stability are some distinct advantages of the systems. However, the importance of environmentally benign processes has been repeatedly stressed in recent years. Many efforts have been

focused on eliminating or decreasing environmentally hazardous substances. Methanol vapour and its oxidized products can create major impact on our atmosphere. DMC is being considered as a possible replacement for toxic alkylating agents.

This part of the chapter deals with a brief study of aniline alkylation using DMC. Using methanol as the alkylating agent, we have noticed that with respect to stability, selectivity and activity $Zn_{0.8}Co_{0.2}Fe_2O_4$ was the best alkylating catalyst. Preliminary studies using DMC also revealed that the same catalyst system is the best possible one among the spinel systems discussed so far. Hence this system has been selected as a model for evaluating the efficiency of DMC as an alkylating agent.

4.7.1. Effect of reaction temperature: A series of experiments were performed in the temperature range of 200-300 °C using 3 g catalyst in a vapor-phase reactor. DMC to aniline molar ratio was maintained at 2. Unlike the experiments using methanol, here temperature has a marked effect on selectivities of the products. At low temperature NMA selectivity was high, but quickly decreased with increase in temperature. Increase in temperature increased N,N-dialkylation rate upto 280 °C and thereafter it suddenly decreased. The other products include DMC fractions, benzene and toluene. No toluidines were detected throughout the experiments. The results are summarised in the following table (Table.4.7.1).

Product distribution, Wt %	Reaction temperature, °C			
	200	250	280	300
Aniline conversion	31.30	50.53	62.30	50.35
NMA	24.99	37.31	32.78	22.30
NNDMA	1.07	6.03	16.74	7.21
Others	5.24	7.20	12.78	20.85
Selectivity				
NMA	79.84	73.83	52.62	44.29
NNDMA	4.28	11.93	26.87	14.32

Table 4.7.1. Product distribution and selectivity data of aniline alkylation using DMC as a function of reaction temperature over $Zn_{0.8}Co_{0.2}Fe_2O_4$. Catalyst amount 3 g, flow rate 4 ml/h, TOS 1 h and molar ratio (DMC to aniline) 2.

4.7.2. Effect of feed molar ratio: In order to understand the optimum DMC-aniline feed-mix ratio a series of experiments were carried out at different molar ratios of DMC and aniline. The result is shown in Fig. 4.7.2. At low DMC concentration selectivity for NMA was increased whereas at high DMC concentration more amount of di-substituted product was detected.

4.7.3. Effect of contact time: Optimum feed flow rate for NMA formation was 4ml/hr (WHSV 1.2 h⁻¹). At low flow rate more amount of NNDMA was formed due to the high contact time with the catalyst. At sufficiently high flow rate aniline conversion and alkylation activity significantly diminished. The results are shown in Fig. 4.7.3.

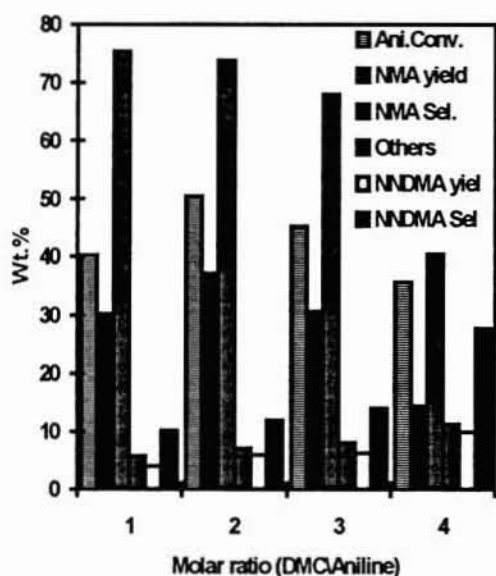


Fig. 4.7.2. Effect of feed molar ratio on aniline alkylation using DMC over $Zn_{0.8}Co_{0.2}Fe_2O_4$. Reaction temperature 250 °C, flow rate 4 ml/h, catalyst amount 3 g.

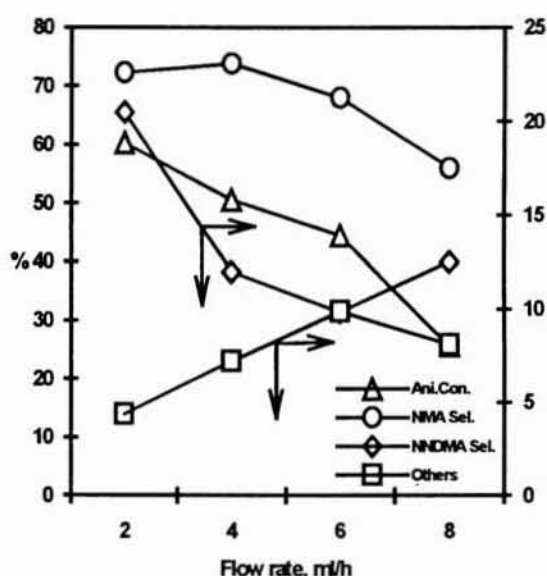


Fig. 4.7.3. Effect of feed flow rate on aniline alkylation using DMC over $Zn_{0.8}Co_{0.2}Fe_2O_4$. Molar ratio (DMC to aniline) 2, reaction temperature 250 °C, catalyst amount 3 g.

The above discussion clearly indicates that DMC can act as an effective N-alkylating agent at sufficiently low temperature, where methanol shows only mild activity. However, unlike methanol, DMC afforded both mono and di-substitution on nitrogen leading to less selectivity for NMA. A comparison of various aspects of

alkylation using methanol and DMC over $Zn_{0.8}Co_{0.2}Fe_2O_4$ is made in the following figure (Fig: 4.7.4.).

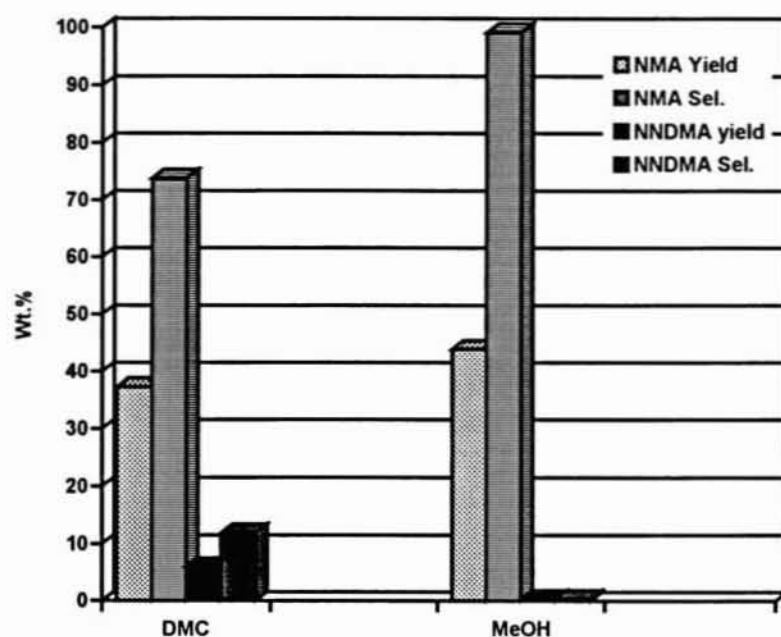


Fig. 4.7.4. A comparison of aniline alkylation using methanol and dimethyl carbonate. In both cases molar ratio (alkylating agent to aniline) was maintained 2. Reaction temperature-for alkylation using methanol 350 °C, for alkylation using DMC 250 °C ; catalyst amount 3 g.

4.8. KINETICS OF ANILINE ALKYLATION

Kinetic parameters such as activation energy (E_a), rate constants and Arrhenous frequency factor (A) for aniline conversion was determined using $Zn_{0.8}Co_{0.2}Fe_2O_4$ as a model system. At sufficiently high concentration of methanol (a methanol to aniline molar ratio of 10), reaction can be assumed to be pseudo-first order with respect to aniline. The product distribution at different temperatures and contact time (W/F) values are measured (Table. 4.8.1). To determine the reaction rate parameters for the conversion of aniline from the results presented in Table.4.8.1, the following differential equation can be used:

$$-dC_{\text{aniline}}/d(W/F) = kC_{\text{aniline}} \quad (1)$$

where W is the weight of the catalyst in grams and F is the flow rate of the feed in mol h^{-1} . Integrating (1) yields:

$$-\ln(1-X_A) = k(W/F) \quad (2)$$

Where X_A is the aniline conversion. Plots of $-\ln(1-X_A)$ against W/F will give straight lines passing through the origin, from which rate constant k can be calculated.

Reaction temperature, $^{\circ}\text{C}$	Contact time, W/F , g h mol^{-1}	$-\ln(1-X_A)$
260	0.100	0.082
	0.150	0.040
	0.188	0.048
	0.250	0.136
280	0.100	0.040
	0.150	0.041
	0.188	0.054
	0.250	0.102
	0.375	0.220
300	0.100	0.061
	0.150	0.084
	0.188	0.153
	0.250	0.192
320	0.100	0.087
	0.188	0.143
	0.250	0.179
	0.375	0.303

Reaction conditions : molar ratio of MeOH to aniline 10; 1 atm.; TOS 2 h.

Table 4.8.1 Aniline methylation data for kinetic studies.

As shown in Fig. 4.8.1, the straight lines passing through zero imply that the first methylation of aniline is a pseudo-first-order reaction with respect to the aniline

concentration. Thus the k values at different reaction temperatures were calculated; The data are presented in Table 2.8.2.

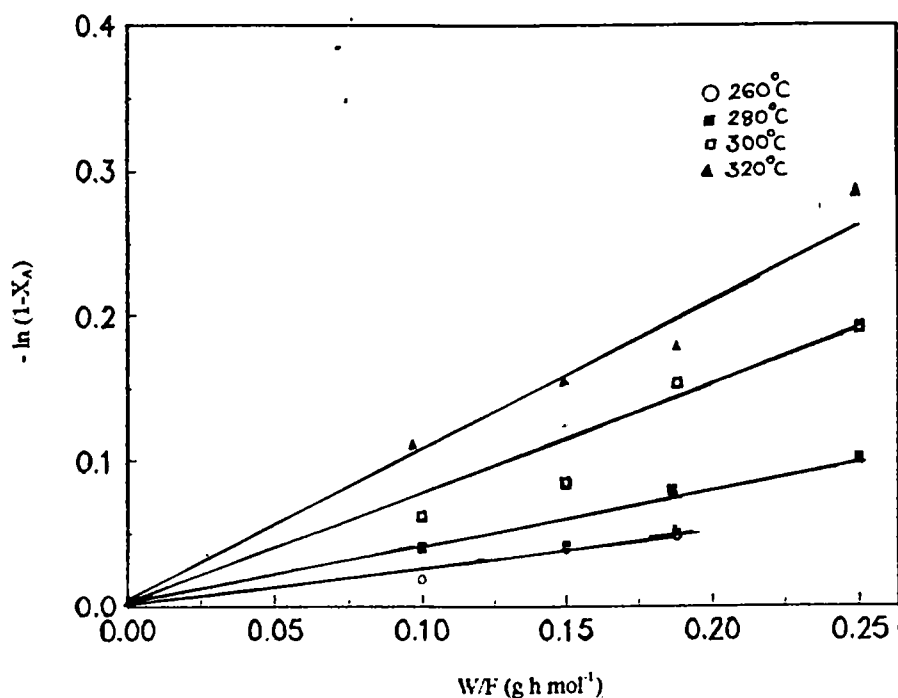


Fig. 4.8.1. Evaluation of rate constants at different reaction temperatures of aniline alkylation over $Zn_{0.8}Co_{0.2}Fe_2O_4$.

Using the Arrhenius equation,

$$k = Ae^{-E_a/RT}$$

the activation energy E_a and frequency factor A can be calculated. Fig.4.8.2 shows the Arrhenius plot from which the activation energy and frequency factor are calculated. Data are presented in Table 4.8.2.

k ($mol\ h^{-1}\ g^{-1}$)	$(-\ln k)$	$\frac{10^3 K}{T}$
0.3708	0.9920	1.870
0.4912	0.7110	1.808
0.7864	0.2403	1.745
1.1484	-0.1384	1.686

Frequency factor, A ($mol\ h^{-1}\ g^{-1}$) = 4.457×10^4
 Activation energy, E_a ($kJmol^{-1}$) = 52.20

Table 4.8.2. Kinetic parameters of N-monomethylation of aniline over $Zn_{0.8}Co_{0.2}Fe_2O_4$.

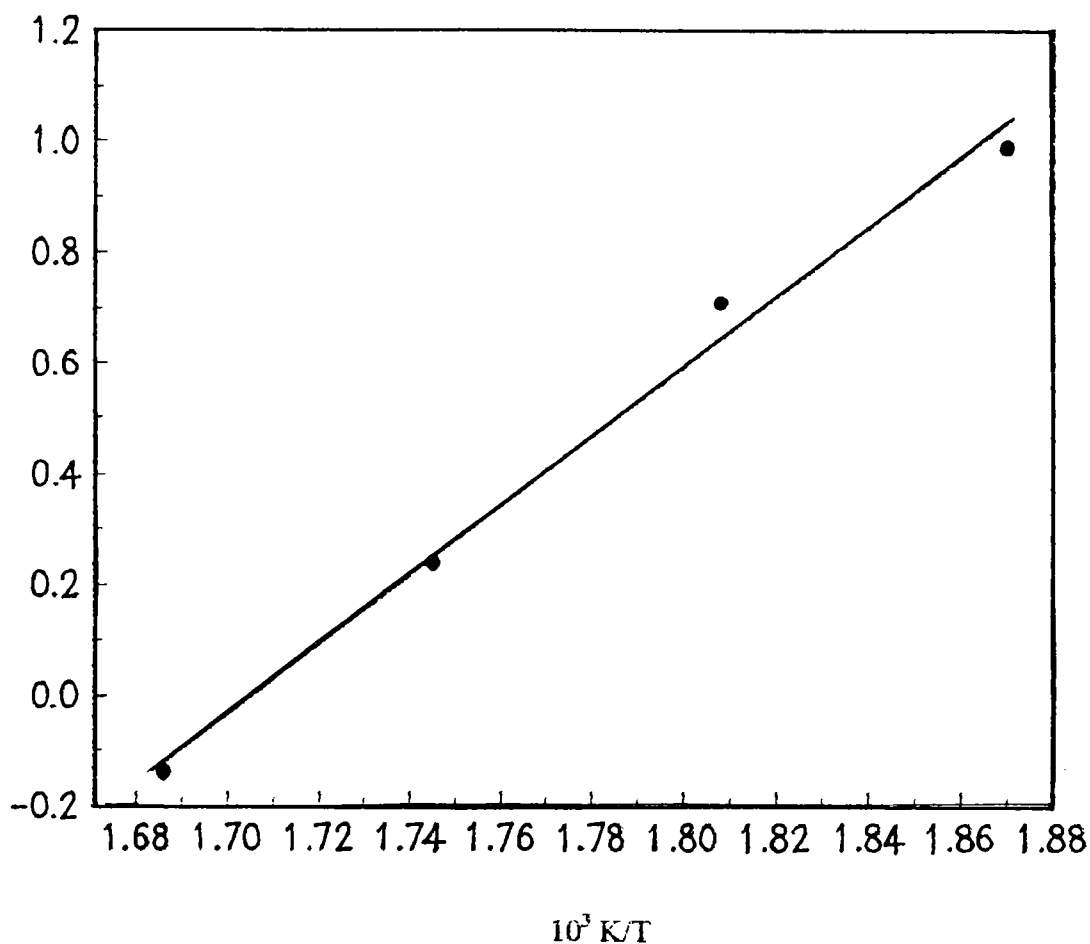


Fig. 4.8.2. Arrhenius plot of aniline methylation over $\text{Zn}_{0.8}\text{Co}_{0.2}\text{Fe}_2\text{O}_4$.

The activation energy calculated for $\text{Zn}_{0.8}\text{Co}_{0.2}\text{Fe}_2\text{O}_4$ is considerably lesser than the one calculated for γ -alumina by An-Nanko *et al.* [18] for which the activation energy value was 62.7 kJ mol^{-1} . Similarly for MgO catalyst, the activation energy of the first methylation was reported to be 67.8 kJ mol^{-1} [30].

4.9. COMPARISON WITH γ -ALUMINA AND ZEOLITES

Various types of zeolites and metal oxides have been tried for aniline alkylation. Among the metal oxides γ -alumina is one of the widely studied systems. Metal exchanged metallosilicates are also extensively studied. The product distribution data in aniline alkylation over various metallosilicates are summarized below (Table 4.9.1) [31] whereas the results obtained using γ -alumina as a catalyst are presented in

Table 4.9.2 [18]. The activity data of the most active ferrite systems are also included in the same table.

Catalyst	Conversion	Selectivity, %		
		NMA	NNDMA	Others
Silicalite	3.2	87.6	12.4	Nil
[Al]ZSM-5	71.4	51.7	36.8	11.5
[Fe]ZSM-5	30.1	79.1	15.1	5.8
[Ni]ZSM-5	33.7	57.1	39.7	Nil
[Zr]ZSM-5	66.3	78.7	19.8	1.5

Table 4.9.1. Product distribution in aniline alkylation over various metallosilicates. Reaction condition: Reaction temperature 400 °C, LHSV 4.3, TOS 1 h, feed composition aniline:methanol:N₂ 1:3:23

Catalyst	Conversion	Selectivity, %		
		NMA	NNDMA	Others
γ-alumina	34.5	64.2	35.7	0.1
ZnFe ₂ O ₄	51.6	97.8	0.1	0.1
Zn _{0.8} Co _{0.2} Fe ₂ O ₄	50.8	99.5	0.5	Nil
Zn _{0.5} Co _{0.5} Fe ₂ O ₄	36.7	99.8	--	0.1
Zn _{0.8} Ni _{0.2} Fe ₂ O ₄	36.0	96.6	0.4	0.6

Table 4.9.2. Product distribution data of aniline alkylation using methanol over γ-alumina and some ferrosilicates containing Zn, Co and Ni. Reaction conditions: Reaction temperature 350°C, molar ratio (methanol:aniline) 2:1, TOS 2 h.

Metallosilicates displayed poor selectivity for mono alkylation and appreciable conversion was obtained only at sufficiently high reaction temperatures. In addition it was reported that such catalysts are deactivating quickly, so that appropriate regeneration procedures should be adopted for regaining the original activity. With

γ -alumina also selectivity was poor, and the activity decreased with time due to coke formation. Ferrite systems executed excellent selectivity for N-monoalkylation. ZnFe_2O_4 and $\text{Zn}_{0.8}\text{Co}_{0.2}\text{Fe}_2\text{O}_4$ gave good conversion even at comparatively low reaction temperatures. Except ZnFe_2O_4 all other ferrites displayed prolonged stability.

REFERENCES

- [1] Y. Ki Park, K. Yon Park and S. Ihl Woo; *Catalysis Letters*, 26 (1994) 169.
- [2] A.B. Brown and E.E. Reid; *J. Am. Chem. Soc.*, 46 (1924) 1836.
- [3] C.E. Andrews; U.S. Patent, 2 073 671.
- [4] A.G. Hill, J.H. Shipp and A.J. Hill; *Ind. Eng. Chem.*, 43 (1951) 1579.
- [5] Y. Ono; *Cat tech*, March 1997.
- [6] W.W. Kaeding and R.E. Holland; *J. Catal.*, 109 (1988) 212.
- [7] S. Narayanan, V.D. Kumari and S. Sudhakar Rao; *Appl. Catal. A*, 111(1944)133.
- [8] V.Venkat Rao, V.D. Kumari and S. Narayanan; *Appl. Catal.*, 49 (1989) 165.
- [9] K.V.C. Rao, K.R. Sabu and C.G.R. Nair; *Bull. Chem. Soc. Jpn.*, 62 (1989) 2657.
- [10] S. Narayanan and B.P. Prasad; *J.Chem. Soc., Chem. Commun.*, (1992) 1204.
- [11] J.R. Butruille and T.J. Pinna Vaia; *Catal. Lett.*, 12 (1992) 187.
- [12] J.H. Clark, A.P. Kybett, D.J. Macquarrie, S.J. Barlow and P. London; *J. Chem. Soc. Chem. Commun.*, (1989)1353.
- [13] K.G. Ione and O.V. Kikhitiyanin; *Stud. Surf. Sci. Catal.*, 49 (1989) 1073.
- [14] S.I. Woo, J.K. Lee, S.B. Hong, Y.K. Park and Y.S. Uh; *Stud. Suf. Sci. Catal*; 49 (1989) 1095.
- [15] R.R.H.P. Rao, P. Massiani and D. Barthoment; *Catal. Lett.*, 31 (1995) 115.
- [16] R. Bandyopadhyay, P.S. Singh and B.S. Rao; *Appl. Catal.*, 155 (1997) 27.
- [17] S. Narayanan, K. Deshpande; *J. Mol. Catal.*, 135 (1996) 125
- [18] An. Nan Ko, C.L. Yang, Wei-de Zhu, H. EnLin; *Appl. Catal.*, 134 (1996) 53.
- [19] P.S. Singh, R. Bandyopadhyay and B.S. Rao; *Appl. Catal.A*, 136 (1996)177.
- [20] C.S. Narasimhan and C.S. Swamy; *Appl. Catal.*, 2 (1982) 315.
- [21] G.R. Dube and V.S. Darshane; *J. Chem. Soc. Farad. Trans*, 88 (9) (1992) 1299.
- [22] C.S. Narasimhan, C.S. Swami; *Appl. Catal.*, 2 (1982) 315.
- [23] F.C. Romeijn; *Phil. Res. Rep.*, 8 (1953) 304.
- [24] J.P. Jacobs, A. Maltha, J.R.H. Reintjes, T. Drimal, V. Ponec, H.H. Brogersma; *J. Catal.*, 147 (1994) 294.

- [25] S.P. Ghorpade, V.S. Darshane, S.G. Dixit; *Appl. Catal. A*, 166 (1998) 141.
- [26] Z.H. Fu and Y. Ono; *Catal. Lett.*, 18 (1993) 59.
- [27] Y. Ono; *Catalysis Today*, 35 (1997) 15.
- [28] F. Totta, P. Tundo and G. Moraglio; *J. Org. Chem.* 52 (1987) 1300.
- [29] Z.H. Fu and Y. Ono; *Catal. Lett.*, 22 (1993) 277.
- [30] N. Takamiya, Y. Koinuma, K. Ando and S. Murai; *Nippon Kagakukaishi*, (1979) 1452.
- [31] Yong Ki Park, Kun Yon Park and Seong Ihl Woo; *Catal. Lett.*, 26 (1994) 169.

CHAPTER V
ALKYLATION OF PHENOL

5.1. INTRODUCTION

Alkyl phenols are the compounds having the alkyl groups substituted or replaced either in the phenyl ring or in the OH group. Cresols, xylenols, alkoxyphenols and trialkyl substituted phenols are some of the important alkylphenols [1-2]. These are industrially important chemical intermediates in the manufacture of pharmaceuticals, pesticides, plastics and a variety of chemicals. Fig. 5.1.1 gives a glossary of various phenolic compounds of industrial interest.

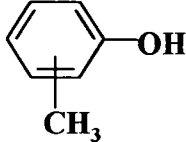
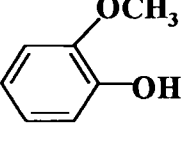
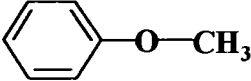
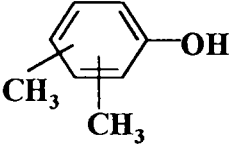
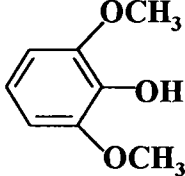
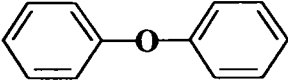
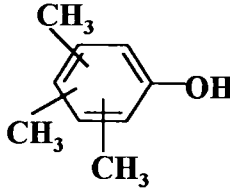
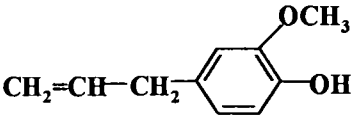
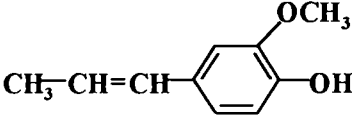
Alkylated phenols	Methoxylated phenols	Phenolic ethers
 <p>Cresol</p>	 <p>Guaiacol</p>	 <p>Anisole</p>
 <p>Xylenol</p>	 <p>2,6-Dimethoxyphenol</p>	 <p>Diphenylether</p>
 <p>Trimethylphenol</p>	 <p>Eugenol</p>	
	 <p>Isoeugenol</p>	

Fig. 5.1.1. Glossary of phenolic compounds.

Among the above discussed phenolic compounds, the most demanding ones are o-cresol and 2,6-xylenol since both of them are extensively being employed for the production of resins, herbicides, insecticides, antioxidants and other chemicals. The

principal market for o-cresol and 2,6-xylenol are for the synthesis of epoxycresol novolak (ECN) and poly(phynylene ether)resins. The aromatic nucleus of alkylphenols can undergo a variety of aromatic electrophilic substitution reactions. Electron density from the hydroxyl group can be fed into the ring. Besides activating the aromatic nucleus, the hydroxyl group controls the orientation of the incoming electrophile. Under acidic conditions phenol (or alkylphenol) reacts with formaldehyde and yields novolaks. Phenolic novolaks are thermoplastic resins having a molecular weight of 500-5000 and a glass-transition temperature of 45-70 °C. The monomer units can be represented as (Fig. 5.1.2):

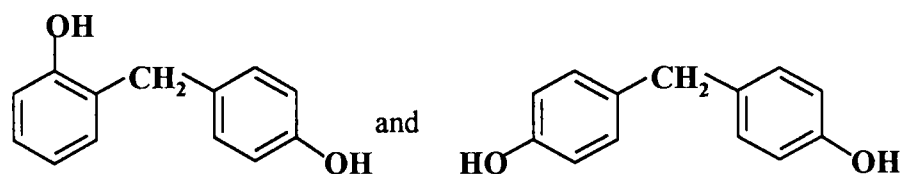


Fig. 5.1.2. Monomer units of phenolic novolak.

Continued reaction leads to novolak polymers having a molecular weight upto 5000. Calixarenes are another industrially valuable products [2]. These are cyclic oligomers of methylene bridged alkylphenols. These molecules are significant in the field of research devoted to host-guest complexation.

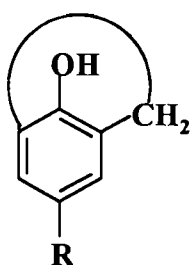


Fig. 5.1.3. Cyclic oligomer unit of methylene bridged alkylphenols.

Other uses of o-cresol include its conversion to a dinitro compound, 4,6-dinitro-2-methylphenol, which is used as a herbicide. About 90-95 % of 2,6-xylenol is being

employed for the production of poly(phenylene oxide) [2]. The poly(phenylene oxide) derived from 2,6-xyleneol is blended with other polymers, and the resulting alloy is widely used in electronic industry. Apart from o-cresol and 2,6-xyleneol, other alkylated phenols like p-cresol, m-cresol and other xyleneol isomers are also being widely employed for many industrial processes. The important applications of various alkyl phenols are represented in the following table (Table 5.1.1).

Alkylphenol	Applications
o-Cresol	in the production of novolak resins, 4,6-dinitro-2-methylphenol (a herbicide) and antioxidants. O-Cresol is a component of cresylic acids, which are used as solvents in a number of coating applications.
m-Cresol	antioxidants, herbicides and insecticides.
p-Cresol	antioxidants. Some derivatives of p-Cresol are used for stabilizing natural and synthetic rubber.
2,6-Xyleneol	poly(phenylene oxide)resin, epoxy resin.

Table 5.1.1. Industrial applications of various alkyl phenols.

The demand for these alkyl phenols has increased in recent years, and catalytic research has been oriented to synthesise selective catalysts for the respective alkyl phenols. The stringent specifications and the demand of these chemicals necessitate the development of catalytic systems and the process for the selective production. Vapour-phase alkylation over environmentally friendly solid acid catalysts is a very good alternative to the conventional route with proton acids or Friedel-Crafts type systems. Several types of catalysts based on zeolites, oxides and hydrotalcite like materials have been advocated for the reaction [3-10]. However, many of these systems showed disadvantages such as lower life time, very high reaction temperature and poor product selectivity. Frequently due to coke formation catalysts deactivate with time on stream. The commercial process for the synthesis of o-cresol and 2,6-xyleneol is based mainly on magnesium oxide and supported vanadium-iron mixed oxide [2]. Oxide catalysts generally show better selectivity than zeolites for o-cresol and

2,6-xyleneol, however in many cases, the major influence on selectivity comes from the acido-basic property of the systems acting as catalysts.

The present chapter contains a detailed discussion on phenol alkylation experiments using ferros spinel systems of Zn, Co and Ni as catalysts. We observed that some ferrite compositions could produce 2,6-xyleneol and o-cresol in high selectivities, and, unlike other conventional systems, their activities remained for longer durations. The chapter is divided into two sections. A detailed discussion on process optimization is given in the first section. We have already observed that surface acid-base properties of ferrites strongly depend on cation distribution and composition. Second section of this chapter deals with reaction network, where a detailed discussion on activity variation with spinel composition and acid-base properties is included.

SECTION I. PROCESS OPTIMIZATION

Alkylation experiments were carried out in a fixed-bed vapour-phase reactor at 280-400 °C under atmospheric pressure. 3 g catalyst was charged during each experiment. Prior to the run, the catalyst was activated in flowing air at 500 °C for 2 h and then brought down to the required reaction temperatures by using a current of nitrogen gas of high purity. After terminating the flow of nitrogen, the feed mixture (methanol and phenol) was admitted into the reactor by means of a syringe pump. Weight hourly space velocity (WHSV) was varied from 1.27 h⁻¹ to 3.1 h⁻¹. Liquid products were analyzed using Shimadzu GC 15A gas chromatograph fitted with FID and using a FAP-S-10% on 60/80 Chromosorb W(AW) column. Products were identified using GC-MS and GC-FTIR studies. During the catalytic run some amount of methanol was simultaneously consumed by the gasification due to some side reactions giving non-condensable products like CO, CO₂ and CH₄. Gaseous products were analyzed using Porapak-Q column and TCD. Phenol conversion and product yield were expressed in Wt.%. The selectivities (S) of o-cresol and 2,6-xyleneol were expressed as follows:

$$S_{\text{o-cresol}} (\%) = \frac{\text{Yield of o-cresol}}{\text{Total conversion of phenol}} \times 100$$

$$S_{\text{2,6-xyleneol}} (\%) = \frac{\text{Yield of 2,6-xyleneol}}{\text{Total conversion of phenol}} \times 100$$

A blank run was carried out at 350°C with no catalyst in the reactor indicating negligible thermal reaction.

5.2. Co_{1-x}Ni_xFe₂O₄ TYPE SYSTEMS

5.2.1. Effect of reaction temperature: The activities and selectivities of the catalysts as a function of reaction temperature are shown in Table 5.2.1. As the temperature was increased from 300 °C the yield of both o-cresol and 2,6-xyleneol increased apparently. However temperature does not show any marked influence on O-alkylation and anisole concentration remained less than 3 % over all catalysts throughout the temperature range studied. It can be seen from the table that all catalysts are highly liable to form only ortho methylated products, viz. o-cresol and 2,6-xyleneol, with total ortho selectivity more than 96%. Also, it is clear from the alkylation studies that there is hardly any xyleneol isomers under the experimental conditions used. With an increase in temperature, the consecutive methylation of o-cresol to 2,6-xyleneol increased; maximum yield of 2,6-xyleneol was observed at 350°C. Further increase in temperature did not enhance the alkylation rate, but some phenol started decomposition and formed products like benzene and toluene. At higher temperatures, the analysis of vapour products indicated the presence of considerable amount of formaldehyde, oxides of carbon and C₁ and C₂ hydrocarbons, indicating the generation of strong acid sites on the catalyst surface, where methanol undergoes decomposition in greater extent. The generation of new acid sites has further been confirmed by passing methanol alone over the catalysts, where decomposition rate was found to be increased considerably after 350 °C.

Reaction temp., °C	Product distribution*					
	Phenol conversion	o-Cresol yield	2,6-Xylenol yield	Anisole yield	o-Cresol selectivity	2,6-Xylenol selectivity
Co₁Ni_{1-x}Fe₂O₄ (x = 0, 0.2, 0.5, 0.8 and 1)						
x = 0						
300	60.00	38.70	20.27	1.06	63.45	33.17
325	85.69	38.20	42.42	2.77	44.63	49.56
350	92.25	16.87	70.20	2.87	18.62	77.48
400	85.77	34.44	41.83	0.64	43.18	52.80
x = 0.2						
300	49.34	32.51	16.01	0.17	65.65	32.23
325	70.12	34.20	34.92	0.77	48.93	49.96
350	80.32	23.72	54.50	1.52	29.75	68.34
400	69.34	40.31	28.77	0.53	57.69	41.14
x = 0.5						
300	48.42	29.72	18.70	0.22	60.72	38.44
325	65.70	29.21	34.52	0.48	45.49	53.76
350	79.32	25.50	51.59	0.59	32.70	65.95
400	66.52	31.07	33.20	0.53	44.94	51.23
x = 0.8						
300	46.52	27.29	19.02	Nil	58.93	41.07
325	64.34	28.21	35.72	0.05	44.13	55.87
350	88.06	23.21	58.01	0.05	28.27	70.65
400	67.23	27.58	38.23	0.06	41.91	58.00
x = 1.0						
300	20.72	16.40	4.21	0.17	78.50	20.15
325	36.43	28.50	7.21	0.33	79.07	20.00
350	43.25	33.70	6.82	Nil	81.16	16.87
400	32.33	27.20	5.13	Nil	84.13	15.87

* Other products include benzene, toluene and traces of phenolic ethers.

Table 5.2.1. Effect of reaction temperature on phenol conversion and product yield and selectivities. WHSV 1.27 h⁻¹, TOS 2 h, and methanol-phenol molar ratio 7:1.

5.2.2. Selection of phenol to methanol molar ratio: Different molar ratios of phenol to methanol viz. 2, 5 and 7 were performed at 350 °C over CoFe₂O₄. Major products, o-cresol and 2,6-xylenol, showed linear dependence with feed ratio. At lower methanol to phenol ratio conversion was less and a gradual increase in o-cresol yield was observed upto the molar ratio of 5. The increase in o-cresol concentration is

associated with a simultaneous rise in 2,6-xylenol concentration. However, maximum value of 2,6-xylenol yield was observed at feed-mix ratio of 7 whereas o-cresol concentration remained more or less unaffected after a feed-mix ratio of 5. Hence the feed-mix ratio 7 was maintained throughout the experiments. o-Cresol and 2,6-xylenol showed selectivity more than 96 % for the sum of both products. Increase in the molar ratio enhances the ring alkylation rate, which leads to the formidable formation of alkylated phenols. The following table (Table 5.2.2) illustrates the influence of feed molar ratio on phenol methylation.

Molar ratio (MeOH/PhOH)	2	5	7
Product distribution, Wt. %			
Non-aromatics	Nil	Nil	0.40
Benzene	0.07	0.08	0.03
Toluene	0.34	0.37	0.23
Anisole	1.89	3.03	2.87
Unreacted phenol	51.37	18.23	7.75
o-Cresol	11.21	17.44	16.87
2,6-Xylenol	30.71	60.85	70.20
Other alkylphenols	2.50	0.05	0.80
Others	1.75	Nil	0.80
Phenol conversion	48.63	81.77	92.25
Selectivity			
o-Cresol	23.13	22.27	18.62
2,6-Xylenol	63.35	77.72	77.40

Table 5.2.2. Effect of methanol to phenol molar ratio on phenol conversion and selectivities of o-cresol and 2,6-xylenol over CoFe_2O_4 . Reaction temperature $350\text{ }^\circ\text{C}$, WHSV 1.27 h^{-1} and TOS 2 h.

5.2.3. Effect of contact time: The influence of contact time (WHSV) on phenol conversion and product yield at $350\text{ }^\circ\text{C}$ performed over CoFe_2O_4 is depicted in Fig. 5.2.1. o-Cresol was formed as the major product at lower contact time regions; however, considerable amount of 2,6-xylenol was also detected along with o-cresol. Increase in contact time increases 2,6-xylenol yield, and this was associated with a corresponding decrease in the o-cresol yield, indicating consecutive methylation of the latter over the catalyst surface at high contact time. Traces of benzene and toluene

were also detected at high contact time regions, but anisole concentration virtually remained unaffected with space velocity variations.

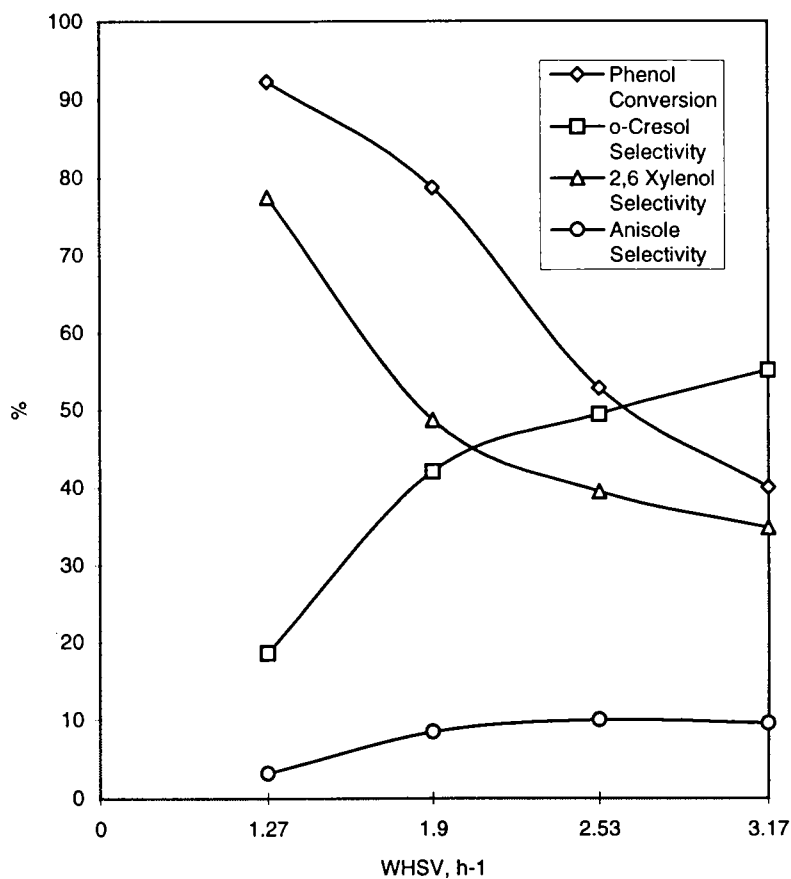


Fig. 5.2.1. Effect of contact time on phenol conversion and product selectivities over CoFe_2O_4 . Reaction temperature 350°C , feed molar ratio (methanol to phenol) 7, TOS 2 h.

5.2.4. Composition effect of catalysts: Catalytic activity as a function of composition is shown in Fig. 5.2.2. The influence of Co-Ni composition is a decisive factor for catalytic activity. Maximum yield for 2,6-xylenol was observed on the systems with the lowest 'x' value, *i.e.* CoFe_2O_4 . As 'x' increases activity for secondary alkylation reduces; however total ortho selectivity was always observed to be above 96% regardless the composition of the systems.

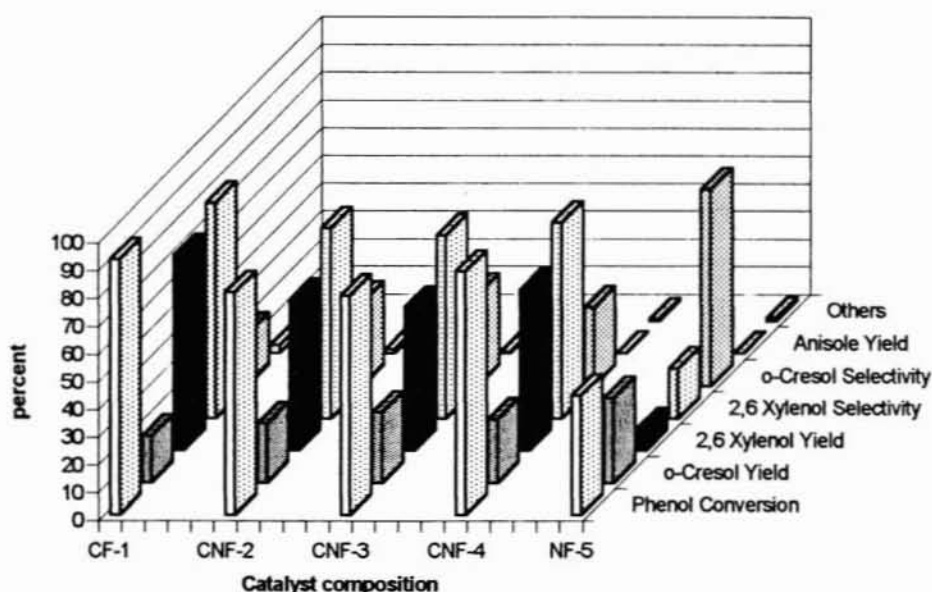


Fig. 5.2.2. Product distribution and selectivity pattern of phenol alkylation using MeOH over different Co-Ni-ferrite systems. Reaction temperature 350 °C, methanol to phenol molar ratio 7, WHSV 1.27 h⁻¹ and TOS 2 h. Catalyst designation: CF-1 (CoFe₂O₄); CNF-2 (Co_{0.8}Ni_{0.2}Fe₂O₄); CNF-3 (Co_{0.5}Ni_{0.5}Fe₂O₄); CNF-4 (Co_{0.2}Ni_{0.8}Fe₂O₄); NF-5 (NiFe₂O₄).

5.2.5. Effect of time on stream: Time on stream studies under the experimental conditions of WHSV 1.27 h⁻¹ and reaction temperature 350 °C were carried out over a period of 10 hours (Fig. 5.2.3). Among the systems CoFe₂O₄ showed excellent stability; both Co_{0.8}Ni_{0.2}Fe₂O₄ and Co_{0.5}Ni_{0.5}Fe₂O₄ showed slight deactivation whereas rapid deactivation was observed for Co_{0.2}Ni_{0.8}Fe₂O₄ and NiFe₂O₄.

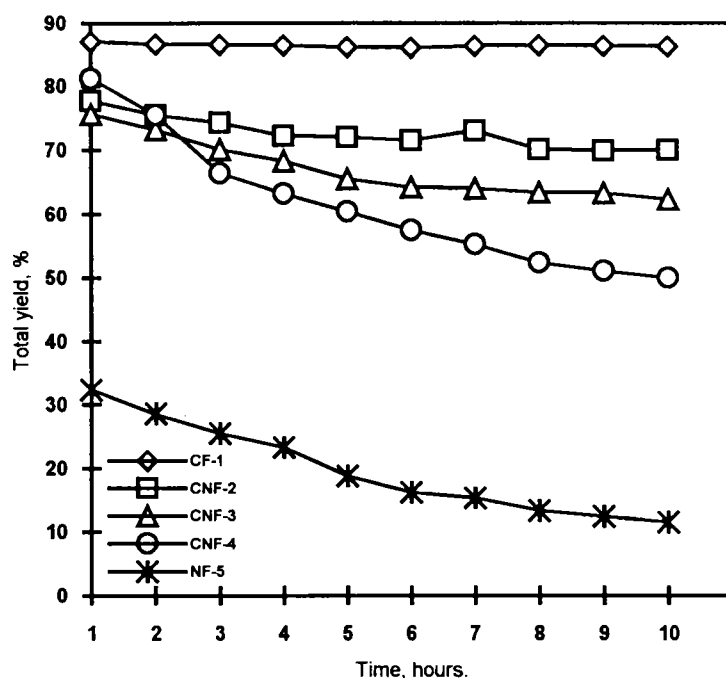


Fig. 5.2.3. Stability study of different Co-Ni ferrite systems in ortho alkylation of phenol using methanol as the alkylating agent. Total yield (o-cresol+2,6-xylene) is plotted against time in hours. Reaction temperature 350 °C, methanol-phenol molar ratio 7:1 and WHSV 1.27 h⁻¹. Catalyst designation: CF-1 (CoFe₂O₄); CNF-2 (Co_{0.8}Ni_{0.2}Fe₂O₄); CNF-3 (Co_{0.5}Ni_{0.5}Fe₂O₄); CNF-4 (Co_{0.2}Ni_{0.8}Fe₂O₄); NF-5 (NiFe₂O₄).

5.2.6. Effect of water in the feed: From the above discussions we have seen that at a feed ratio (methanol to aniline) of 7 Co-Ni systems can effectively alkylate phenol in the ortho positions. 350 °C is found to be the most suitable reaction temperature. Since we are using excess of methanol and also since the reaction is performed in a vapor-phase set-up, some amount of methanol will be lost due to decomposition or side reactions. In order to minimise these side reactions and, hence, to recover maximum methanol after the reaction, we have studied the influence of water in the feed. Another advantage of using water is that steam will prevent or suppress the coke formation and will activate the catalyst surface. The data obtained were presented in the following table (Table 5.2.3). As can be seen from the table, water in small quantities suppressed significantly the methanol consumption without affecting much the product yields.

Product distribution	Feed composition (MeOH:H ₂ O:PhOH)		
	Without water	6:1:1	5:2:1
Non aromatics	0.40	Nil	Nil
Benzene	0.03	0.65	0.25
Toluene	0.23	0.63	0.30
Anisole	2.87	0.10	0.10
Unreacted phenol	7.75	10.04	37.82
o-Cresol	16.87	19.53	18.30
2,6-Xylenol	70.20	68.28	42.31
Other alkylphenols	0.80	0.45	0.33
Others	0.80	0.21	0.17
Phenol conversion	92.25	89.96	62.18
Selectivity			
o-Cresol	18.62	21.73	29.63
2,6-Xylenol	77.48	75.98	68.50
Methanol conversion	62.20	51.17	42.20

Table 5.2.3. Effect of water in the feed. Catalyst CoFe₂O₄, flow rate 4 ml/h, reaction temperature 350 °C, catalyst amount 3 g, and TOS 1 h.

5.3. Zn_{1-x}Co_xFe₂O₄-TYPE SYSTEMS

5.3.1. Effect of catalyst composition: A series of experiments were performed to evaluate the catalytic activities of different Zn-Ni ferrites. The results obtained are summarized in the following table (Table 5.3.1). It is clear from the table that, pure Zn-ferrite is not so active, but activity increased as Zn is being substituted with Co. Thus unlike the previously discussed aniline alkylation reactions, where activity is mainly due to the iron concentration in the octahedral sites, here the Co²⁺ ions, which always occupy the octahedral sites, influence the reaction rate.

$Zn_{1-x}Co_xFe_2O_4$					
Product distribution, Wt. %	x = 0	x = 0.2	x = 0.5	x = 0.8	x = 1.0
Benzene	Nil	Nil	Nil	Nil	0.03
Toluene	Nil	Nil	Nil	Nil	0.63
Anisole	0.8	0.8	Nil	0.07	2.87
Unreacted phenol	74.16	59.87	45.13	25.16	7.75
o-Cresol	18.50	19.77	33.50	21.76	16.87
2,6-Xylenol	7.24	18.50	21.13	48.45	70.20
Others	0.03	0.01	Nil	Nil	1.00
Phenol conversion	25.84	40.13	54.87	74.84	92.25
Selectivity					
Anisole	3.01	2.09	--	0.5	3.00
o-Cresol	69.70	51.65	61.32	30.99	18.62
2,6-Xylenol	27.27	48.34	38.67	69.00	77.40

Table 5.3.1. Product distribution data of phenol methylation using methanol over different Zn-Co ferrites. Reaction temperature 350 °C, WHSV 1.27 h⁻¹, methanol-phenol molar ratio 7:1 and TOS 1 h.

5.3.2. Effect of reaction temperature: The results of the alkylation of phenol in the temperature range 300-400 °C over $Zn_{0.2}Co_{0.8}Fe_2O_4$ are given in Table 5.3.2. In general, an increase in temperature seems to increase the phenol conversion. The products formed in this temperature range are mainly o-cresol and 2,6-xylenol. Below 350 °C o-cresol selectivity was more, and after 350 °C 2,6-xylenol selectivity increased at the expense of o-cresol selectivity, indicating the generation of new sites in the temperature range 350-400 °C where more amount of o-cresol can undergo further alkylation. As in the case of Co-Ni systems, at higher temperature phenol decomposition rate is also enhanced as indicated by more side products.

Product distribution, Wt. %	Reaction temperature, °C			
	300	325	350	400
Phenol conversion	25.74	42.00	54.87	65.34
o-Cresol yield	18.20	20.21	33.50	24.63
2,6-Xylenol yield	7.47	21.71	21.13	35.20
Others	0.07	0.08	0.24	5.51
o-Cresol selectivity	70.70	48.11	61.32	37.70
2,6-Xylenol selectivity	29.02	51.69	38.67	53.90

Table 5.3.2. Effect of reaction temperature on phenol alkylation using methanol over $Zn_{0.2}Co_{0.8}Fe_2O_4$. Reaction conditions: Feed molar ratio (methanol-phenol) 7:1; WHSV 1.27 h^{-1} and TOS 2 h.

5.3.3. Effect of feed flow rate: Alkylation experiment was carried out at different space velocities as indicated by the Fig. 5.3.1. Studies on the effect of contact time on the conversion of phenol and the selectivity for o-cresol and 2,6-xylenol showed that the activity was maximum at feed flow rate of 4 ml/h. The selectivity for 2,6-xylenol increased with increasing contact time (decreasing flow rate). Investigation of the effect of feed flow rate indicated that the reaction can be studied conveniently at flow rate 3 or 4 ml/h, as a further increase in flow rate did not improve the conversion to any great extent.

5.3.4. Selection of feed molar ratio: Figure 5.3.2 describes the effect of feed molar ratio on phenol methylation. Increase in methanol concentration increased both phenol conversion and 2,6-xylenol yield. At lower feed-mix ratio (methanol to phenol), selectivity for o-cresol was more. 2,6-Xylenol yield increased linearly with molar ratio. However, phenol conversion decreased at sufficiently high methanol concentration, since the availability of phenol molecules in the neighbouring sites of a coordinated methanol is comparatively less in a highly diluted phenol solution.

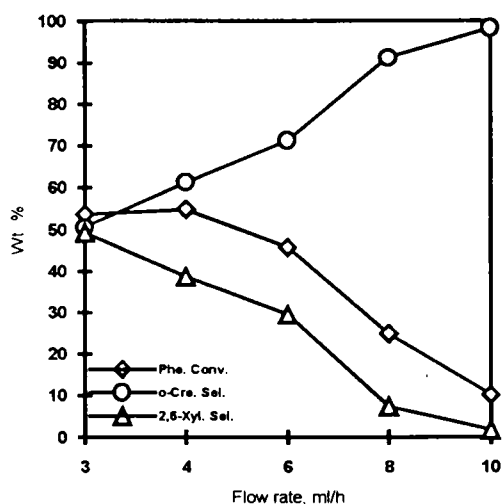


Fig. 5.3.1. Effect of feed flow rate on phenol alkylation over $Zn_{0.2}Co_{0.8}Fe_2O_4$. Reaction temperature $350\text{ }^\circ\text{C}$, molar ratio (methanol to phenol) 7, TOS 2 h.

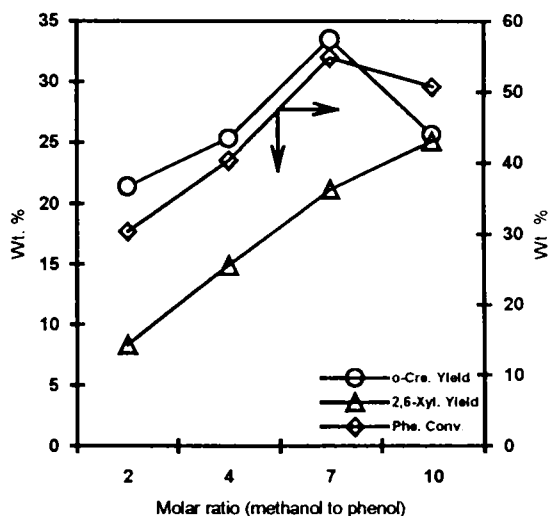


Fig. 5.3.2. Effect of feed molar ratio on phenol alkylation over $Zn_{0.2}Co_{0.8}Fe_2O_4$. Reaction temperature $350\text{ }^\circ\text{C}$, WHSV 1.27 h^{-1} , TOS 2 h.

5.4. $Zn_{1-x}Ni_xFe_2O_4$ -TYPE SYSTEMS

5.4.1 Influence of catalyst composition: Variation of catalytic activity as a function of composition is given in the following table (Table 5.4.1).

$Zn_{1-x}Ni_xFe_2O_4$	x = 0	x = 0.2	x = 0.5	x = 0.8	x = 1.0
Benzene	Nil	Nil	Nil	Nil	0.30
Toluene	Nil	Nil	Nil	Nil	0.46
Anisole	0.80	0.30	Nil	0.41	Nil
Unreacted phenol	73.66	80.37	73.31	57.00	56.75
o-Cresol	18.50	15.40	26.69	27.60	30.70
2,6-Xylenol	7.24	4.00	20.00	15.00	7.82
Phenol conversion	26.34	19.63	6.69	43	43.25
Selectivity					
o-Cresol	69.70	78.45	74.93	64.18	79.69
2,6-Xylenol	27.27	20.37	25.06	34.88	20.30

Table 5.4.1. Activity data of $Zn_{1-x}Ni_xFe_2O_4$ -type ferrispinels for phenol alkylation using methanol as the alkylating agent. Reaction temperature $350\text{ }^\circ\text{C}$, WHSV 1.27 h^{-1} and TOS 2 h.

ZnFe₂O₄ showed only mild activity. As 'x' is increased the activity first decreased and then increased. However, all Zn-Ni systems executed less activity compared to the corresponding Zn-Co and Co-Ni systems. The poor activity can be accounted for by the low acidity possessed by Zn-Ni systems.

5.4.2. Effect of reaction temperature and contact time: Unlike the other two systems described so far, maximum activities of Zn-Ni systems were obtained at 380°C. At still higher temperatures conversion and selectivities were decreased. Data are presented in Fig. 5.4.1. Influence of contact time is also studied. Increase in contact time increased phenol conversion and 2,6-xylenol selectivities, whereas at lower contact times secondary alkylation rate decreased and, consequently, o-cresol selectivity increased as shown in the Fig 5.4.2.

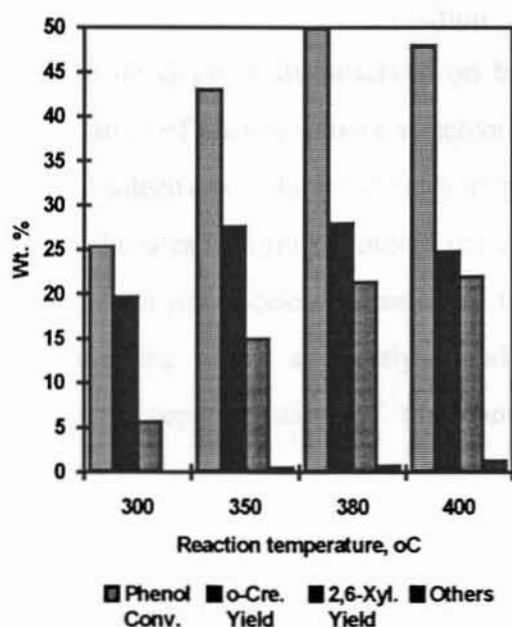


Fig. 5.4.1. Effect of reaction temperature on phenol methylation over Zn_{0.2}Ni_{0.8}Fe₂O₄. WHSV 1.27 h⁻¹, methanol-phenol molar ratio 7:1 and TOS 2 h.

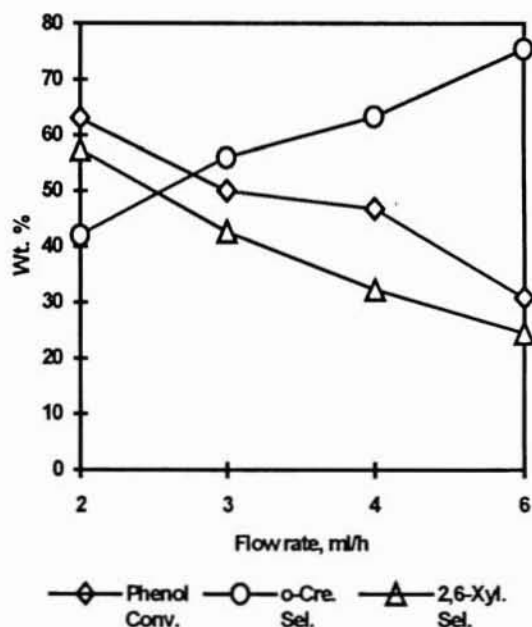


Fig. 5.4.2. Effect of feed flow rate on phenol methylation over Zn_{0.2}Ni_{0.8}Fe₂O₄. Reaction temperature 380 °C, molar ratio (methanol-phenol) 7:1 and TOS 2 h.

SECTION II. REACTION PATHWAYS

5.5. GENERAL CATALYTIC PATHWAY

Alkylation of phenol with methanol gives several products such as cresols, xylenols, anisole and higher alkyl phenols. Selectivity of products depends to a large extent on the acid-base properties of the systems and upto a certain extent on the experimental conditions. Several mechanisms have been proposed for phenol alkylation over acidic catalysts [3]. It is postulated that phenol methylation over strong acid catalysts proceeds through the initial formation of anisole followed by the intramolecular rearrangement of methyl group to form o-cresol. The methyl group in the ortho position can further undergo isomerization to form meta and para isomers. The formation of meta and para isomers is accelerated at higher temperatures and with stronger acid catalysts. Xylenol isomers are produced by the consecutive methylation of cresol isomers. Another plausible route involves direct C-alkylation giving cresols and xylenols, without the formation of anisole as an intermediate. This type of mechanism is generally observed on basic and bifunctional systems. In such cases methylation of phenol is more selective to ortho positions and yield o-cresol and 2,6-xylenol selectively. On these catalysts phenol adsorbs dissociatively on a pair of basic and acidic sites to form a protonic site and an adsorbed phenolate species, respectively. This proton site accelerates methanol to produce a carbonium ion, which reacts with phenolic ring of an adjacently adsorbed phenolate species at ortho position. A schematic representation of the above mentioned two routes is shown below (Fig.5.5.1):

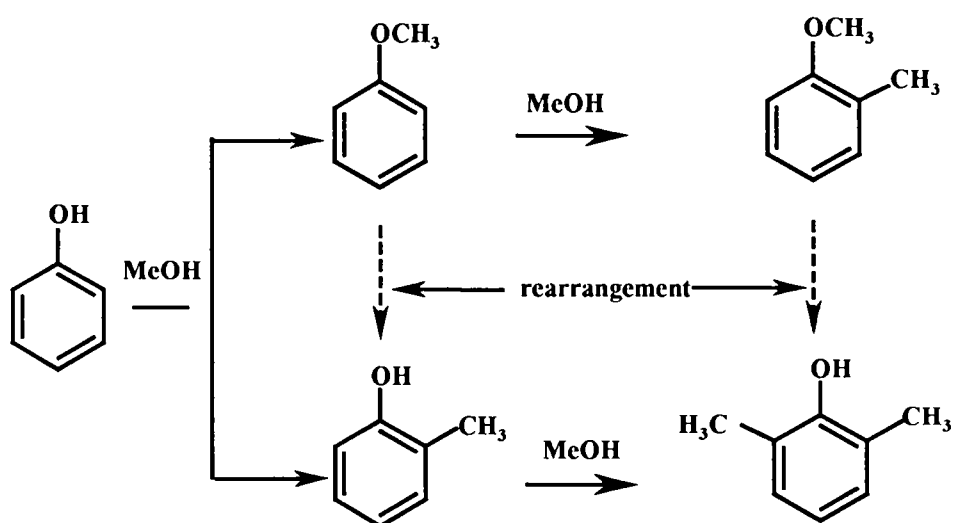


Fig. 5.5.1. A schematic representation of phenol alkylation using methanol.

Several papers and patents have been published on the alkylation of phenol with methanol in the presence of catalytic systems having varying acid-base properties, such as γ -alumina [11], silica-alumina [12], supported phosphoric acid [13], magnesium oxide [14], mixed oxides [15], zeolites [16-19] and acid solids such as Nafion-H [20] and metal phosphates [4]. On this subject literature data are scattered and in many cases inaccessible. Strong controversy is existing regarding the role of acid-base sites for the reaction. Tanabe and Nishizaki [12] reported that highly acidic catalysts are more active but less selective to ortho alkylation. However, Benzohariava and Al.Zahari [7] claimed that catalysts with strong acid sites favour O-alkylation and weak acid sites or strong basic sites favour C-alkylation. Santhacesaria and Grasso [3] compared the behaviour of catalysts with different acidic characteristics and reported that in the adsorption of reagents geometric factors play a fundamental role in affecting selectivity. Additionally they pointed out that Brønsted acid sites are responsible for coke formation. It was reported that in medium pore zeolites like H-ZSM5, activity is strongly dependent on the crystalline size, *i.e.* phenol conversion is completely dominated by the intra-crystalline molecular diffusion [21].

5.6. ACTIVITY AND SURFACE PROPERTIES OF THE PRESENT SYSTEMS:

From the detailed investigation of phenol methylation using methanol as the alkylating agent, we have seen that CoFe_2O_4 is the most selective and active catalyst for ortho alkylation of phenol. Substitution of Zn^{2+} ions in $\text{Zn}_{1-x}\text{Co}_x\text{Fe}_2\text{O}_4$ series and Ni^{2+} ions in $\text{Co}_{1-x}\text{Ni}_x\text{Fe}_2\text{O}_4$ series by Co^{2+} ions also increased their selectivity and activity towards ortho methylation, indicating the unique role played by the Co^{2+} ions. The catalytic effectiveness to a greater extent is determined by the cation distribution in the ferrosipinel lattice. Both acidic and basic characters vary with composition and, therefore, the variation of acid-base properties with composition is an important factor in explaining the catalytic activities of the present systems.

While studying the influence of contact time (WHSV) on phenol conversion and product selectivities over all the systems, we have noticed that o-cresol was the major product at lower contact times (high flow rates). Increase in contact time increased the 2,6-xylenol yield, and this was always observed with a corresponding decrease in o-cresol yield. This clearly indicates the consecutive methylation of o-cresol over the catalyst surface at high contact times. In all cases anisole concentration was negligible and did not show any marked variation with space velocity changes. Hence, the bimolecular mechanism as suggested by Pienotzzia and Nordquest [17], in which anisole served as its own alkylating agent cannot be considered in the present systems (Fig. 5.6.1). If anisole is acting as an intermediate, the rearrangement step would be significantly influenced by space velocity changes and one can expect more anisole at high space velocities.

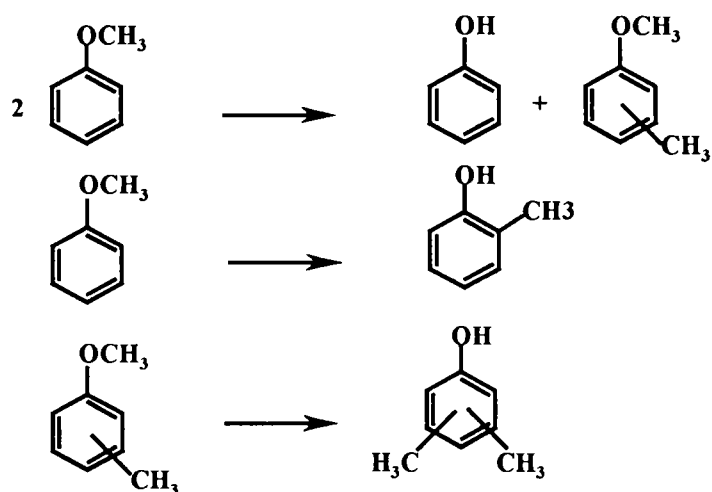


Fig. 5.6.1. Reactions of anisole- Transalkylation and rearrangements.

The above argument was further confirmed by passing anisole alone over the catalysts, where neither phenol nor any alkylated phenols could be detected. Additionally, when a feed mixture of o-cresol and methanol was passed over these catalysts enormous amount of 2,6-xyleneol (more than 78% over CoFe_2O_4) was detected (Table 5.6.1).

Product distribution	Wt. %
Non aromatics	0.05
Benzene	0.06
Toluene	0.04
Anisole	1.23
Phenol	2.5
Unreacted o-cresol	17.25
2,6-Xylenol	78.04
Methyl anisole	0.30
Other alkyl phenols	0.17
Others	0.30
o-Cresol conversion	82.75
2,6-Xylenol selectivity	94.44

Table. 5.6.1. Methylation of o-Cresol using methanol over CoFe_2O_4 . Reaction temperature 350°C , methanol - o-cresol molar ratio 3 and WHSV 1.3 h^{-1} .

Even at high contact times, selectivity for 2-methyl anisole was less than 1% at all temperatures. However, with increase in o-cresol contact time slight decrease in 2,6-xylenol selectivity was noticed. Traces of higher alkyl phenols were detected at this stage. From these observations it can be inferred that, o-cresol formed as a primary alkylated product undergoes secondary alkylation to give 2,6-xylenol rather than O-alkylation to give anisole followed by o-cresol and 2,6-xylenol. Hence the reaction path can be expressed as (Fig. 5.6.2):

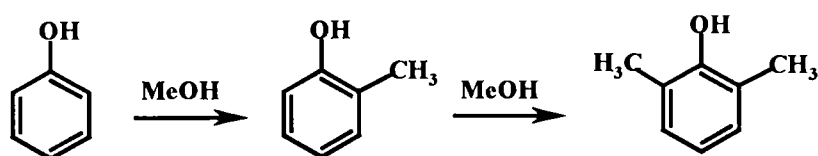


Fig. 5.6.2. Direct C-alkylation of phenol. 2,6-Xylenol is formed by the consecutive methylation of the initially formed o-Cresol.

Since the alkylation of phenol is essentially an acid-base reaction, the catalytic activity and product selectivity depend strongly on the acid-base properties of catalysts. All the ferrosphenel systems are highly selective to ortho alkylation. Generally, selectivity of products upto a greater extent depend on the nature of the acid sites. According to Tanabe and Nishizaki [12], the Brønsted acid sites strongly interact with the aromatic ring. Consequently, phenol molecule will lie parallel to the catalyst surface (Fig. 5.6.3) and, therefore, all positions of the ring will become equally accessible for the incoming group leading to poor selectivity for ortho alkylation.

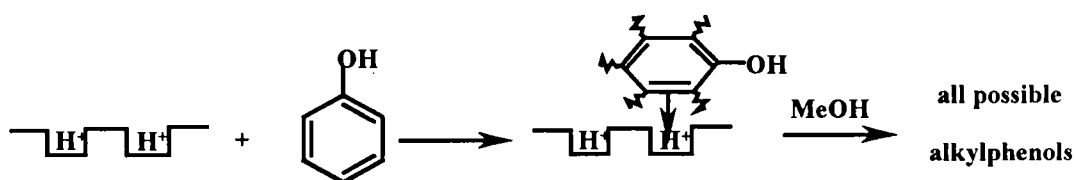


Fig. 5.6.3. Parallel orientation of benzene ring on the catalyst surface containing strong Brønsted acid sites.

But, using the ferrosphinel catalysts, under the optimized conditions, the total ortho selectivity always exceeded 96 %. Additionally we could not detect any xylene or cresol isomers. Consequently, phenol adsorption is never parallel to the surface in the case of ferrosphinel systems. High ortho selectivity can be explained by assuming vertical orientation of adsorbed phenol on the Lewis sites, as postulated for γ -alumina surface by Klemm *et al.* [22]. Vertical orientation prevents the aromatic ring from directly interacting with strong acid sites on the surface. According to this scheme, phenol molecule will interact with Lewis acid-base centers giving a phenolate ion adsorbed on the acid site and a hydrogen ion bound to the basic site. This proton site accelerates methanol to produce a carbonium ion, which reacts with benzene ring of an adjacently adsorbed phenolate species at ortho position (Fig. 5.6.4).

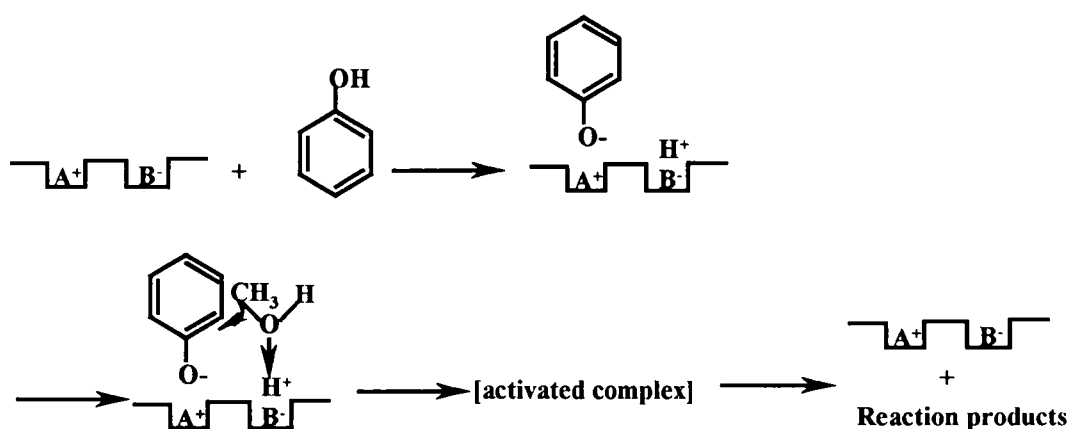


Fig. 5.6.4. Reaction mechanism of phenol alkylation using methanol - role of Lewis acid-base centers.

In the $\text{Co}_{1-x}\text{Ni}_x\text{Fe}_2\text{O}_4$ -type series, the catalytic activity follows the order $\text{CoFe}_2\text{O}_4 > \text{Co}_{0.8}\text{Ni}_{0.2}\text{Fe}_2\text{O}_4 > \text{Co}_{0.5}\text{Ni}_{0.5}\text{Fe}_2\text{O}_4 \approx \text{Co}_{0.2}\text{Ni}_{0.8}\text{Fe}_2\text{O}_4 > \text{NiFe}_2\text{O}_4$, with a total ortho selectivity always greater than 96 %. We have already understood that, substitution of Co^{2+} by Ni^{2+} increased the basicity of the system with simultaneous decrease in their acidity, as observed from the limiting concentration of electron acceptors adsorbed and their alcohol dehydration activities. The 2,6-xylene/o-cresol ratio is found to be influenced by the Ni^{2+} substitution, which is least when Ni^{2+} is

completely substituted. As explained before, Ni^{2+} substitution reduces the acidity of the system which tends to suppress the secondary alkylation activity. This conclusion is in agreement with that reported by Seitara Namba *et al.*[23] according to which stronger acid sites are required for secondary alkylation reaction to yield 2,6-xyleneol, whereas only weaker acid sites are needed for the formation of primary alkylated product, o-cresol. We believe that a controlled interplay of strength as well as the number of acidic sites determine the product selectivity and catalytic activity.

In $\text{Zn}_{1-x}\text{Co}_x\text{Fe}_2\text{O}_4$ series also activity and selectivity to ortho alkylation increased substantially with Co concentration. Activity follows the order $\text{CoFe}_2\text{O}_4 > \text{Zn}_{0.2}\text{Co}_{0.8}\text{Fe}_2\text{O}_4 > \text{Zn}_{0.5}\text{Co}_{0.5}\text{Fe}_2\text{O}_4 > \text{Zn}_{0.8}\text{Co}_{0.2}\text{Fe}_2\text{O}_4 > \text{ZnFe}_2\text{O}_4$. It is interesting to notice that this order is just opposite to that for aniline methylation, where we observed decrease in NMA yield progressively with Co^{2+} substitution. We have noticed that Co-addition decreased the basicity of the systems. In both aniline and phenol alkylation reactions the initial step involves adsorption and polarization of substrate molecules due to the combined effect of acid-base site pairs. Since aniline is less polar than phenol, even minute variation in basic site concentration due to Co-substitution will seriously reflect in the activity pattern. Also, since aniline is a very strong base even very weak acid centers can effectively coordinate with aniline. Hence in aniline alkylation, it is the basicity of the system, rather than acidity, that influences the catalytic activity. Phenol itself is highly polar and even very weak basic sites can easily remove a H^+ from phenolic O-H bond. Therefore in phenol alkylation it is the acidity rather than basicity controls the catalytic activity. Hence, phenol alkylation activity increased with Co-substitution in $\text{Zn}_{1-x}\text{Co}_x\text{Fe}_2\text{O}_4$ type systems.

Among the systems tried $\text{Zn}_{1-x}\text{Ni}_x\text{Fe}_2\text{O}_4$ series is least active for phenol methylation. The low activity can be due to the low acidity possessed by this system. Ni-addition progressively removes acidic sites originally present in zinc-system and correspondingly lesser amount of alkylated phenols were formed.

5.7. ALKYLATION OF PHENOL USING DIMETHYL CARBONATE

Dimethyl carbonate (DMC) is a non-toxic chemical and is often being mentioned as a possible replacement for toxic alkylating agents. So this part of the chapter deals with some preliminary studies using DMC as an alkylating agent for phenol methylation. CoFe_2O_4 has been selected as a model system.

The product distribution data of one such experiment at 300 °C and at a feed flow rate of 3 ml/h are presented in the following table (Table 5.7.1):

Product distribution	Wt. %
Non aromatics	2.51
Anisole	3.72
Unreacted phenol	39.92
Methyl anisole	Nil
o-Cresol	38.50
2,6-Xylenol	15.30
Others	0.05
Phenol conversion	60.08
o-Cresol selectivity	64.08
2,6-Xylenol selectivity	25.47

Table 5.7.1. Product distribution and selectivity data of phenol methylation using DMC over CoFe_2O_4 . Reaction temperature 300 °C, feed flow rate 3 ml/h, catalyst amount 3 g, DMC-phenol molar ratio 3 and TOS 1 h.

The Table (5.7.2) illustrates the effect of molar ratio of DMC to phenol on conversion and selectivities. Highest conversion and product selectivities were recorded at a feed ratio of 3.

In another set of experiments the effect of reaction temperature is studied. The optimum temperature range was found to be 300-350 °C. At low temperature o-cresol selectivity was more. Increase in temperature increased both phenol conversion and 2,6-xylenol yield upto 350 °C. The results are presented in Fig 5.7.1.

Product distribution	Feed molar ratio (DMC:Phenol)	
	2:1	3:1
Non aromatics	1.27	2.51
Anisole	3.93	3.72
Phenol	57.67	39.93
Methyl anisole	Nil	Nil
o-Cresol	26.37	38.50
2,6-Xylenol	10.49	15.30
Others	0.26	0.05
Phenol conversion	42.33	60.08
o-Cresol selectivity	62.30	64.08
2,6-Xylenol selectivity	24.78	25.47

Table 5.7.2. Effect of feed molar ratio on product distribution over CoFe_2O_4 . Reaction temperature $300\text{ }^\circ\text{C}$, flow rate 4 ml/h and catalyst amount 3 g .

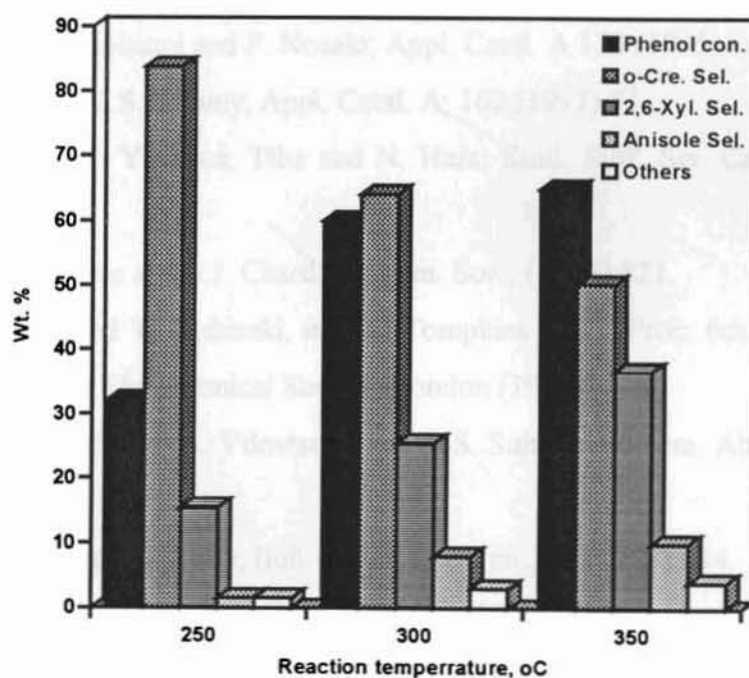


Fig. 5.7.1. Influence of reaction temperature on phenol conversion and product selectivities over CoFe_2O_4 using DMC as the alkylating agent. Feed molar ratio (DMC to phenol) 3, flow rate 3 ml/h and catalyst amount 3 g .

REFERENCES:

- [1] H. Feige, in: B. Elvers, S. Hawkins, G. Schultz (Eds.); Ullmann's Encyclopedia of Industrial Chemistry, Vol. A19, 5th ed., VCH. Weinheim, 1999, p. 313.
- [2] R. Dowbenko, in: J.I. Kroschwitz, Mary Houl-Grant (Eds.); Kirk-Othmer Encyclopedia of Chemical Technology, 4th ed., Vol. 2, 1992, p. 106.
- [3] E. Santhacesaria, D. Grasso, D. Galosa and S. Carra; Appl. Catal., 64 (1990) 83.
- [4] F. Nozaki and I. Kimura; Bull. Chem. Soc. Jpn 50 (1977) 614.
- [5] K. Li, I. Wang and K. Chang; Ind. Eng. Chem. Res., 32 (1993) 1007.
- [6] M.C. Samolada, E. Grgoriadou, Z. Kiparissides and I.A. Vasalos; J. Catal., 152 (1995) 52.
- [7] C. Bezouhanova and M.A. Al.Zihari; Appl. Catal., 83 (1992) 45.
- [8] S. Sato, K. Koisumi and F. Nozaki; Appl. Catal. A 133 (1995) L7.
- [9] S. Velu and C.S. Swamy; Appl. Catal. A; 162 (1997) 81.
- [10] S. Namba, T. Yashima, Tiba and N. Hara; Stud. Surf. Sci. Catal., 5 (1980) 105.
- [11] N.M. Cullinane and S.J. Chard; J. Chem. Soc., (1945) 821.
- [12] K. Tanabe and T. Nishizaki, in F.C. Tompkins (Ed.), Proc. 6th Int. Congress on Catalysis, The Chemical Society, London (1977).
- [13] N.D. Limankina, F.A. Vdovtsova and A.S. Sultanov; Chem. Abst., 89 (1976) 17640.
- [14] F. Nozaki and I. Kimura; Bull. Chem. Soc. Jpn., 50 (1977) 614.
- [15] J.A. Sharp and R.E. Dean; Brit. Patent, 1 125 087 (1968).
- [16] S. Balasme, P. Baltrame, P.L. Baltrame, P. Carniti, L. Forni and G. Zuretti; Appl. Catal., 13 (1984) 161.
- [17] R. Pierantozzi and A.F. Nordquist; Appl. Catal., 263 (1986) 21.
- [18] P.D. Chantal, S. Kaliaguine and J.L. Grandmaison; Appl. Catal., 18 (1985) 133.
- [19] M. Renaud, P.D. Chantal and S. Kaliaguine; Can. J. Chem. Eng., 64 (1986) 787.

- [20] J. Kaspi and G.A. Olah; *J. Org. Chem.*, 43 (1978) 3142.
- [21] E. Santacesaria, M. Di Serio, P. Clambelli, D. Gelosa and S. Carra; *Appl. Catal.* 64 (1990) 101.
- [22] L.H. Klemm, C.E. Klopfenstein and J. Shabtai; *J. Org. Chem.*, 35 (1970) 1069.
- [23] S. Namba, T. Yashima, Y. Itaba and N. Hara, in: *Catalysis by Zeolites*, B. Imelik *et al.* (Editors), Elsevier Scientific Publishing Company, Amsterdam (1980), p. 105.

CHAPTER VI

SUMMARY AND CONCLUSIONS

6.1. SUMMARY OF THE WORK

Spinel type compounds have attracted much attention due to their peculiar type of cation distribution, mechanical and chemical stability and their ability to withstand reducing atmosphere. However, the conventional ceramic route for the preparation of these materials gives non-homogeneous, aggregate particles with low surface area and large particle size. The recently developed low temperature methods have the advantages that, such methods often give homogeneous fine ferrite particles with very high surface areas. The present thesis is devoted to prepare ferrospinels containing Zn, Co and Ni via low temperature method and to evaluate the activities of these systems for phenol and aniline alkylation using a vapour phase silica reactor. The work is presented in six chapters.

Introduction and literature survey about heterogeneous catalyst systems are included in **Chapter I**. A detailed description on spinel structure and their catalytic effectiveness for various reactions are also presented in this chapter. **Chapter II** deals with various experimental procedures adopted for the present work. **Chapter III** is mainly oriented to explain characterization data and to study and understand surface properties of the systems. The catalysts were synthesized via co-precipitation route. All the systems were thoroughly characterized by adopting various physico-chemical techniques. Spinel phase formation has been confirmed from XRD and DR-IR data. SEM photographs indicated fine particles of approximately 50 nm. All these materials possessed sufficiently high surface areas as against those prepared by the conventional high temperature methods. Pore sizes are distributed in the range of 20-200 Å. Two independent methods were adopted for acidity basicity measurements. For the determination of basicity the electron acceptor adsorption experiments were performed. The limiting amount of electron acceptors adsorbed and their electron affinity values have been correlated with basicity of the systems. Isopropanol and cyclohexanol decomposition studies were performed to evaluate the acidity of the systems. Since dehydration is an acid catalysed reaction the dehydration activities of the systems have been taken as a measure of their acid strength. Redox properties of

the systems have been compared after performing oxidative dehydrogenation of ethyl benzene.

Alkyl anilines are important intermediates for the production of many useful materials such as dyes, pharmaceuticals, pesticides and explosives. A detailed discussion on aniline alkylation activities using present systems is presented in **Chapter IV**. Ferrospinels of Zn-Co and Zn-Ni are found to be highly active and selective for N-monoalkylation of aniline leading to N-methylaniline. The chapter is divided into two sections. The procedure adopted for the process-optimization to yield N-methylaniline selectively and in better yield is presented in a systematic way in the first section. Selectivity and activity of the systems depend strongly on acid-base properties. In the second section of this chapter the plausible reaction network and the associated mechanisms are discussed. Catalytic activities have been correlated with surface acid-base and structural properties. Kinetic studies were performed using $\text{Zn}_{0.8}\text{Co}_{0.2}\text{Fe}_2\text{O}_4$ as a model system. Reaction was found to be pseudo first order with respect to aniline at sufficiently high concentration of methanol. Finally, a brief study was made using dimethyl carbonate as an alkylating agent.

Alkylphenols such as o-cresol and 2,6-xyleneol are industrially valuable products. The demand for these products has increased in recent years owing to the numerous uses of substituted phenols. **Chapter V** focuses on the alkylation of phenol using methanol over the ferrospinel systems. $\text{Co}_{1-x}\text{Ni}_x\text{Fe}_2\text{O}_4$ and $\text{Zn}_{1-x}\text{Co}_x\text{Fe}_2\text{O}_4$ type systems are particularly selective and active for ortho methylation of phenol leading to o-cresol and 2,6-xyleneol. CoFe_2O_4 is found to be the most active and stable catalyst. Under the optimized conditions, the total ortho selectivity (i.e. o-cresol + 2,6-xyleneol) exceeded 96%, whereas the individual selectivities depend largely on process parameters.

6.2. CONCLUSIONS:

- ◆ Unlike the spinels prepared by the conventional solid state ceramic methods, the ferrites containing Zn, Co and Ni prepared via low temperature route produced homogeneous and fine ferrite particles with high surface areas.

- ◆ Adsorption experiments using electron acceptors having different electron affinity values revealed the variation of the electron donor properties of the spinel surface with composition. Ni-containing systems are most basic whereas Co-containing systems are least basic. Zn-Containing systems show intermediate basicity values.

- ◆ As revealed from the alcohol dehydration experiments, the influence of various metal ions on acidity can be represented as $\text{Co} > \text{Zn} \gg \text{Ni}$.

- ◆ Presence of Fe^{3+} and Co^{2+} ions in the octahedral sites of the spinel matrix significantly enhanced ethylbenzene dehydrogenation. Activity decreased during Ni-doping in both Zn and Co-ferrites. In $\text{Zn}_{1-x}\text{Ni}_x\text{Fe}_2\text{O}_4$, Ni-addition replaces equivalent amounts of Fe^{3+} ions from octahedral to tetrahedral sites, whereas in $\text{Co}_x\text{Ni}_{1-x}\text{Fe}_2\text{O}_4$ only the $\text{Co}^{2+}/\text{Ni}^{2+}$ ratio varies during Ni-substitution. Hence it is the Co^{2+} and / or Fe^{3+} concentration in the octahedral sites that determines the redox properties of the systems.

- ◆ For the oxidative dehydrogenation of ethyl benzene, the catalyst oxygen has a major effect on the reaction rates, whereas the gas phase oxygen serves only in reoxidizing the catalyst itself. The identical Mossbauer isomer shift values of fresh and used ZnFe_2O_4 and CoFe_2O_4 revealed the absence of major bulk reduction during the reaction.

- ◆ $\text{Zn}_{0.8}\text{Co}_{0.2}\text{Fe}_2\text{O}_4$ exhibits excellent selectivity and high yield for N-methylaniline even at comparatively low temperatures and methanol to aniline molar ratios. ZnFe_2O_4 , though exhibits high activity in the initial period of the run, deactivates quickly as the reaction proceeds. This can be attributed to the normal spinel structure of ZnFe_2O_4 , where the reduced Fe^{3+} ions are unable to regain their original state through redox migration.

- ◆ Alkylation of aniline over $Zn_{0.8}Co_{0.2}Fe_2O_4$ is pseudo first order with respect to aniline at sufficiently high concentration of methanol in the feed. Activation energy calculated is considerably lower than the values reported for γ -alumina and MgO.
- ◆ Dimethyl carbonate can also be employed for the alkylation of both phenol and aniline.